INVESTIGATION OF SOIL AND GROUNDWATER CONTAMINATION USING INTEGRATED GEOPHYSICAL AND GEOCHEMICAL METHODS AT KATAEREGI MINING SITE, NIGER STATE, NIGERIA

BY

JAMILU, Shehu PhD/SPS/2018/8326

DEPARTMENT OF PHYSICS

SCHOOL OF PHYSICAL SCIENCES FEDERAL UNIVERSITY OF TECHNOLOGY, MINNA.

AUGUST, 2023

ABSTRACT

Seismic refraction method, Resistivity method, Airborne magnetic data and geochemical analysis of soil and water were conducted to investigate the mineralisation potential of Kataeregi (Latitudes 09º21'N and 09º25'N and Longitudes 006º17'E and 006º22'E) and also to check the effect of mining activities on soil and groundwater in the study area. Aeromagnetic data acquired from Nigeria Geological Survey Agency was used to analyse and interpret the magnetic signatures using different filters. The 2-D resistivity technique using Wenner array was adopted with the help of SAS 1000 Terrameter, the data was interpreted using RES2DINV. Five traverses were occupied with a distance of 100 m apart, readings were repeated three times 10 m, 30 m and 50 m respectively with resistivity values ranging from 5.95 Ωm to 572 Ωm. The low resistivity values of less than 10 Ωm was observed at the top soil and may be suggestive of slimes or mine waste, with the depth of contamination ranging from 0- 2 m. IP locates the passages of the zones of anomalies aligning NE – SW direction. 12 channel seismograph was used for seismic data acquisition and seisOpt@2D software was used for data interpretation. Tomography model revealed three distinctive layers of top soil with velocity of 600 m/s, weathered/fractured layer has a velocity of 2000 m/s and fresh basement with a velocity of 2850 m/s. The 3-DEuler deconvolution locate and estimate the depth to various anomalous bodies with depth to source body between 30 m and 428.5 m. The results revealed lineaments trending majorly in NE-SW directions. The FVD anomaly map reveals the oval and linear shapes anomalies with values between -5.78 to 0.34 nT/m, the ASA amplitude map reveals wide range of values between 0.03 to 0.76 nT/m, the TDR map showed variations in anomalies with values ranging from -0.06 to 1.42 rad/m**.** Five

groundwater samples were collected and ten elements were analysed. The results showed Cadmium ranges from 0.000 mg/L to 0.003 mg/L. Copper ranges between 0.000 m/L and 0.515 mg/L and Zinc ranges from 0.000 mg/L to 0.111 mg/L. Iron concentration varies from 0.03 mg/L and 13.6 mg/L, arsenic ranges from 0.002 mg/L to 0.026 mg/L. Nitrate concentration level was far above the WHO and NSDWQ standard with the values ranging from 16.50 mg/L to 323.7 mg/L, well $_1$, well$_3$ and well$_4$ values are all above tolerable limit. Mercury has concentration level ranging from 0.000 mg/L to 0.022 mg/L with well$_2$ been the possible contaminant, while chromium has values ranging from 0.000 mg/L to 0.080 mg/L with well$_1$ having the value above the NSDWQ standard, lead concentration value ranging between 0.000 mg/L and 0.001 mg/L. The results of the analysed soil samples revealed soil pH ranged from 6.08 to 8.12 which is indicative of moderately alkaline, Ar values ranged from 4.23 mg/kg to 12.05 mg/kg, Ni values ranged between 4.00 mg/kg and 70.0 mg/kg and is above the standard. Fe ranged from 0.72 mg/kg to 16.03 mg/kg, Hg values ranged between 0.11 and 1.01which is also above the standard set by CSQG/WHO, Cd values ranged from 4.76 mg/kg to 9.32 mg/kg which is highly concentrated and Cr ranged between 9.89 mg/kg and 27.00 mg/kg. Cu values ranged from 99.78 mg/kg to 111.9 mg/kg while Pb values ranged between 1.0 mg/kg and 6.07 mg/kg and Zn values ranged from 9.91 mg/kg to 13.0 mg/kg. Concentrations of Ar, Ni, Hg, Cd and Cr are above the CSQG/WHO standard while that of Fe is found to be below the standard set by CSQG/WHO and Cu, Pb, and Zn are within the permissible range. Generally inverse models of the tomography lines show low resistivity values of less than 10 Ωm observed at the top soil which is indicative of mine wastes as a result of the mining activities, the depth to mine residue was estimated to be around 0 - 2 m with resistivity

values ranging from 5.95 Ωm to 572 Ωm. The chargeability suggest the continuity of the vein with the depth not exceeding 30 m. The correlation between the seismic refraction and electrical resistivity revealed three layers each. The result of geochemical parameters on the analysed groundwater are within the limit set by WHO, NSDWQ. However the activity of artisanal mining in the area has impacted on the environment.

TABLE OF CONTENTS

CHAPTER ONE

1.0 INTRODUCTION

CHAPTER TWO 2.0 LITERATURE REVIEW

CHAPTER THREE

3.0 MATERIALS AND METHODS

CHAPTER FOUR

4.0 RESULTS AND DISCUSSION

LIST OF TABLES

LIST OF FIGURES

LIST OF PLATE

LIST OF ABBREVIATIONS

Current-	I
Resistivity	ρ
Resistance-	R
Self-Potential-	SP
Ohm-meter-	Ωm
Millisecond	msec
United Nations Children's Fund	UNICEF
Office for the Coordination of Humanitarian Affairs	OCHA
Médecins Sans Frontières	MSF
United Nations Development Programme	UNDP
Nigerian Standard for Drinking Water Quality	NSDWQ
Electrical Resistivity Tomography	ERT
Seismic Refraction Tomography	SRT
Induced Polarisation	IP
Total Magnetic Intensity	TMI
Potentially Toxic Elements PTEs Volcanic Massive Sulphide	VMS
Sedimentary Exhalative	SEDEX
Iron Oxide Copper Gold	IOCG
Vertical Electrical Sounding	VES
Kilometre-	km
Metres-	m

Metre square- m^2

Current density-   J

Apparent Resistivity-   ρa

Root Mean Square-   RMS

Conductivity   **σ**

Changeability   M

Magnetic susceptibility   k

North-   N

2-Dimentional   2D

Universal Transverse Mercator   UTM

East- West-   E-W

Cadmium   Cd

Cobalt   Co Zinc   Zn

 Arsenic   Ar Chromium   Cr

Copper   Cu

Lead   Pb

Mercury   Hg

 Iron   Fe

Nitrate   Ni

Potential of hydrogen   pH

Gram   g

Milligram   mg Kilogram

                                   kg

World Health Organisation   WHO

Canadian Soil Quality Guidelines	CSQG
European Union	EU
United State Environmental Programme	USEPA
Commission of the European Communities	CEC
Reduced to Equator	RTE
Analytical signal	ASA
First vertical derivative	FVD

CHAPTER ONE

1.0   INTRODUCTION

1.1 Background to the study

The sustainable management of waste approach aimed at global environmental quality, and environmental quality is a prerequisite for a rise in per capital welfare over a period of time (Beatrice and Jussi, 2013). Water and sanitation are among the basic requirements for life (Mara & Evans, 2011). According to United Nations Sustainable Development goals on water and sanitation, about 2 billion people in the world are living in areas classified as water stress. The availability of water resources in quality and quantity is a prerequisite in dealing with the sustainability of the resources (Mara and Evans, 2011). Rapid population increase across the globe has resulted in an increase in food production, thereby putting a lot of stress on water resources (Kalaivanan *et al*., 2017). In recent times people have resorted to groundwater for their potable use, especially in developing

countries (Massally *et al*., 2017). Observations have shown that the reliance on groundwater resources has risen because of quality issues associated with the use of surface water. The quality of groundwater varies spatially in response to geogenic and anthropogenic factors (Annapoorna & Janardhana, 2015) which warrants an assessment of the water quality to serve the purpose for which it is used.

Efficient management of waste is a global concern requiring extensive research and developmental work towards exploring newer application for a sustainable and environmentally sound management. The problem of waste management is a primordial one and presents issues in developing countries in Africa, particularly Nigeria (Beatrice & Jussi, 2013). The earth subsurface has become the safest and most abundant source of potable water in comparison to the earth's surface as it is often shielded from direct human activities. However, any undetected contamination of this resource poses a threat to the well-being and continuous existence of man in the environment. Contamination is the pollution involving constituents that are hazardous to health because of their nature or quality (Adelusi *et al*., 2013). Groundwater is transmitted through a deep aquifer comprising unconsolidated weathered materials that form the overlying mantle or regolith (Morrison *et al*., 2003).

Recently, cases of contamination has been reported i n m a n y a r t i c l e and this has led to the use of seismic refraction, magnetic, very low frequency, electromagnetic, geochemical and electrical resistivity tomography methods to map the contaminants within the subsurface since geophysical methods have been found useful in mapping area(s) of contaminated soil and groundwater based on their ability to measure certain physical properties of the subsurface structures that can harbor groundwater and its contaminants (Adebayo *et al.*, 2015*).*

Mining generates a large quantum of tailing otherwise termed as slimes or leach residue, basically a mixture of fine disintegrated mineral particles and fluid, which needs to be disposed safely without causing any environmental hazard like leaching and erosion by wind or water. The global legacy of mining and disposal of tailings had been for more than few centuries (Orisakwe *et al*., 2012). Tailings facilities consist of tailings pond or lagoons, tailings dam and tailings transport systems (generally pipelines). Usually a very large area is required to contain the tailings which is man-made, and is the most critical element of these facilities. The surface disposal site is to be characterised for its subsurface nature in order to understand its role in mapping the subsurface geological formation in terms of it geophysical parameters in and around the waste disposal site (Rolland & Karunakar, 2011).

A mining site is usually a complex industrial system handling huge amounts of rocks in order to extract from them a lower or marginal amount of valuable metals or minerals. It comprises thus two activities: extraction and ore processing. The sheer mass of the handled material implies that the valuable commodity is extracted or concentrated near site, and most of the waste is disposed of nearby. The specificity of mine waste required adapted regulations and standards (Alexandros *et al*., 2010). Several near surface geophysical explorations methods can be adopted in integration with geological mapping or lithology analysis to better understand the subsurface geological settings below the waste disposal site. The thickness of the weathered zone (overburden), presence of intrusive bodies, dipping bodies are some of the geological inferences expected from geophysical investigation. These inferences are to be corroborated with hydrological and geochemical results from the study area to concretise the geophysical findings (Adelusi *et al*., 2013).

Geophysics has two major advantages which makes it a suitable tool for environmental impact assessment. It is non-invasive or non-destructive and it can give continuous subsurface information along a profile. Consequently, geophysics has an important role to play in contaminated land assessment. Several authors had engaged geophysical methods such as aeromagnetic and electrical resistivity methods, seismic tomography and hydrochemical measurements in mapping dumpsite pollution in both basement complex and sedimentary terrains of Nigeria and other parts of the world

(Bayode & Adeniyi, 2014; Adelusi *et al*., 2013; Adebayo *et al.,* 2015; Osazuwa & Abdullahi, 2008 & Rolland & Karunakar, 2011).

1.2 Statement of the Research Problem

The world Health Organisation (WHO, fact sheet No 112, 1996), estimated that every eight seconds a child died from water related disease and that each year more than five million people died from illness linked to unsafe drinking water or inadequate sanitation.

The use of machines in the crushing, grinding and milling of crystalline rocks hosting gold deposits during processing can pollutes the air and affect human by inhaling the dust and in plant either by settling on the leave or through intake from the soil. This could lead to serious health challenges such as respiratory tract infections.

With the global recession causing the price of precious metals to soar, impoverished villagers in Bagega, Zamfara State, Nigeria in 2010 had to turned to mining the area's gold deposits but gold vein were mingle with lead and as result the villager's low-tech mining methods were sending clouds of lead-laced dust into the air. The miners, unknowingly carrying the powerful toxic on their clothes and skin, brought it into their homes where their children breathed it in. This has led to the deaths of 163 people

including 111 children, with discovery of 355 cases (UNEP Report, 2011). This is one of the many lead poisoning epidemics with low and middle income countries.

1.3 Scope and Limitations of the Study

The scope of the study covers an area of 500 m by 500 m and is limited to electrical resistivity tomography, Induced Polarisation (chargeability), Seismic refraction tomography, airborne magnetic data and geochemical analysis of soil and groundwater in around the study area.

1.4 Justification for the Study

The study area has been going through series of mining activities without proper survey and with indiscriminate dumping of mine waste or leach residues without regards to local geology and hydrogeology. The reported danger often associated with mining necessitates a detailed structural framework for the eco-friendly extraction of mineral and also to delineate the potential mineralisation zones and locates the areas that are possibly been contaminated as well as to proper solution that can reduce the effect of mining to environment.

Focus has mainly been on dumpsite thereby neglecting other areas of possible contamination such as mine waste, oil spillage arising from mechanics and filling station.

1.5 Aim and Objectives of the Study

The aim of the research is to investigate groundwater and soil contamination at a mining site.

The objective of the study are to:

i. delineate structurally controlled mineralisation zone in the study area ii. delineate lateral and depth extent of contaminated leach residue or slimes below the surface iii. map out subsurface structures below the ground surface that could act as pathways for the flow of the contaminant (permeability, fractured zones, fault lines and lithologic contact) iv. determine the physiochemical properties of water in the study area

v. correlate the result of generated leach residue or slimes on the nearby groundwater through hydro-chemical analysis of water samples with international best practices   vi. classify the water for various purposes and their percentage compliance with World Health Organisation (WHO) and Nigerian Standard for Drinking Water Quality (NSDWQ) vii. determine and analyse the properties of the subsurface soil through physiochemical analysis

1.6 Description of the Study Area

The study area (Kataeregi) is located 39 km along Minna – Bida road, in Katcha Local Government Area of Niger State, North-central Nigeria (Figure 1.1). The area is part of Bida Sheet 184 NE and is located between Latitudes 09º21'N and 09º25'N and Longitudes 006º17'E and 006º22'E. It lies between the geographical coordinates of Northing's 1038000 – 1037700 mN and Easthing's 206030 – 206455 mE in the Universal Traverse Mercator (UTM) Minna Zone 31. The topographic elevation around the site ranges from 335.0 to 365.0 m above mean sea level and generally slopes gently from the north towards the southern part. The area has a climate characterised by two seasons; the wet season and the dry season. The wet season starts from around mid-April and ends in October with an average rainfall of 1500 mm to 2000 mm while the dry

season starts around November and ends in March with an average maximum temperature of about 33 ˚C (Bayode and Adeniyi, 2014).

The vegetation of the area consist of broad leaved Savannah woodland with some of the trees reaching about 10 meter in height.. The predominant vegetation consist of shrubs and grasses (Adesoye, 1986). Basically, the study area consist of low-lying terrain and gentle hills.
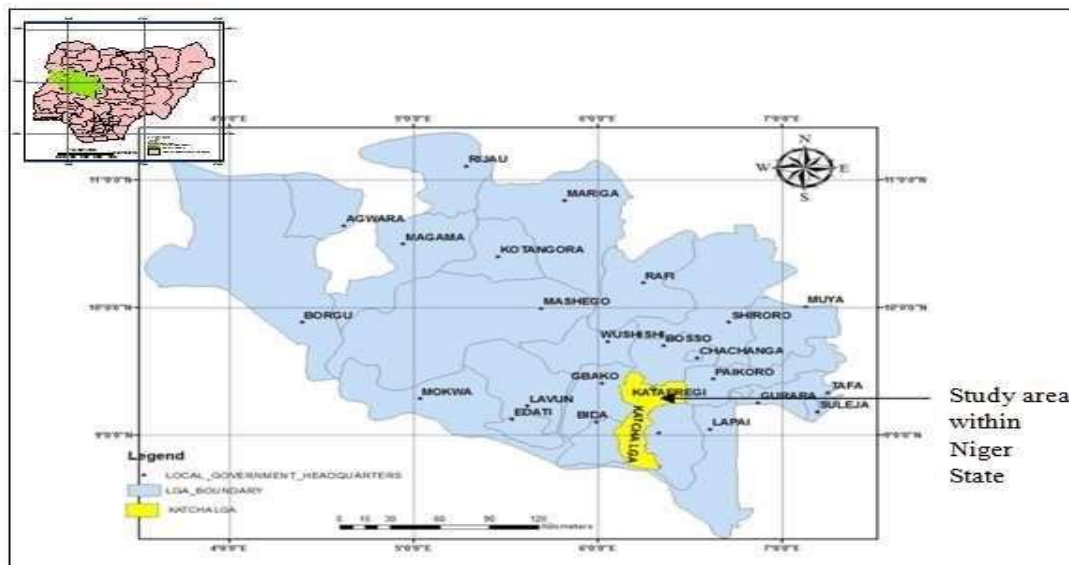
Figure 1.1 Location map of Kataeregi, Niger State, Nigeria (Omanayin *et al*., 2016).

1.7 Management of Mining, Quarrying and Ore-Processing Waste

Mining-selected waste (or simply mining waste) can be defined as part of the materials that result from the exploration, mining and processing of substances governed by legislation on mines and quarries. It may consist of natural materials without any modification other than crushing (ordinary mining waste, unusable mineralised materials) or of natural materials, processed to varying degrees during the ore-processing and enrichment phases, and possibly containing chemical, inorganic and organic additives (Figure 1.1). Overburden and topsoil are classified as waste (Commission of the European Communities (CEC), 2000)**.**

23
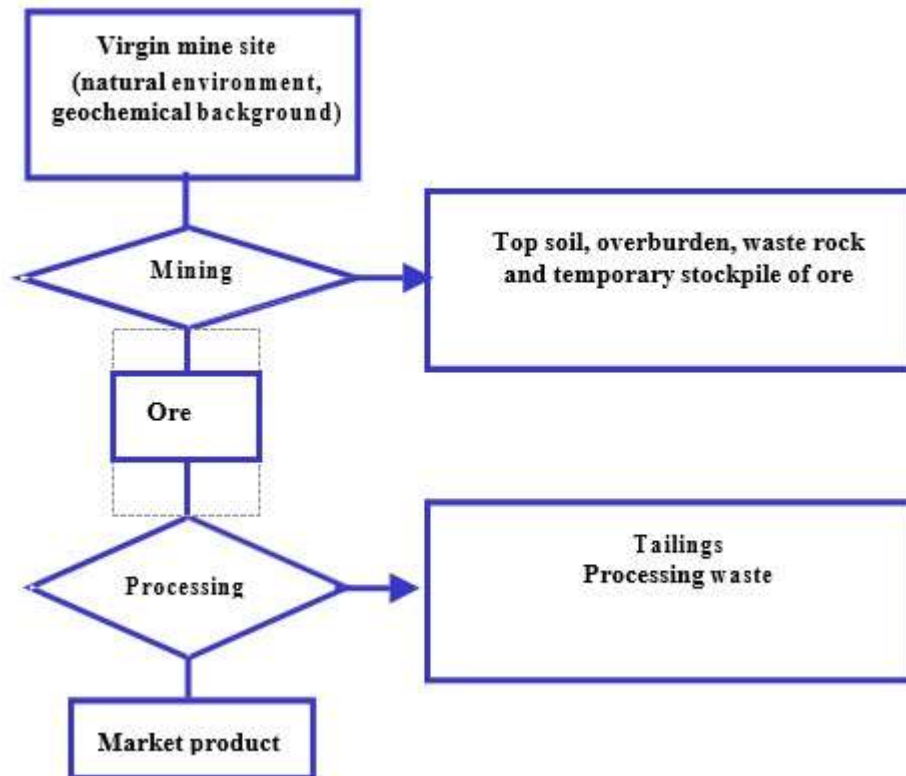
Figure 1:2: Mining waste types (UNEP, 1996)

Waste can affect the environment through one or more of the following intrinsic criteria:

a. its chemical and mineralogical composition,

b. its physical properties,

c. its volume and the surface occupied,

d. the waste disposal method.

Besides these parameters, one must also take into account extrinsic parameters such as:

a. climatic conditions liable to modify the disposal conditions,

b. geographic and geological location,

c. existing targets liable to be affected (man and his environment).

1.8 Types of mining waste

1. Topsoil and Overburden

2. Waste rock (mine rock piles)

3. Tailings (processing waste)

1.8.1. Waste rock

Waste rock is hence durably unused extraction products that is generally stored indefinitely in a landfill site which, for economic reasons associated with transport costs, is located in the immediate vicinity of the main mining centre. The quantity of mining waste that can be stored at a mining centre varies considerably and mainly depends o n the selectivity of the mining method. As a r u l e opencast pits and quarries generate much more mining waste than an underground mine (Ritcey, 1989).

The main type of waste rock is generated by surface (or barren rock) stripping to expose the shallow ore. This is rock that is weathered to varying degrees, although increasingly fresh with depth and showing the geological characteristics of the local surrounding material. Its composition is similar to the rocks of the sector. The largest (in tonnage) quantity of barren rock comes from stripping for opencast mines. In underground mines, these barren rocks are generated by the passages (shafts, crosscuts) (Douglas & Lawson, 2000).

1.8.2 Tailings (processing waste)

At a mine, an ore mill normally abuts on the extraction centre to produce the first marketable products (metallic concentrates, sorted ore, and ingots). The technological

processes are very different according to the type of substance mined, and the modernity of the technologies employed (Douglas & Lawson, 2000).

Mill waste is generally referred to as tailings, or releases or effluents. It is generated by the various mineral-upgrading processes employed to meet demand. For a given mineral, it will have different physicochemical properties according to the conditions in which it has been generated. It is found in solid, liquid and gaseous form. Waste is generated at all levels of the recovery process to upgrade the minerals, within the same process chain, and is considered as ultimate or stripped of useful elements. Its content depends on the time that it was generated (UNEP, 1996).

1.9 Assessment of mining related risk: potential sources of pollution

Every ore, whether metallic or non-metallic, is rarely mono-minerallic, but composed of a complex mineral paragenesis liable to contain a large number of potential pollutants, in addition to the material to be upgraded. Moreover, industrial processing methods use chemical components, which may also create pollution. These components are present in small quantities and are often organic, dissociating fairly rapidly in other molecules (Ritcey, 1989).

Consequently, analysis of the "pollutant potential" of the extraction and physical preparation of an ore, must take into account the "pollutant potential" of each mineral species, including those resulting from the *in situ* weathering of the primary minerals making up this ore and its surroundings. Since excavation and reworking gives rise to different physicochemical conditions from those prevailing in the deposit in place, the

chemistry of the elements concerned must also be considered (Commission of the European Communities, 2000)

Some mineral species are believed to be stable in the natural environment and harmless to man and the environment, apart from possible detriment attributable to the "fines" fraction. The "pollutant potential" of this type of ore has to be analysed individually in accordance with the processes employed for their conversion and for their adaptation to their intended use. Ores that fall into this category include aluminium (bauxite), tin (cassiterite), iron, manganese, talc, titanium (rutile or ilmenite), and zirconium (Ritcey, 1989). Analysis of the "pollutant potential" associated with ore processing has to take into account the industrial method(s) used to process the concerned ore in order to extract the useful components (e.g. flotation, cyaniding, and amalgamation) (Ritcey, 1989).

The recent priority given to the diversification of the Nigerian economy, the development of the solid mineral sector has become very active. The focus on how to locate and develop metalliferous deposits in the country has taken a centre stage. Gold deposit is by far the most important exploration target in the schist belts of Nigeria and contains world class potential gold reserves. Structural and hydrothermal alterations, which are critically important in controlling gold mineralization throughout the schist belts can be mapped out using geophysical methods (Ejepu *et al*., 2018).

Lithologic units, lithologic boundaries, fractures and mineral accumulations are more accurately identified and delineated using the combination of surface geological mapping, geophysical data, and geochemical data on subsurface samples. Recent improvement in the analysis of geophysical data and enhancement transforms, have

increased geophysical dataset resolution, so that very insidious changes in responses can be seen (Amstrong & Rodeghiero, 2006).

Geological and geophysical interpretation of the area will be done to gain insight into the structural setting, lithological contacts and possible alteration zones as well as identify prospective structurally controlled mineralisation of the area. Primarily, mineralisation in Nigeria is mostly lithologically and structurally controlled. Structures include faults, shear zones (lineament), pegmatites, quartz and quartzite veins. The methodology for the research is to capture the general trends of surface and subsurface structures. The exercise comprises surface geological mapping, lithologic and structural analysis of geophysical and geochemical data (Ajakaiye *et al*., 1991).

In order to confirm the location of the different contacts encountered, we also provided measurements in induced polarisation (IP). This imagery gives detailed information on the different heterogeneities existing within the prospected field. Resistivity and chargeability are well known geophysical methods and are traditionally applied to mineral exploration. Given the configuration of the prospected area which is very rugged and given its quality which is strongly fractured, the coupling between these two techniques, electrical resistivity and induced polarization, seems essential. Indeed, the contribution of the chargeability response makes it possible both to confirm the results of the response of the electrical resistivity at the level of the ground prospected and also to distinguish these results from those relating to the clay materials which accumulate in fractures (Ibrahim *et al*., 2019).

Magnetic minerals present in soils may either be inherited from the parent rocks (lithogenic origin) formed during pedogenesis (pedogenic origin) or may stem from

anthropogenic activities (secondary ferromagnetic materials). Hematite and magnetite are common minerals that occur as primary and secondary minerals in soil and provide a major sink for pollutants such as heavy metals in soils. They have been known as major minerals contributing to the magnetic susceptibility of a soil (Brempong *et al*., 2016). In addition to the presence of these minerals, the content of Fe, Mn, Cr, Co and Ni also affect magnetic susceptibility of the soil (Brempong *et al*., 2016). Magnetic susceptibility is a measure of the ability of any substance to be magnetised. In geology, magnetic susceptibility is one characteristic of a mineral type. The term "heavy metal" refers to any metallic chemical element that has a relatively high density. The use of magnetic measurements as a representation of chemical methods is largely approved because pollutants and magnetic particles are related (Hanesch & Scholger, 2002). Bityukova *et al*. (1999) reported close relationships of magnetic susceptibility with heavy metal contamination in soil has been proven by combined analyses of chemical and magnetic data. Magnetic susceptibility thus provides an indicator of heavy metal contamination of soils. Salehi *et al.* (2013) successfully measured road traffic pollution by evaluating the spatial distribution of magnetic susceptibility in the nearby soils. In the light of the current challenges in improving economic base of the country, there is a need to derive detailed information on the extent, the trend and depth to structures (e.g., dykes, shear or fracture/fault zones) that might be controlling emplacement of mineral deposits in the area. Regional features are of fundamental importance in selection of targets for mineral exploration, while localize features such as contact and shear zones are responsible for the localisation of the mineral deposits (Olomo *et al.,* 2018). These geologic features could be either directly observed or interpreted from data sets such as aeromagnetic and Landsat imageries.

Magnetic properties of different types of soil display different aspects of soil mineralogy. The minerals that are present in soil are either natural (through lithogenesis, pedogenesis) or of anthropogenic origin (industrial residues). The magnetic mineral content of the soil can be expressed in very broad terms by its magnetic susceptibility (Mücella-Canbay, 2010). Magnetic susceptibility is a measure of iron-bearing components in a material and it can be used to identify the type of the material on which the test is conducted as well as the amount of the iron-bearing minerals that the material contains. The determination of magnetic susceptibility can be a useful, sensitive and fast method which provides an important parameter used in mineralogy and granulometry.

The knowledge of the structural setting and subsurface sequence of an area is crucial in hazard assessment and natural resource exploration. Infrastructures sited on geological structures such as fault are prone to high structural damages (Adebiyi *et al.*, 2021). Geological mapping for geologic structures is difficult in areas with subdued surface relief, limited rock outcrops, or where the faults are mostly buried beneath large accumulations of sediment.

Primary mineralisation in Nigeria is largely lithological and structurally controlled. Solid mineral exploration requires interpretation of high-resolution airborne data, usually aimed at delineating possible rocks, zones and structures that may serve as hosts ((Tawey *et al.*, 2020*).*). Soil is the main source of nutrient for crops. Soil also provides support for plant growth in various ways. Knowledge about soil health and its maintenance is critical to sustaining crop productivity. However, this is a general assessment made by farmers. A scientific assessment is possible through detailed physical and chemical analysis of the soil.

A healthy soil is always the foundation of the food production system. Soils help to produces healthy crops. Plants obtain nutrients from two natural sources of soils. They are organic matter and the minerals. The organic matter includes any plant or animal material that returns to the soil and goes through the decomposition process. In addition to providing nutrients and habitat to organisms that are living in the soil, the soil organic matter also binds the soil particles to form soil aggregates and improves the water holding capacity of soils. Soils are the bases for survival of life on earth (Balasubramanian, 2017).

1.10 Heavy Metal Toxicity in Gold Mine Environment

Heavy metals play a vital role in metabolic and physiological processes of plant, humans and microorganism. Heavy metal like Zn, Cu, Ni, Co and Cr function as micronutrients and are important in redox-processes. They are important in the stabilisation of molecules through electrostatic interaction, regulation of osmotic pressure and cofactors of numerous enzymes and electrons transport chain (Smejkalora *et al.*, 2003).The non-essentials heavy metal like Ag, As, Cd, Pb, and Hg are of no biological importance to living organism and are very toxic when found in the ecosystem (Vega *et al.,* 2006).

Table 1.1: Heavy Metal Toxicity in Gold Mine Environment (Harish & David, 2015)

Constituents	Acceptable Concentration	Effect on Human body
Arsenic (As)	High toxicity	Damages skin, lungs, kidney and bladder
Cadmium (Cd)	6.4 – 11.7 mg/kg	Causes kidney stone and Damage liver
Nickel (Ni)	3 – 100 mg/kg	Asthma, lungs and cancer
Lead (Pb)	1 – 32 mg/kg	Damage kidney and causes blood pressure
Copper (Cu)	5 – 70 mg/kg	Brain damage, kidney and liver
Zinc (Zn)	8.9 – 65.7 mg/kg	Cancer, Headache, asthma and diarrhea
Mercury (Hg)	1.32kg (for every I kg of gold)	Damages kidney

Other mineral exist in a mining site like Cobalt (Co), Chromium (C)

1.11 Characteristics of Gold Mine Tailings

Tailings are a mixture of finely ground rock that is left after retrieval of the precious minerals and water used in the processing. Tailings are characterised by poor physical properties like poor aggregation, high hydraulic conductivity, fine texture and very limited cohesion ability. These properties make tailings different from soil (Blight & Fourie, 2005) and the lack of cohesion is responsible for the varied moisture content and temperature seen in the toxic waste.

1.12 Zamfara State Lead Poisoning Epidemic

A series of lead poisonings in Zamfara State, Nigeria, led to the deaths of at least 163 people between March and June 2010, including 111 children. Nigerian Federal Ministry of Health figures, state the discovery of 355 cases with 46 percent proving fatal. This is one of the many lead poisoning epidemics with low and middle income countries (Yi-chun *et al.,* 2012).

With the global recession causing the price of precious metals to soar, impoverished villagers had turned to mining the area's gold deposits. But the gold veins were mingled with lead, and as a result the villagers' low-tech mining methods were sending clouds of lead-laced dust into the air (UNICEF, 2010). The miners, unknowingly carrying the powerful toxin on their clothes and skin, brought it into their homes where their children breathed it in (OCHA Report, 2011). The result was perhaps the worst outbreak of lead poisoning in history, killing over 400 children in Bagega and neighbouring villages. In response, the Nigerian government pledged to clean up the lead-contaminated topsoil and provide medical care to the stricken children. But by mid-2012, there was no sign of the promised funds (UNEP Report, 2011).

Changes in animals can provide an early warning of the presence of disease or a dangerous change in the environment. As the extent of the lead poisoning became clear, there had been warning signs of lead contamination in the animal populations. The villagers were asked if any animals in the area had died, and they mentioned the disappearing of ducks earlier in the year but said that they did not think it was important. The death of these animals was a missed clue that could have alerted authorities of the crisis earlier. These ducks were sentinels (warning signs) of an environmental hazard (MSF Report, 2010).

Lead is a naturally occurring heavy metal, but it is unusual to find such high levels of lead in these communities. Zamfara State is an agricultural region, and traditionally most villagers relied on farming to earn a living. However, the area was also rich in many minerals, including gold. In recent years, the price of gold had risen and many villagers had started mining gold to earn more money (Yi-chun *et al.,* 2012). This outbreak has

been challenging for public health officials because it is difficult to remove lead from the environment. All of the contaminated soil must be removed from the villages and replaced with clean soil. This process is expensive, and some regions in Zamfara are still waiting for the contaminated soil in their villages to be removed. Since children cannot be treated for lead poisoning until the environment is clean, treatment has been delayed in some villages (UNEP Report, 2011).

Effective interventions have prevented many deaths, and thousands of children who were exposed to lead have been treated. Children will continue to be treated, and contaminated soil will continue to be removed from the remaining villages. The exposed children will also require long-term support. Although there are still many challenges, public health officials have made important progress in stopping this outbreak (OCHA Report, 2011).

The response to the mass lead poisoning in Zamfara State has involved multiple agencies, including WHO, United Nations Children's Fund (UNICEF), United Nations Development Programme (UNDP), United Nations Environment Programme (UNEP) - Office for the Coordination of Humanitarian Affairs (OCHA) Joint Environment Unit, Médecins Sans Frontières (MSF), the US CDC, the Blacksmith Institute, TerraGraphics Environmental Engineering Inc, and the Artisanal Gold Council, working with authorities and leaders at community, state and federal levels.

1.13 Groundwater Contamination

Groundwater contamination (also called groundwater pollution) occurs when pollutants are released to the ground and make their way down into the groundwater. This type of water pollution can also occur naturally due to the presence of minor and unwanted

constituent, contaminant or impurity in the groundwater. Movement of water and dispersion within the aquifer spreads the pollutant over a wider area (Custodio, 2013). Its advancing boundary, often called a plume edge, can intersect with groundwater wells , making the water supplies unsafe for humans and wildlife. The movement of the plume, called a plume front, may be analysed through a hydrological transport model or groundwater model. Analysis of groundwater pollution may focus

on soil characteristics and site hydrogeology, hydrology, geology and the nature of the contaminants. These natural contaminants are health problems if presents above tolerable limits. In addition to natural contaminants groundwater is often polluted by human activities (Ezugwu, 2015).

1.14 Contaminants Types

Contaminants found in groundwater cover a broad range of physical, inorganic chemical, organic chemical, bacteriological, and radioactive parameters. Contaminants in groundwater are summarised as inorganic and physical contaminants in Table 1.2.

Table 1.2: Inorganic contaminants found in groundwater (Ezugwu, 2015)

Contaminants	Source to groundwater	Potential health and other effects
Cadmium	Found in low concentrations in rocks, coal and petroleum and enters the ground and surface water when dissolved by acidic waters. May enter the environment from industrial discharge, mining waste, metal plating, water pipes, batteries, paints and pigments, plastic stabilizers and landfill leachate.	Replaces zinc biochemically in the body and causes high blood pressure, liver and kidney damage, and anemia. Destroys testicular tissue and red blood cells. Toxic

Chloride	May be associated with the presence of sodium in drinking water when present in high concentrations. Often from saltwater intrusion, mineral dissolution, industrial and domestic waste.	Deteriorates plumbing, water heaters and municipal works equipment at high levels. Above maximum contaminant level, taste becomes noticeable
Chromium	Enters environment from old mining operations, runoff and leaching into groundwater, fossil fuel combustion, cement-plant emissions, mineral leaching, and waste incineration. Used metal plating and a cooking-tower water additive.	Chromium III is a nutritionally essential element. Chromium IV is much more toxic than chromium III and causes liver and kidney damage, internal haemorrhaging, respiratory damage, dermatitis, and ulcers on the skin at high concentration.
Dissolved solids	Occur naturally but also enters environment from man-made sources such as landfill leachate, feedlots, or sewage. A measure of the dissolved ''salt''	May have an influence on the acceptability of water in general. May be indicative of the presence of excess concentrations of substance not included in the safe water Drinking

	or minerals in the water. May also include some dissolved organic compound.	Act. Which would make water objectionable. High concentrations of dissolved solids shorten the life of hot water heaters.
Copper	Enters environment from metal plating, industrial and domestic waste, mining and mineral leaching.	Can cause stomach and intestinal distress, liver and kidney damage, anaemia in high doses. Imparts an adverse taste and significant staining to cloths and fixtures. Essential trace element but toxic to plants and algae at moderate levels.
Aluminium	Occur naturally in some rocks and drainage from mines.	Can precipitate out of water after treatment causing increased turbidity or discoloured water.
Fluoride	Occurs naturally as an addictive to municipal water supplies; widely used in industries.	Decreases incidence of tooth decay but high levels can stain or mottle teeth. Causes crippling bone disorder (calcification of the bones and joints) at very high levels.
Hardness	Results of metallic ions dissolved in the water, reported as concentration of calcium carbonate. Calcium carbonate is derived from dissolved limestone or discharges from operating or abandoned mines.	Decreases the lather formation of soap and increases scale formation in hotwater heaters and low pressure boilers at high levels.
Iron	Occurs naturally as a mineral from sediment and rocks or from mining, industrial wastes and corroding.	Imparts a bitter astringent taste to water and a brownish colour to laundered clothing and plumbing fixtures.

Lead	Enters environment from industry, mining, plumbing, gasoline, coal, and as a water	Affects red blood cells chemistry, delays normal physical and mental development in babies and young

	additive	children. Causes slight defects in attention span, hearing and learning in children. Can cause slight increase in blood pressure in some adults. Probable carcinogen.
Manganese's	Occurs naturally as a mineral from sediment and rocks or from mining and industrial waste.	Cause aesthetic and economic damage, and imparts brownish stains to laundry. Affects taste of water, and causes dark brown or black stains on plumbing fixtures. Relatively non- toxic to animals but toxic to plants at high levels.
Nitrate	Occurs naturally in mineral deposits, soils, seawater, freshwater systems, the atmosphere, and biota. More stable form of combined nitrogen in oxygenated water. Found in the highest levels in groundwater under extensively developed areas. Enters the environment from fertilizer, feedlots, and sewage.	Toxicity results from the body's natural breakdown of nitrate to nitrite. Causes "blue baby disease", or methemoglobinemia, which threatens oxygen- carrying capacity of the blood.

Silver	Enters environment from ore mining and processing, product fabrication, and disposal. Often used in photography, electric and electronic equipment, sterling and electroplating alloy and solder. Because of great economic value of silver,	Can cause cargyria, a blue-gray colouration of the skin, mucous membranes, eyes, and organs in humans and animals with chronic exposure.

	recovery practices are typically used to minimize loss.	
Zinc	Found naturally in water, most frequently in areas where it is minned. Enters the environment from industrial waste, metal plating, and plumbing, and is a major component of sludge.	Aids in the healing of wounds. Causes no ill health effects except in very high doses. Imparts an undesirable taste to water. Toxic to plants at high levels.
pH	Indicate, by numerical expression, the degree to which water is alkaline or acidic. Represented on a scale of 0-14, where 0 is the acidic, 14 is the most alkaline, and 7 is neutral.	High pH causes a bitter taste, water pipes and water using appliances becomes encrusted; depresses the effectiveness of the disinfection of chlorine, thereby causing the need for additional chlorine when pH is high. Low pH water will corrode or dissolve metals and other substance

1.15 Factors that Determine Groundwater Contamination by Residue Leachate

1.15.1 Depth to water table

If the water table is low (far below the ground surface), the leachate will be partially

filtered as it percolates downward through the soil. If the water table is high (close to the

ground surface), the groundwater stands the risk of being contaminated by the time it gets

in contact with the groundwater (Osazuwa & Abdullahi, 2008)

1.15.2 Concentration of contaminants

A high concentration of contaminants in leachate will make the groundwater pollution more likely. Using polluted groundwater causes hazards to public health through poisoning or the spread of diseases (Osazuwa & Abdullahi, 2008). Different mechanism have influence on transport of pollutants e.g. diffusion, adsorption, precipitation, decay, in the groundwater.

1.15.3 Permeability of geologic strata

Highly permeable geologic strata allow leachate to quickly percolate through, receiving little filtration along the way (Osazuwa & Abdullahi, 2008)

1.15.4 Hydrologic settings

Relative vulnerability to pollution by hydrologic settings becomes:

I.   extreme, if (a) bedrock aquifers crop out (especially in karsts area); or bedrock aquifers are overlain by less than 3 m of soil (b) unconfined and gravel aquifers with unsaturated zone less than 3 m thick.

II.   high, if bedrock aquifers are overlain by 3 m sand and gravel, 3-5 m clay or clay- rich till.

III.   moderate, if unconfined aquifers are overlain by 10 m sandy till, or 5-10 m clay rich till, clay or peat.

IV.   low, if confined aquifers low permeable rock such as shale are overlain by 10 m clay-rich till (George, 1992).

1.16 Residue, Landfill Leachate and Public Health

The misconception about the materials placed on solid and residue deposit are basically household and residue deposit materials, they are relatively safe and would not adversely

affect groundwater quality and hence public health. Recent research of numerous toxic chemicals in well waters have proven this belief to be false (Osazuwa & Abdullahi, 2008). One need only to consider the water that was used to clean a garbage and to understand that it is not desirable to have a drop of residue deposit leachate in water meant for drinking and domestic use. The study has shown that in landfill leachate: 32 organic chemicals cause cancer (e.g. vinyl chloride, benzene), 16 cause birth defects (e.g. endrin), and 22 cause genetic effects (e.g. Trichloroethene). 10 inorganic chemicals cause diseases like skin discolouration (e.g. silver), skeletal damage (e.g. Fluoride), nervous system effects (e.g. mercury), central nervous system effects (e.g. Lead), circulatory system effects (e.g. Barium), liver/kidney (e.g. chromium, cadmium) and cancer of the bladder (e.g. Arsenic). World Health Organisation (WHO) also suggest that if sustainable safe drinking water and sanitation services were provided to all each year there would be 200 million fewer diarrhoeal episode, 2.1 million fewer deaths caused by diarrhoea, 76 000 fewer dracunculiasis cases, 150 million fewer schistosomiasis cases and 75 million fewer trachoma cases. Residue deposits present socioeconomic and environmental liability wherever they are: residue deposits are safety and health hazards. They contain many harmful elements such as Uranium (U), Arsenic (As) Radon (Ra), Nickle (Ni), Zinc (Zn), and many other radioactive materials. Human exposure to these elements leads to various acute or chronic illness, such as cell mutation, cancer, respiratory diseases and many more (McGasshan, 2004). Apart from health problems, they can also cause injuries and pollution, such as destruction of buildings during floods or heavy rains, pollution of groundwater and surface water (Manungufala *et al.,* 2005).

1.17 Geophysical Methods Applied to Contamination Studies

The application and limitations of the geophysical methods in environmental problems associated with groundwater contamination due to leachate movement exist. The use of various geophysical techniques for the investigation of groundwater contamination sites is a fairly recent development. The combination of more than one technique at a location is an integrated interpretation results in a reduction of the degree of ambiguity. The success of geophysical exploration technique depends on contrast in physical properties in the subsurface. The following geophysical technique can be successfully applied in contamination investigation because dissolved plume (leachate) can influence resistivity (ρ) or conductivity ($\boldsymbol{\sigma}$), chargeability (M) and magnetic susceptibility (k) (Osazuwa & Abdullahi, 2008). Mathias *et al.* (2017) has found that 2D resistivity is the most suitable geophysical methods for groundwater contamination.

1.18. Effect of Mining activities on the Physical Environment

The observable physical impact of gold mining activity on the land and environment in general ranges from land degradation, loss of vegetation, dust pollution, soil erosion and general reduction in agricultural practices which are shown in Plates I, II, III, and IV respectively.

1.18.1 Loss of vegetation

Mining activities is done by clearing of the site which causes deforestation. Vegetation are destroyed during the process of mining and extraction of minerals from the host rock thereby washing away and exposing fertile top soil Omanayin *et al.* (2016).

Plate I. Loss of vegetation in the processing portion of the area.

1.18.2 Dust pollution

The use of machines in the crushing, grinding and milling of crystalline rocks hosting gold deposits during processing can pollutes the air and affect human by inhaling the dust and in plant either by settling on the leave or through intake from the soil Omanayin *et al.* (2016). This could lead to serious health challenges such

respiratory tract infections (Plate II)

Plate II. Dust pollution arising from crushing and milling of host rock.

1.18.3 Land degradation

The activity of artisanal gold mining in Kataeregi and it environ have led to the destruction of natural landscape (Plate III). Heaps of rock waste and tailings were generated from trenches and series of pits created. This could be hidden place for reptiles and death trap to both human and animals

Plate III. Land destruction due to mining activity at Kataeregi

1.18.4 Soil erosion

The waste generated from the activity of artisanal gold mining in the area leaving large heaps of excavated soils from trenches and tailings generated during processing creates an artificial barrier for surface run-off Omanayin *et al.* (2016). This has led to the modification in the stream channels by disrupting the initial channel and creating new ones (Plate IV).

Plate IV. Development of erosion channel arising from mining activity

2.1 Review of Geological Literature of Nigeria

Generally, Nigeria is divided into two main geological terrains namely;

    i. The basement terrain which comprises of hard rocks, namely; igneous and metamorphic. They are Precambrian age.

    ii. Sedimentary basins in Nigeria out of which Dahomey basin and Niger delta are the most prominent. Others are Borno/Chad basin, Bida basin and Benue trough.

Nigeria lies approximately between latitudes 4° N and 15° N and Longitudes 3° E and 14° E, within the Pan African mobile belt in between the West African and Congo cratons (Figure 2.1). The Geology of Nigeria is dominated by crystalline and sedimentary rocks both occurring approximately in equal proportions (Adegoke & Ajayi, 1988). The crystalline rocks are made up of Precambrian basement complex and the Phanerozoic rocks which occur in the eastern region of the country and in the north central part of Nigeria. The basement complex outcrops in four major areas – North Central, South West as well as the South East (the Oban – Obudu Massifs) and North East (Adamawa Highlands). The complex consists of a wide variety of metamorphic and igneous rocks. Rahaman (1979) divided the basement complex of southwestern Nigeria into five major rock units:

    i. Migmatite – Gnesis – Quartzite complex which comprises biotite and biotite hornblende gneisses, quartzites, quartz schists and small lenses of calcsilicate rocks.

ii. Slightly migmatised to unmigmatised paraschicts and meta-igneous rocks which consists of pelitic schists, quartzite amphibolites, talcose rocks, metaconglomerates, marbles and calc-silicate rocks.

iii. Charnockitic rocks.

iv. Older granites, which comprises rocks varying in composition from granodiorites to true granites and potassic syenite.

v. Unmetamorphosed dolerite dyke believed to be the youngest.

These rocks are believed to be emplaced during the Pan-African Orogeny and are therefore thought to be of Pan-African in age (600±150 m.y.a) (Rahaman, 1988; Odeyemi, 1999).

2.1.1 Migmatite-gneiss-quartzite complex

This complex makes up by far the greatest of the basement complex, about 70%. It consists of high-grade metamorphic rocks, which comprise a variety of gneisses, migmatite, schists, quartz and marbles (Figure 2.1). The gneisses and migmatites are ubiquitous and are intimately mixed together that they are hardly separable on the field. The gneiss may be divided into two types; they are the biotite gneiss and the banded gneiss (Akinloye, 1983). The banded gneiss consist of alternating bands of dark (melanocratic) and light colored (leucocratic) portions with complex gradation between them. Both the quartzites and the marbles form relatively minor concordant layers within the gneiss- migmatite units, although the former being resistant to erosion, commonly features as prominent ridges. The migmatite-gneiss-quartzite complex constitutes the basement into which other crystalline rocks are emplaced. It is invariably, a heterogeneous rock group covering about twenty one states of the federation. The age these rocks is assumed to be 1850 million years (Kelvin, 2005)

2.1.2 Schist belts

These are essentially N-S trending narrow linear zones of low to medium grade metamorphosed supra-crustal (cover) rocks, also called the "younger metasediments" (Figure 2.1). These rocks are host to important mineral deposits, which include Gold, Iron Ore, Talc, Marble, Manganese and Magnesite. They are derived from an ancient (probably Paleoproterozoic, about 2 billion years old) sedimentary and igneous series which were deposited on the pre-existing migmatite-gneiss- quartzite basement. The bulk schist belt is located in the western half of the country, that is, Osun, Oyo, Ogun, Kebbi, Edo, Ondo, Katsina, Kaduna, Niger, Kwara, Kogi and Zamfara States.

2.1.3 Charnockite

This is a coarse-grained granular rock consisting of quartz, feldspar and hypersthene plus other Minerals. The minerals are characteristically fresh, un-decomposed and lacking in inclusions. Some Charnockite may result from crystallisation of magma at great depth under extreme pressure. Others are thought to have arisen by ultrametamorphism of basic igneous rock. The Nigerian Charnockites are different from those of other parts of the world in that they belong to Amphibolite facies rather than the Granulite facies in which Charnockites from other parts of the world are invariably associated. The more facts that the Nigerian Charnockites contain ortho - pyroxenes with dark blue to dark green feldspars would have tempted one to lace them into granulite facies of metamorphism, but then one find them associated with granitic rocks and migmatite gneisses and the pressure to temperature conditions of the Nigerian Basement Complex are indicative of an indisputable amphibolites facies of metamorphism. The Nigerian Charnockites also do not contain garnets.

2.1.4   The pan African granites (older granites)

Large volumes of Pan African granites known as the "Older Granites" in Nigeria intruded all the Pre-existing rocks including the migmatite-gneiss-quartzite complex and the schist belts during the late Proterozoic to early Paleozoic (600 ± 150 million years) rejuvenation of the older crust (i.e. the Pan African Orogeny) (Figure 2.1). Associated with older granites in some places are syenites and bluish-green/green rocks called "Charnockites". Those two rock-types especially the charnockites, occur in many localities in the western and north-central parts of the country. Several types of older granites recognized include: migmatite; granitic gneiss or granite, undeformed pegmatites and quartz vein. The available geochronological data on the older granite show that age on the older granite range from 667 to 518 million years (Odeyemi, 1999).

2.1.5 Younger granites

The younger granites consist of a suite of migmatite rocks that consists essentially of high-level granite intrusions and their volcanic and hypabyssal equivalents, mainly rhyolites and granite porphyries (Figure 2.1). Minor intermediate and basic rocks, which include syenites, trachytes, gabbro's, microgabbro and dolerites are associated with granite bodies. The granite plutons were emplaced in Jurassic (about 160 million years ago) and are called "younger granites" to distinguish them from the older Pan African granites of the Precambrian basement complex which are therefore described as "Older Granites". Three major types of granites have been recognized in the Younger Granite Province on the basis of dominant mafic mineral content. There are; Biotite Granites, Hornblende-Pyroxene-Fayalite granites and Riebeckite Granite.

The granites and other associated rocks occur in form of separate bodies or complexes, which transgress all units of the Basement complex in the North-central part of Nigeria.

2.1.6 Minor felsic and mafic intrusive

These rocks are made up of concordant and discordant dykes, veins and irregular bodies of Pegmatites, aplites, quartz, dolerite, lamprophye, gabbro, pyroxenite and serpentinite. They intruded in places of all the pre-existing rocks of the basement complex. Most of them are considered have been formed during the warming stages of the Pan African Orogeny and are thus the youngest member of the Nigerian Basement complex. Pegmatites which belong to this group is the host rock for the famous Nigerian tourmaline and beryl gemstones in addition to fayalite, columbite and cassiterite (tin ore). Others of less economic importance include Feldspar and micas which commonly include muscovite and lepidolite (Li-bearing mica).
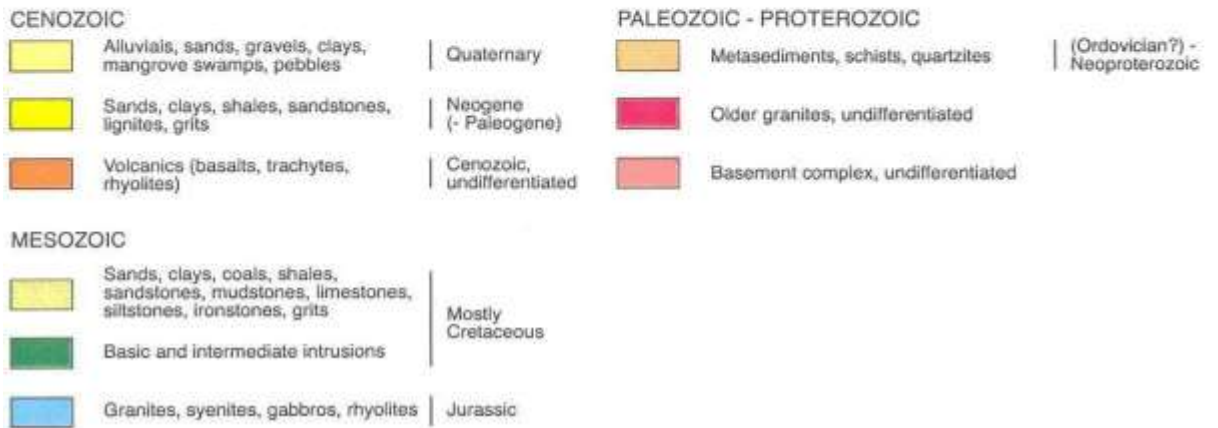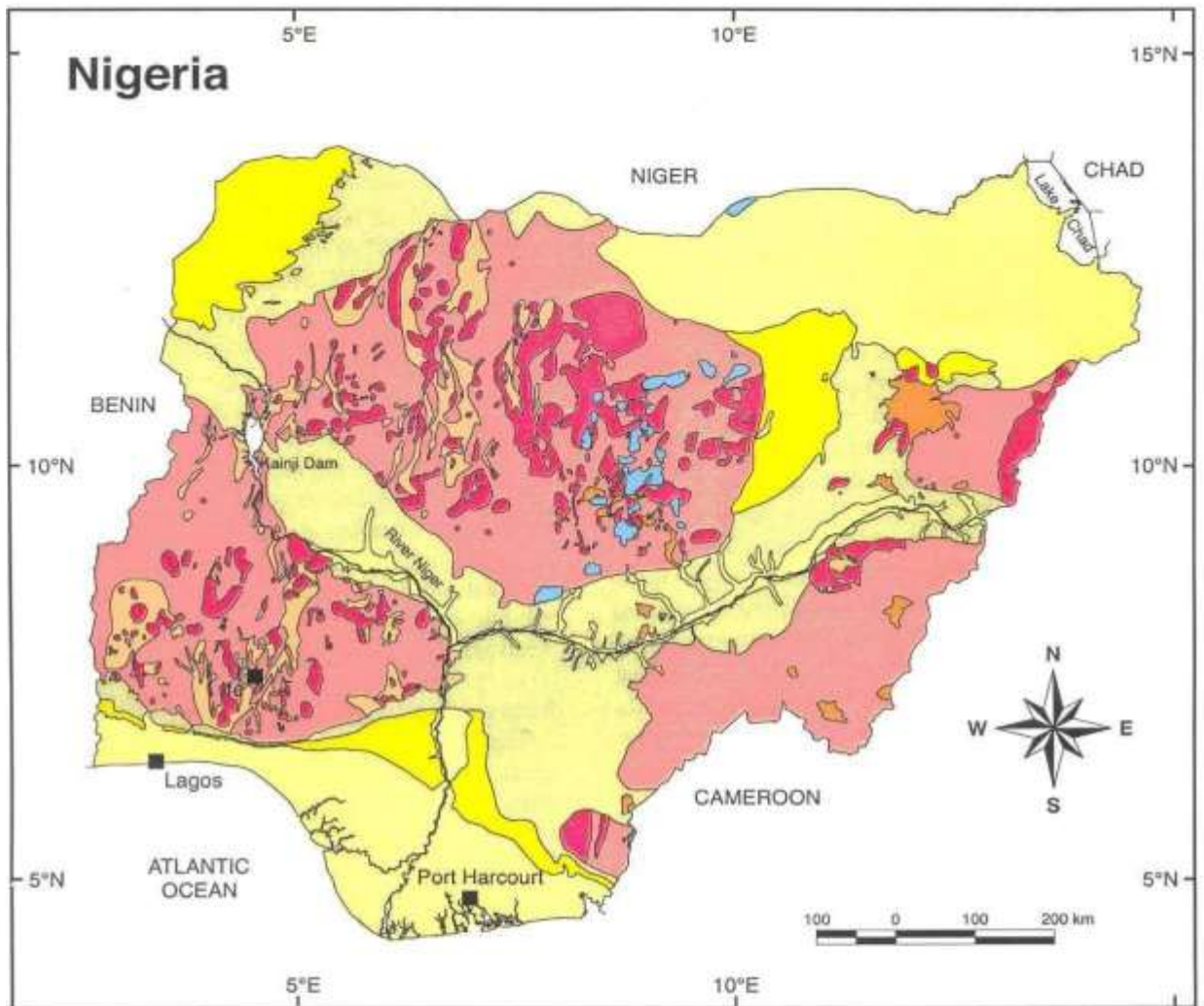
Figure 2.1: Geologic map of Nigeria (Rahaman 1979)

2.2 Review of Geological Literatures of Niger State

Mccurry (1976) described the rock in Minna and named them as older granites, schist and migmatite gneiss complex. The granitites includes rocks varying in composition from granite to tonalite with smaller bodies of syenite (Trustwell & Cope, 1963) recognised three formations around the area: the first is the kusheriki formation at the base of the successions made up of rock of varying lithology structures and texture which show different degree of textures, granitisation and migmatisation. They noticed the impressive parallel structures and traditional contacts within and between metamorphic units and older granite. About half of the landmass of Niger State is underlain by the Basement Complex rocks while the remaining half is occupied by the Cretaceous Sedimentary rocks of the Bida Basin. It lies within the north-central portion of the Nigerian Basement complex rock which is characterized by three lithofacies: the migmatite-gneiss complex, the low grade schist belt and the older granites (Olarewaju *et al*., 1996; Olasehinde, 1999). The geological mapping revealed that the area is underlain by granite and gneiss which in most locations are undifferentiated granite gneiss-complex.

The rocks are found in East-west (E-W) trending vain and joints, which are at times filled by aplites or quartz. The rocks are also broken into builders and show the effect of weathering in form of colour change and loose rock fragment (Ajibade *et al*., 1976). They further described magmatite along the Minna-Kwakuti and Gwada road to have formed as a result of magmatic injection into low-grade schist. There are two types of generation of magmatite – the one formed earlier during eburnean and the Pan-Africa magmatite which are formed by magmatic injection into low-grade schist during the emplacement of the pan-africa granites (Ajibade *et al*., 1976).

The schist belts area occur as two elongated bodies separated by the older granite suite (Figure 2.2). The tips of the two formations are separated by a 40 km expanse of the older granite suite (Ajibade *et al*., 2008). However this study indicates a much smaller separation of less than 10 km. The Birnin-Gwari formation lies to the west of the older granite (the Minna Batholith) while the Kushaka formation lies to the East. A gravity survey model conducted over the area showed that the two formations have a maximum thickness of 11 and 6 km respectively.

The sedimentary formations belong to the Bida Basin of deposition, the Bida Basin otherwise known as the mid-Niger Basin or the Nupe Basin is a NW–SE trending intracratonic sedimentary basin extending from Kontagora in Niger State to areas slightly beyond Lokoja in the south (Figure 2.2). Its total length is estimated at 400 km with a maximum width of about 160 km which tapers to less than 60 km at Dekina. The largest portion of the basin (the northern part), occurs in the southern half of Niger State (Idris-Nda *et al*., 2015).
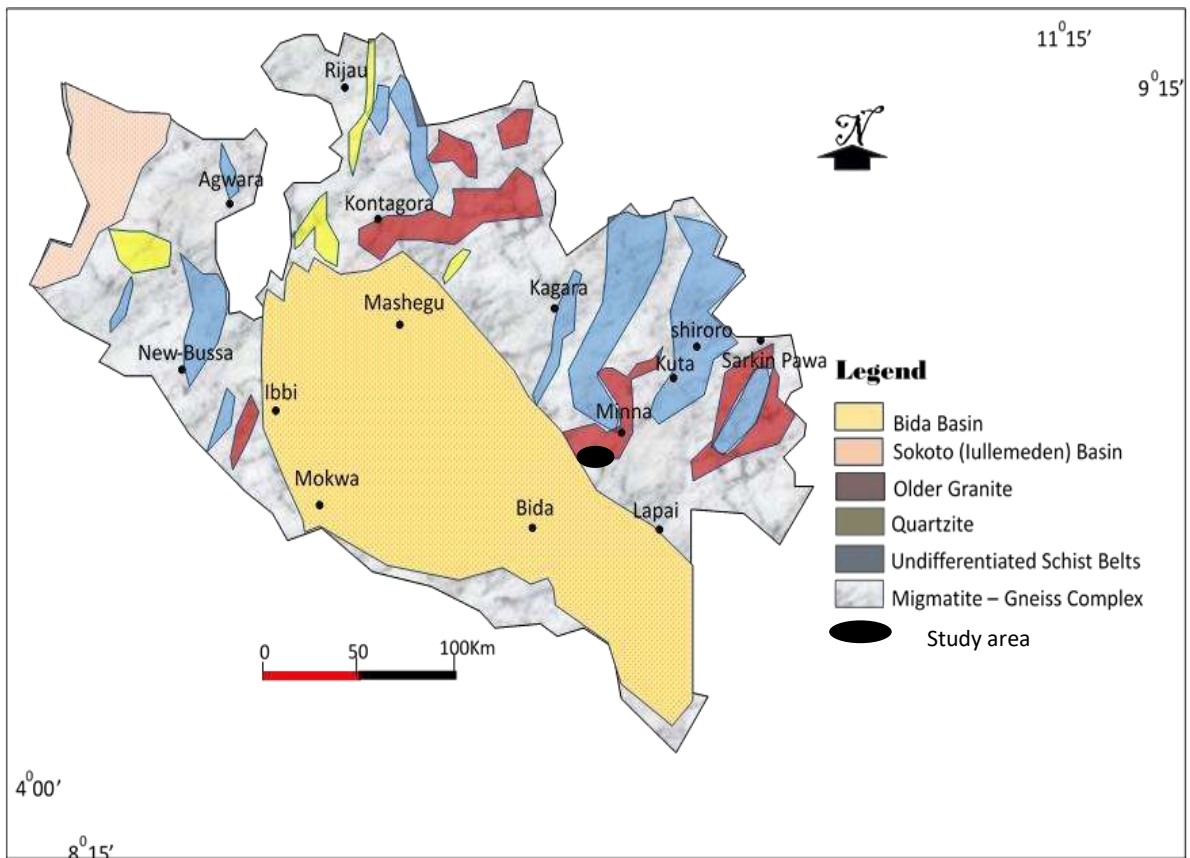
Figure 2.2: Geological map of Niger State showing the study area (Idris-Nda *et al*., 2018)

2.3 Hydrogeology of the Basement Complex Terrain

Study of groundwater with reference to geologic environment is known as hydrogeology. Generally, locating sites for well or borehole in area underlain by basement complex rocks is a difficult task (Rahaman, 1988). The extreme variation in lithology and structure coupled with highly localised water producing zones make geological, hydro geophysical exploration for groundwater difficult. Among the factors which are considered for well location in basement complex areas include high topographical features where it is related to high bedrock relief (e.g. ridges). This is important factor for wells located on hill tops and valley sides, because bedrock ridges' crest (when present) acts as radiating center for ground water as water normally drain along steep

slopes and hill tops to pint of discharge in adjacent lowlands (Olorunfemi & Olayinka, 1992). In crystalline rocks, weathered, partially weathered, fractured zones form aquifers. The nature and extent of weathering varies and depends mostly on the presence of fractures at depth and favorable morphological features at the surface. In metamorphic terrains, fault breccias are useful guides for location of well sites. Ideal conditions for groundwater aquifers exists when such features like reef cut across a narrow part of a valley with good recharge area, but hornblende gneiss and metabasic dykes acts as barriers for groundwater flow.

However, in weathered rocks, both intergranular and fracture porosities exist. The clay content in the weathered portion, reduce the permeability to some extent. In hard rock area, the weathered and fracture aquifers are capable of yielding sufficient quantities of water to meet the needs of a small community or village. In the area underlain by crystalline rocks, groundwater is stored in the buried stream channel and the weathered layer, joints and fractures. The groundwater is good unless it is polluted through human, industrial and agricultural act ivities. In the study area, the groundwater is primarily recharged by rainfall and small amount form lateral groundwater flow and from river channel where possible.

The basement complex rocks are crystalline rocks of low porosity and permeability. In this geologic environment, groundwater accumulation depends on the following;

   i. The degree of weathering and thickness of overburden ii. The degree and nature of fracturing of the rocks iii. The presence and absence of clays above the weathered zone and its

        effect on rate of infiltration of water into the aquifer.

   iv.   The hydrological continuity (permeability) of the weathered zone.

v. Sources of recharge in the area include river, stream, precipitation Cracks, fractures bedrocks depression, graben and weather basement are the geologic structure basement terrain that favour groundwater accumulation, various types of aquifer include unconfined, confined, leak, perched and idealised aquifers, while porosity, permeability and transmisivity are the parameters of an aquifer.

2.4 Geology of the study area

The area consists of mixed geology of both basement and sedimentary rocks. The rocks units consist of schists, migmatites, gneisses, granites, quartzite of Precambrian age (> 550 million years old) (Idris-Nda *et al*., 2018). The area is dominated by schistose rocks that serves as host to auriferous quartz vein where the mining is taking place (Figure 2.3). The schists are intercalated with amphibolites observable along the

River Chanchaga, the schists had already been mapped and considered as part of the Kusharki Schists. The schists are intruded by plutonic rock and exposed at sabon Eregi and Kataeregi with xenoliths of phyllites. The study area is dominated by migmatitesgneisses complex and granites at the North and South-eastern parts and Bida sandstone to the extreme South-western part (Omanayin *et al.,* 2016). The sedimentary terrain falls within the Bida Basin of central Nigeria and covers the central and southern part of the state. The rocks of the basin comprise of conglomerates, sandstones, siltstones, mudstones and ironstones (Idris-Nda *et al*.,

2018).
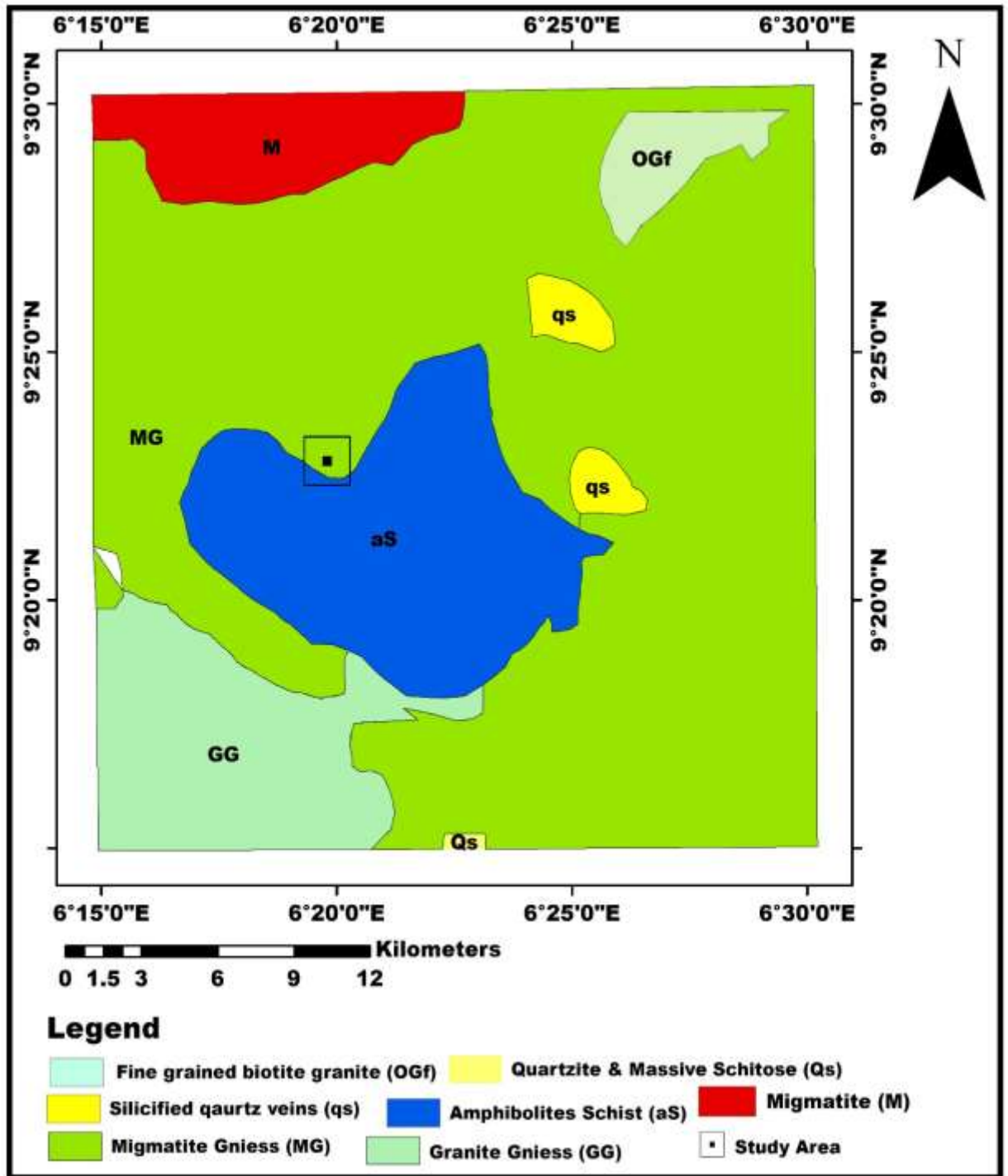
Figure 2.3: Geological map of the study area

2.5 Review of Geophysical and Geochemical Literatures

Researchers have carried out a lot of study over the waste dumpsites, waste residue/slims

and landfills employing electrical resistivity, seismic and geochemical methods. The

results indicate the ability of the methods to detect variation in fluid content and chemical composition.

Adebiyi *et al.* (2021) uses structural interpretation of magnetic and satellite remotely sensed data of Osun State, Southwestern, Nigeria The magnetic lineament map reveals that the structural trend in the area is dominant by NE-SW and NNE-SSW. These structural trends were found to be consistent with the regional tectonics of the Southwest Basement of Nigeria. The NE-SW is the most conspicuous structural trend in the study area.

Tawey *et al. (*2020*)* utilises application of aeromagnetic data to assess the structures and solid mineral potentials in part of north central Nigeria. The result indicates that lineaments mapped trending in the ENE-WSW followed by WNW-ESE with some NESW, NNE-SSW and NNW-SSE trends. The second vertical derivative (SVD) map also helped in delineating structures and possible mineralization zones that are pronounced within the study area, around high analytic signal zones. Delineated possible and favorable mineralisation zones from second vertical derivative map correlate with portion of the study area with rocks showing high analytic signal amplitude suggesting the rocks to be of later magmatic intrusions where mineralisation fluids solidify within the host rocks.

Ibrahim *et al.* (2019): applied induced polarisation and resistivity to the determination of the location of metalliferous veins in the Taroucht and Tabesbaste Areas (Eastern Anti-Atlas, Morocco), in order to obtain a better recognition of the different structural contacts and to define the alignment of mineralized veins in barite and galena at the level of the study area, we used the technique of electrical tomography. The resulting response,

in the form of electrical imaging, informed us in detail about the different zones of heterogeneity existing in the prospected soil. In induced polarisation, the pseudosections obtained were able to locate the passages of the zones of anomalies encountered and thus confirm their alignments defined by the electrical resistivity measurement results

Seidu & Ewusi (2018) conducted a research to assess the groundwater quality using hydro-geochemical indices and statistical analysis in a mining area at Tarkwa, Ghana. According to the results of the analysis there are two main hydrogeochemical facies which are: Ca^{2+}-Mg^{2+}-Cl^- SO_4^{2-} and Ca^{2+}-$Mg^{2+-HCO3}$, these two constitute 92 % of the total samples. The two most dominant water types in the area are CaHCO3 and Mixed CaMgCl type, which gives an indication that fresh water types are available in the area. It is observed from the Gibbs plot that 72 % of the samples are controlled by rock weathering and 28 % are controlled by precipitation.

Yusuf *et al*. (2018a) assessed the spatial patterns in soil properties at Mokwa which strongly influence high crop yields using electrical resistivity method. Three geologic features (claystone, sandstones and conglomerated) were identified at various locations among others like; weathered basement, fresh basement, fractured and aquifer zones. Areas with low resistivity in soil properties were considered as bleached claystone grains and sandstone with relatively high humus content and cation exchange capacity with their picks at a point. This was due to high level of water content which strongly influences the crop yields. This method has proved to be suitable for soil and water investigations

Yusuf *et al*. (2018b) conducted a research aimed at investigating the groundwater quality and soil cultivation viability using resistivity and geochemical approach at Mokwa. The

result from geo-electrical imaging method revealed that leachate migration into subsurface as well as ingress into the surrounding soils and groundwater up to the depth of 20 m. Physiochemical analysis was also used to support the earlier assertion, fractured zone was revealed to be the weakest zone as a result of leachate migration. VES data revealed the shallowest water table of about 7 m, indicating that the groundwater was already contaminated by leachate invasion.

Ejepu *et al*. (2018) used integrated geosciences prospecting for gold mineralization in Kwakuti, North-Central Nigeria, it was observed that schist occupies moderate to low elevation areas and they display high magnetic field intensity values. The migmatites are dotted with quartz veins which constitute the gold mineralisation zone. Gold concentration distribution pattern in the area is skewed NE-SW, thereby suggesting that the NE-SE structures control the mineralization. Mining activities will be more efficient if directed along the NE-SW structurally trend.

Idris-Nda *et al.* (2018) looked at the Socio-Economic Impacts of Artisanal and SmallScale Mining in Parts of Niger State, Central Nigeria. The activities of artisanal miners result in many devastating impacts on the environment which includes land degradation, pollution of soil and water, erosion, desertification and waste disposal. The most obvious to any casual observer is the land degradation created by open mine pits. However, the most serious impact, which affects the health of the population results from contamination of soils, surface water bodies and crops are the Potentially Toxic Elements (PTEs) such as lead, copper, zinc, together with arsenic which has posed serious challenges to the health of the populace. Mitigation Strategies involves Disaster Risk Reduction strategies in solid minerals mining in the state which will involve revisiting

the current practices towards improving operations in this potential revenue generating sector.

Olomo *et al.* (2018) applied integrated approach involving aeromagnetic and land sat for delineating structures and its implication on mineralisation Enhancement of the magnetic anomalies observed from the interpreted magnetic anomaly map involved the use of reduction to equator, wavelength, upward continuation and derivative filters. The 3-D Euler deconvolution and radial spectral analysis were applied to locate and estimate the depth to various anomalous bodies, with depth to source body between 50 m and 500 m. The processed images revealed lineaments trending majorly in NE-SW directions diagnostic of primary structures of potential targets for mineralisation in the area. Generally, coincidence of both Landsat and aeromagnetic lineaments trends were observed in the study area, which suggested that these lineaments reflect real continuous fault/fractures in depth

Eugeniusz *et al*. (2017) used electrical resistivity data sets for the evaluation of the pollution concentration level within landfill ground water monitoring at Warsaw, Poland, the results revealed that the base was not leakage-free. Another two landfills were established in the past, when no containment systems were legally required. The geoelectrical investigation was the final part of an overall analytical assessment of the contaminated sites. The study was aimed at pollution spatial migration analyses and the interpretation of results, for further design of the reclamation and restoration plans.

Nataliya *et al.* (2017) applied electrical resistivity tomography to trace the geoelectric zoning of the waste samples at Kemerovo, Russia. The zones of increased conductivity in oxidized mine tailings indicated local areas with high acid production potential and

coexisting acidic pore solution. In non-oxidized tailings, high conductivity of the mineral skeleton was observed. There was a migration of drainage outside the tailings, its direction monitored by geophysical data. Chemical analysis confirmed that the concentrations of chemical in groundwater samples were higher than the maximum permissible concentration.

Oyeyemi *et al.* (2017) used geoelectrical and geotechnical investigations for subsoil characterisation, at Ota, Ogun State, Nigeria, two ERT lines were conducted for 2D geoelectrical resistivity measurements using wenner array configuration in combination with four cone penetration data, two geoelectrical layers were interpreted to be loose silty and compacted clayey sand lithological units with resistivity values ranging from 50 - 280 Ωm and 10 - 74 Ωm respectively. A water saturated portion with resistivity values ≤ 3 Ωm due to lagoon – water incursion was equally observed at the base of the second clayey sand layer ERT line T_2.

Saad *et al.* (2017) used 2D resistivity imaging and seismic refraction tomography to identify sediment depositional origin at Sungai Batu, Malaysia. A region with low resistivity value of 10 – 50 Ωm indicated the presence of saturated alluvium (sand and clay) which are transported from land and the moist zone was identified with resistivity < 100 Ωm. The resistivity value > 300 Ωm indicated a river bed. The seismic revealed the river bed with velocity of > 3600 m/s at a depth > 10 m while velocity value of < 1400 m/s show as moist/saturated alluvium zone which consist of clay and sand.

Zielke & Vermeulen (2017) utilised geophysics as a delineation tool for groundwater flow paths and contaminants along a graben at Lappeenranta, Finland, geophysical modelling indicated zones of elevated conductivity associated with fault planes, tailings

dams, discard dumps and quarries. Additionally, groundwater chemistry obtained at high conductivity zones suggested seepage into both the shallow weathered aquifer and the deeper fractured aquifer underlying the study area. The study demonstrated that applied geophysics in combination with geo-hydrological data is a useful tool for detecting contaminant groundwater flow paths.

Ganiyu *et al*. (2016) investigated groundwater contamination due to leachate migration in a solid waste disposal site at Ibadan Southwest, Nigeria using geophysical and hydrochemical methods. The inverse resistivity models of the subsurface from 2D and 3D imaging revealed low resistivity values less than 10 Ωm suspected to be leachate, the extent of migration was more pronounced in the southern part of the dump site, the physio-chemical analyses of groundwater samples was found to be within the limits of WHO/NSDWQ for drinking purpose. Generally the groundwater in the area is of hard, fresh and alkaline in nature.

Benson *et al.* (2016) trace metal contamination characteristics and health risks assessment of *Commelina africana* L. and Psammitic Sandflats in the Niger

Delta, Nigeria the average carcinogenic risks are below 1.0×10^{-6} threshold values, and the sandflat soils are not considered to pose significant health effects to children and adult males and females. The concentrations varied with the sample locations; and the levels of Pb (0.05 to 0.08 mg/kg) at all locations are found to be significantly below permissible level of 0.3 mg/kg.

Andres *et al.* (2016) used electrical resistivity tomography and Induced Polarisation for Mapping the Subsurface of Alluvial Fans: A Case Study in Punata (Bolivia), This research attempts to use geoelectrical methods, for mapping the subsurface in alluvial

fans and to demonstrate its applicability; the Punata alluvial fan was used as a case study. The resistivity measurements proved to be a good tool for mapping the subsurface in the fan, especially when used in combination with induced polarisation parameters (i.e., Normalised Chargeability). The Punata alluvial fan characterisation indicated that the top part of the subsurface is composed of boulders in a matrix of finer particles and that the grain size decreases with depth; the electrical resistivity of these deposits ranged from 200 to 1000 Ωm, while the values of normalised chargeability were lower than 0.05 mS/m.

Brempong *et al.* (2016) uses magnetic susceptibility measurements to determine pollution of agricultural soils in road proximity. The results showed three most important trends: 1) the samples collected near the road have higher values of magnetic susceptibility and mean heavy metals content than those collected far from the road exhaust; 2) some of the sample areas undisturbed by erosion and weathering have significant magnetic susceptibility and heavy metals contents; 3) some of the sample areas washed away by erosion are believed to be deposited in Owabi Dam due to their low ground reliefs. Therefore, future research should concentrate on Owabi Dam which may be polluted by the runoff from these heavy metals.

Omanayin *et al.* (2016) investigated Water quality within the neighbourhood of Kataeregi artisanal gold mining sites, North-Central Nigeria. Water samples were analysed for domestic and agricultural purposes, the concentration Fe and Pb far exceed World Health Organisation (WHO) and Nigerian Standard for Drinking Water Quality (NSDWQ) prescribed limits for irrigation, portability and other domestic purposes.

Adebayo *et al.* (2015) carried out studies at Ede town, southwestern Nigeria to delineate contamination plumes at olubonku dump site using geophysical and geochemical approach, with the view to assess the degree and extent of impact of waste dump site on the quality of the groundwater. The VES delineated three subsurface layers, the soil sampled indicated chemical concentration of K, Ca, Mn, Zn, Ni, Cu, Cr and Fe while the water analysed showed increase in concentration of nitrate exceeding WHO limit.

Ameloko & Ojigbo (2015) applied 2D surface resistivity survey around two power houses in Covenant University Ota, Ogun State, Nigeria to investigate the possible spread within the subsurface, of disposed used hydrocarbon products. The study delineated three subsurface geoelectric layers with resistivity values ranging from 57 Ωm to 1258 Ωm on all the profiles. The high resistivity values 800 Ωm – 1258 Ωm on traverse 1 near the power house behind College of Science and Technology (CST) building may be as a result of the contamination arising from the disposed hydrocarbon products.

Dimitri *et al.* (2015) used integration of geophysical methods in the diagnostic of a diesel contaminated site in Santa Ernestina (Sp, Brazil). The results indicated the punctual occurrence of shallow zones of low resistivity close to the place of contaminants infiltration, associated to the action of natural attenuation processes. The model presented zones of high chargeability associated to the probable presence of metallic minerals formed during and after the action of biodegradation processes. The results set pointed to a general scenario of an advanced stage of decontamination in the area, with effective natural attenuation processes

Ganiyu *et al.* (2015) delineate leachate plume migration using electrical resistivity imaging, the method was successful in mapping at Ibadan Southwest, Nigeria, and the

contaminant leachate plume and to characterise the dumpsite in terms of subsurface resistivity distribution of leachate, waste material and soil condition beneath the dumpsite. The result also indicated that the western part of the dumpsite has the possibility of been contaminating the shallow groundwater. The horizontal and vertical extent were also delineated.

Ezugwu (2015) examines the contaminants, their sources to groundwater and the potential health effects.The results shows that the water may be contaminated. It is recommended that groundwater be monitored periodically and treated before use, if pollutant are found to exist above tolerable levels to ensure that it is fit for its intended purpose.

Moghaddam *et al*. (2015) time-lapse electrical resistivity tomography (ERT) surveys were conducted along 7 longitudinal lines in the downstream of the Latian dam in Jajrood (Iran), in order to detect the contamination resulting from the direct injection of a saltwater solution in to the saturated zone in the area. To investigate the pollutant quantities affecting the resistivity of this zone, the temperature and electrical conductivity measurement were carried out using a self-recording device during 20 days (before and after the injection). The results obtained from the self- recording device measurements and ERT surveys indicated that in addition to the salt concentration changes in water, the resistivity changes in the saturated zone were dependent on other factors such as the lithology and absorption of contaminants by the subsurface layers.

Tamma Rao *et al.* (2014): used electrical resistivity tomography methods for delineation of groundwater contamination and potential zones, two main applications of electrical resistivity tomography (ERT) methods have been addressed covering characterisation of

leachate movement from a composting area of a Sugar Mill in Southern India. Good correlation has been obtained between ERT and groundwater quality assessments as well as from groundwater monitoring data sets. The study helped in conceptualization of hydro geologic framework in basaltic

terrain.

Umar *et al.* (2014) used electrical resistivity techniques and chemical analysis in the study of leachate at Sungai Sedi, to investigate the pattern of leachate pollutant in soil at landfill site and groundwater below the dumping area. The maximum leachate infiltration was estimated at 4-6 m depth vertically, resistivity values were observed to be ranging from 1-10 Ωm representing the most contaminated zones while the chemical analysis indicates the presence of heavy metals in soils and water in and around the waste disposal site.

Bayode & Adeniyi (2014) a review Integrated geophysical and hydrochemical investigation of pollution were employed at Ilara-Mokin Southwestern, Nigeria. The results indicates of both poorly conductive bodies and leachate saturated near subsurface soil. The geoelectric section delineated four subsurface layers: top soil, weathered layer, weathered/fractured layer which are considered as the aquifer unit and the fresh basement bed rock. The relatively low resistivity of 6 – 50 ohm-m suggested that the area around the dump site has been impacted and the 2-D images shows that the leachate depth of migration varies from about 2.5 – 7.5 m along the traverse. The hydrochemical parameters from the collected samples generally indicate that the values are within the WHO (2004) limit.

David *et al.* (2014) applied geoelectrical method for investigating mine dumps at Reno Nevada, the results reflect lithology, pore water saturation and dissolved solid in pore water. If the pore water has a pH less less than 5, conductivity maps can indicate acid generating potential. Most mine dump material is electrically conducive relative to host materials forming dump edges and bottoms.

Salehi *et al.* (2013) used Relationship between Magnetic Susceptibility and Heavy Metals Concentration in Polluted Soils of Lenjanat Region, Isfahan. Geochemical analysis of soil samples showed close correlation between Cd, Ni and Fe. Cd concentration was the highest of all the elements studied. The correlation between the analyzed metals and magnetic susceptibility are positive and significant for Fe and Cu. Results suggests that magnetic susceptibility can be used as a guideline to find contaminated urban areas with Fe and Cu in this region.

Adelusi *et al.* (2013) mapped out groundwater contamination using geophysical and hydrochemistry method, wenner profiling, VLF EM, VES and water quality analysis were integrated at Aule area, Akure, there exist good correlation between the geophysical and hydrochemical methods due to the hydrocarbon contamination in some wells. The hydrocarbon from the nearby filling station and suspected impacted zones are characterised by relatively high resistivity (> 200 Ωm) and low conductivity responses. There has been the movement of the hydrocarbon contamination plume down to depths of about 9.26 m horizontally and vertically.

Jolanta (2013) investigated soil contamination using resistivity and induced polarization methods Bukow, southern Poland, the results of induced polarisation allowed some of the contaminated zones to be unambiguously identified. The results obtained also show

that the post mining waste and hydrotechnical objects built on them influence the underground water, and areas of contamination can be identified successfully by the combination of resistivity and induced polarization imaging, even in the complex lithological structure.

Sayed *et al.* (2012) usesd seismic refraction and resistivity imaging for assessment of groundwater seepage under a dam site at Southwest Saudi Arabia. Four distinctive layers were identified includes: topmost unconsolidated layer, alluvium that is underlain by saturated alluvium sediment, the third layer is fractured basement and followed by hard massive bedrock with relatively high velocity. These indicated that the site is affected by faulting that resulted in depressions, these depressions are considered zones of permeability and represent a favourable pathway for groundwater flow. The resistivity imaging also confirmed that where low resistivity exist with thickness up to 22 m and a layer of alluvial sediment saturated with groundwater, may indicate possible seepage flow.

Orisakwe *et al.* (2012) assessed heavy metals health risk assessment for population via consumption of food crops and fruits in owerri, south eastern, Nigeria, the results shows the concentration of Pb, Cd, and Ni in Ohaji exceeded the maximum allowable concentrations for agricultural soil as recommended by EU.

Rolland & Karunakar (2011) geophysical prospecting as a tool for site characterisation for mining dump site has been considered in India. It was concluded that surface geophysical techniques like ERT (2D resistivity tomography), ground magnetic and borehole seismic studies can be integrated with each other as an ideal tool in mapping the geophysical characteristics of subsurface formations in and around the disposal site.

Raymond & Felix (2011) investigate heavy metals in contaminated soils: a review of sources, chemistry, risks and best available strategies for remediation. Remediation of heavy metal contaminated soils is necessary to reduce the associated risks, make the land resources available for agricultural production, enhance food security and scale down land tenure problems arising from changes in the land use pattern.

Mücella-Canbay (2010) Investigate the relation between heavy metal contamination of soil and its magnetic susceptibility. The value of magnetic susceptibility is observed to vary between 12.10-5 and 84.10-5 SI in the upper layers of the soil samples in on-site measurements. On the other hand, the mass-specific magnetic susceptibility of the samples changes between 2.10-5 and 202.10-5 SI in the laboratory measurements. The geochemical analysis is carried out and the heavy metal content consisting of Pb, Cu, Zn, Co, Cd and Ni is determined using the atomic absorption spectrometry method. Additionally, the correlation coefficient is determined from the comparison of magnetic susceptibility with the heavy metal concentrations.

Alex & Olyphant (2010) mapped out the variability of groundwater quality in an abandoned tailings deposit at Southern Indiana, USA using electromagnetic Geophysical Techniques, a correlation was observed between subsurface hydraulic conductivity and terrain conductivity measurements (R^2=0.66) indicating an instrument response to soil permeability. The study indicates that shallow electrical geophysical exploration can be used to locate groundwater contamination plumes when subsurface hydraulic properties are taken into account.

Alabi *et al.* (2010) interprete induced polarisation for subsurface characterisation to evaluate the potential of the method when structural properties of the subsurface are required. It addresses one of the potential near-surface applications of the IP method, namely lithological characterization. The study shows that IP imaging is a promising tool for mapping lithological contrasts in unconsolidated sediments and to clarify difficulties in lithological interpretation observed in other geophysical methods. The profiles obtained in the study area depicted two layers; the first layer with consistent and considerable high chargeability signatures at depth of 20 m indicates sand formation. The second layer predicted to be clay with low IP effects was observed at various depths for all the profiles.

Alexandros *et al*. (2010) an environmental impacts of unmanaged solid waste at a former metal mining and ore processing site was conducted at Kirki, Greece, the potential impacts are the contamination of surface water, soil and groundwater, the definition of pathways conceptual models, and the design of a monitoring network were significantly easier and more efficient due to the availability of field methods. This strategy does not replace, but improve, the traditional approach with laboratory analyses, and it helped to keep cost under control.

Olubunmi & Olanipekun (2010) evaluate the Status of Heavy Metal Pollution of Sediment of AgbabuSS Bitumen Deposit Area, Nigeria. From the analysis of variance with Statistical Analysis System (SAS), the mean concentration of metals in sediment in the two seasons (α level=0.05) are not significantly different which implied that the metals were held firmly in the matrix of sediment.

Ramalho *et al.* (2009) used geophysical methods to characterize an abandoned uranium mining site, Portugal, 2D schematic models have been constructed, showing alteration and faults zones at depth. These fault zones control groundwater circulation and therefore, future water circulation problems with negative environmental impact may be predicted and prevented.

Ugwu & Nwosu (2009) examines the effect of waste dumps on groundwater in Choba using geophysical method, the result of the survey interpreted by IPI2WIN and offix software's show two characteristic curve types: type A curve at the dumpsite and type H curve away from the dumpsite, the other result further indicates that the first two layers at the dumpsite has resistivity 59.91 and 20.10 ohms meter respectively, on the other hand the result shows that groundwater at the dumpsite is polluted because of the high conductivity. This was confirm by laboratory analysis from the study area.

Cabala *et al.* (2008) used geochemical and geophysical to study the historical Zn – Pb ore processing waste dump areas in southern Poland, the mineral composition of wastes was identified using XRD method, the results distinctly showed high concentration of metals, thereby posing great danger to the occupant of the area. Remediation method was suggested because environmental issues cannot be resolved quickly.

Umar *et al.* (2008) applied geophysical techniques in the study of hydrocarboncontaminated soil at Sungai Kandis, Klang, Malaysia, the vertical resistivity probe (VRP) results show high apparent resistivity values ranging from 200 to 10000 Ωm associated with oil contaminated layer. The presence of this layer was also detected in the 2D resistivity sections as a thin band of high resistivity values ranging from 60 to

200 Ωm. In the GPR section, the oil contaminated layer exhibits discontinuous, subparallel and chaotic high amplitude reflection patterns.

Osazuwa & Abdullahi (2008) review various geophysical techniques that can be used successfully in areas with moderately complex geology (i.e. contamination plumes). Information gained from geophysical survey can be used to choose optimal locations for placement of boreholes, subsurface sampling and remediation.

Salisbury & Snyders (2007) utilises Application of Seismic Methods to Mineral Exploration in Canada, 2D and 3D surveys have successfully detected and imaged large massive sulphide deposits such as the magmatic and volcanic massive sulphide (VMS) deposits in Sudbury and Bathurst and should also be useful for detection of massive sedimentary exhalative (SEDEX) and iron oxide copper gold (IOCG) deposits.

Manungufala *et al.* (2005) investigate the slimes dams mine dumps and landfills (residue deposits) as environmental constraints to low cost housing projects in Gauteng, South Africa to examine the potential health hazards associated with residue deposits and possible rehabilitation or mitigation measures, prescribed such as revegetation rock cladding of tailings dams and environmental legislation.

Shitivelman (2003) employed shallow seismic methods to engineering, environmental and groundwater investigation Lod, Israel, and observed that the method can be an effective tool for studying the shallow subsurface for various application, the information on shear wave velocity distribution in the shallow subsurface, obtained from shear wave surveys, can make investigation problems related to site evaluation for seismic risk assessment.

Alvin *et al.* (1997) Mapped out groundwater contamination using dc resistivity and very low frequency (VLF) geophysical methods at Utah Country, Utah, the electrical resistivity and VLF data correlate well, and vertical cross-sections and contour maps generated from the data helped in mapping the contaminant plume, which was delineated as an area of high interpreted resistivities.

In view of the reviewed previous works in the study area (and its environs) and the methods, the present study utilises both electrical resistivity (electrical resistivity tomography and induce polarisation), seismic refraction tomography airborne magnetic data and geochemical analysis of soil and water to re-evaluates groundwater contamination, re-evaluates the heavy metals presents in both the soil and groundwater and to also delineate mineralised zones in the study area. Airborne magnetic data was also used to identify mineralised zones, identify subsurface structures that can aid the flow of contaminant and to correlate the result with geophysical data. The use of electrical resistivity tomography, induced polarisation and seismic refraction tomography methods helps in achieving the objective of the research which has never been used in the study area.

CHAPTER THREE

3.0 MATERIALS AND METHODS

3.1 Materials

3.1.1 Instruments for electrical resistivity tomography and induced polarization methods

1. Terrameter (SAS 1000 series) for measuring the earth resistance

2. Metal Electrodes

3. Tape Rule

4. Labelled Tag (used in locating station position) 5. Hammer (used in driving the electrodes into the ground)

6. Electric Cables.

7. Data sheet for field data capturing

8. RES2DINV Software for interpreting apparent resistivity.

9. Global positioning system

3.1.1.1 Tape rule

These are narrow, woven fabric used for linear measurements. Each tape is 2 cm thick and 100 m long.

3.1.1.2 Electric cables

These are composed of one or more electric conductors covered by insulators used for transmitting electric current from the resistivity meter to the electrodes. Red cables connect the tetramer to the potential electrodes while the blue cables connect the current electrodes to the tetramer. Each cable is about 100 m long each. They are rolled on a metal reel for easy conveyance.

3.1.1.3 Hammer and cutlass

It is a hand tool consisting of a shaft with a metal head of 2 kg at right angles to it, used mainly for driving the electrodes into the ground. Its shaft is wooden. The cutlass as used to clear the path along which measurement are to be taken.

3.1.1.4 Terrameter

It measures the resistance of the subsurface layers and can also measure the voltage of the power source. The equipment has an in-built system of reducing the effect of noise. The instruments portable and fixed with rechargeable battery. Tetrameter is powered by a 12 V battery.

3.1.1.5 Electrodes

This is a metal rod which is about 30 cm long, with which the cable is connected, it transmits current from the resistivity meter and also receive potential impulse.

3.1.1.6 Global positioning system and compass clinometer

These equipment were used for taking coordinates and bearing. GPS was used for taking the latitudes, longitudes and elevation of various locations. It is portable and handy. The compass clinometer was used to take direction of the profiles.

3.1.2 Instruments for seismic refraction tomography method

i. Seismograph was used to store the arrival time of signal. It consists of recording unit and is connected to 12 geophones, it been powered by 12 v battery.

ii. Geophones were used to detect seismic ground motions. Geophones are seismic detectors that convert mechanical energy to electrical energy. iii. Metal plate iv. Hammer was used to strike the metal plate to generate pulse

v. Transducer is attached to the hammer. To enhances the conversion of ground motion to electrical signal.

vi. Cables used in connecting all the geophone to the seismograph. Polarity is considered in doing the connection such that the positive terminal of the geophones is clip to the positive terminal of cable.

vii. Tape was used in taking measurement and to decide where to bury geophones and offset distance from shot. **viii.** SeisOpt@2D software was used to analyse seismic data

3.1.3 Airborne magnetic data

High resolution magnetic data was acquired from the Nigerian Geological Survey Agency. The data were processed to the following:

a. Production of total magnetic intensity (TMI)

b. The total magnetic intensity (TMI) anomalies were subjected to reduction to equator (RTE) to subdue the effect of the low latitude region

c. The RTE anomalies structural lineaments were extracted using Centre for exploration targeting (CET)

d. The Rose diagram which reveals the trends dissecting the study area was determined

e. The reduced to equator anomaly data was subjected to the first vertical derivative, analytical signal and tilt derivative to enhance the near-surface using oasis montaj.

f. The depths to the concealed structures were estimated using 3-D Euler deconvolution technique.

3.2 Methodology

3.2.1 Reconnaissance survey

This involves the general site overview and familiarisation. It set the tune for every other activity to be carried out. Through reconnaissance survey, appropriate portion of the site is delineated out for geophysical investigation, based on parameters like; sanitary structures, proximity of streams, topographical profile, presence of rock outcrops and their lithologies, etc. This also defines the type of method to be adopted. When carrying out this investigation mining pits, cesspits and tailings were avoided in situating the machine point. The most probable and active mining site were considered and identified. The type of rock outcrop is an indication of the bedrock in that area. Generally reconnaissance survey involves; topographical, environmental and social overview of the site.

3.2.2 Field procedure/data collection for electrical resistivity tomography and induced polarisation methods

Electrical Resistivity Tomography and Induced Polarisation investigations was conducted using ABEM Terameter (SAS 1000 Series) along the traverses (T_0, T_1, T_2, T_3, and T_4). The ERT lines have a length of 500 m each and was acquired using wenner array with (maximum and minimum) electrode spacing of 10.0 m, 30.0 m and 50.0 m respectively. The apparent resistivity and chargeability data was processed and inverted using RES2DINV code, employing a least-square inversion modelling technique with regularisation technique (Loke, 2001).

The wenner electrode array has one current electrode (C_1) followed by two potential electrodes, (P_1 and P_2) and ends with second current electrode (C_2). The current and

potential electrodes was maintained at a regular fixed distance from each other (starting at a = 10 m) and are progressively moved along the traverse line. The geometric factor (k) for the wenner array equals $2\pi a$. Measurements commenced at one end of the traverse line with electrode spacing a = 10 m at electrode position 1, 2, 3 and 4. (C_1, P_1, P_2 and C_2) was shifted to a distance of 10 m, the active electrode position being 2, 3, 4 and 5. The procedure was continued to the end of the traverse line. At each measurement, the resistivity meter displayed earth resistance value, chargeability was also displayed and the corresponding root mean square (rms) error of the reading. The apparent resistivity of the subsurface was computed using the formula $\rho a = 2\pi a R$

where a is the electrode spacing and R is the earth resistance value.

3.2.3 Seismic refraction tomography field procedure/data collection

Seismic survey was undertaken along 4 lines (A - D) using 12-channel seismograph, length of spread of 12 geophones was 55 m, shot point was -5 m from first geophones for forward shots, reverse shot was at maximum of +5 m, overlap at 50 m from the end of spread and energy source- (hammer 15 lb). Geophones with natural frequency around 40 Hz provided the adequate signals with usable frequency content.

3.2.4 Sample collection, preparation and digestion for geochemical analysis Five

water samples were collected from the untreated well and mine pits around the mining site, the groundwater samples from the fetched bucket which was cleansed with distilled water was then transferred into plastic bottles which was capped and clearly labelled. The water temperature, electrical conductivity, and pH of all the water samples were measured and recorded on the field. The concentration of lead, zinc, nitrate, arsenic, iron, copper chromium, mercury and cadmium were determined.

Five soil samples within and around the mining waste site were collected from five profile pits dug. This pit size is necessary for easier and clear observation of all soil horizons from the bottom to the top of the pit. The samples were randomly collected at a depth interval of $0 - 2$ m. The soil samples were poured into prepared plastic bottles which were capped and lebelled properly. The samples were subjected to air and oven dried to ensure constant weight, gently crush and sieved. The samples (1.5 g) were placed in 100 cm^3 flask and treated with a mixture of solvent, the mixture were swirled gently and digested for fifteen minutes. The mixture was allowed to cool and diluted to 50 cm^3, heated gently and then filtered. The filtered was then diluted to 100 cm^3 and analysed.

3.2.5 Electrical resistivity tomography and induced polarisation data processing 2D resistivity imaging were obtained from the inversion of data along the traverses that was established within the mining site. The output were presented in form of subsurface image, which is a useful system for electrical resistivity tomography.

The final output from RES2DINV displays three section, i.e., measured and calculated apparent resistivity, pseudo-sections and the inverse model resistivity section. The pseudo-sections are a qualitative way of presenting the spatial variation of the measured or calculated apparent resistivity in cross section and do not reflect the true depth, Wenner array were used to for the computation of the pseudo-sections. The inverse model section will shows the true depth and true formation resistivity (Umar *et al*., 2014). The same method was repeated for induced polarisation (IP) until the image were obtained. The data were arranged in x, y and z direction and inputted into RES2DINV program.

3.2.6 Seismic refraction tomography data processing

The data that was recorded was uploaded to computer and was processed using SeisOpt@2D system. The first arrival times was picked and inversion of travel time data was carried out. The times versus shot point to geophone distance (Time Distance Curve) were plotted. The slopes of these time-distance segments are inversely proportional to the apparent velocity of seismic waves in that layer of the earth. Tomographic inversion was perform to generate initial velocity model, the time term inversion was first used. This inversion method assumes that the subsurface is vertically stratified without lateral changes in the velocity. The depths to the top of the underlying layers was calculated under each point on the travel time versus offset distance plot.

3.2.7 Electrical resistivity tomography interpretation

Interpretation of inverse resistivity model was basically based on the resistivity value, the range of observed value in all inverse represent uncontaminated or contaminated layers and groundwater within the subsurface to a depth of investigation. The resistivity model was also compared with the results of other methods to confirm its accuracy. The contaminant movement is very much influence by the chemical properties of the soil (Umar *et al*., 2014).

3.2.8 Seismic refraction tomography data interpretation

Shallow seismic method gives information about the subsurface in terms of seismic velocities. The velocities are directly related to the quality, hardness, compaction and water content of the medium. However, as qualitative classification, seismic velocity classification was used for identifying the subsurface rock layers in terms of unconsolidated or compacted sediments and fractured or hard bedrock (Sayed *et al.*

2012).
3.3 Theories of Methods

Different methods exist, but for the purpose of this research electrical resistivity tomography, induced polarization and seismic refraction tomography methods are employed for assessment of mining site.

3.3.1 The Electrical resistivity method

Induced polarisation, self-potential and resistivity are among the electrical survey methods. Electrical methods use direct currents (dc) or low frequency alternating currents to investigate the electrical properties of the subsurface. The induced polarisation method makes use of the capacitive action of the subsurface to locate zones where conductive minerals are disseminated within their host rocks. Self-potential method makes use of natural currents flowing in the ground that are generated by electrochemical processes to locate shallow bodies of anomalous conductivity.

The resistivity method uses current injected into the subsurface to study horizontal and vertical discontinuities in the electrical properties of the ground. Electrical surveys in which currents are made to flow inductively are referred to as electromagnetic (EM) surveys (Kearey *et al.,* 2009).

Electric current has three ways of conducting through rocks namely dielectric, electronic (Ohmic) and electrolytic. Electrolytic conduction occurs by the relatively slow movement of ions within an electrolyte in a rock matrix. Electronic conduction involves rapid movement of electrons in metals. Dielectric conduction occurs in very poor conducting materials (or insulators) when an external alternating current is applied, so causing electrons to be shifted slightly with respect to their nuclei. In most rocks,

conduction is electrolytic as a result of fluids in their pores (Milsom, 2007 and Kearey *et al.,* 2009).

3.3.2 Induced polarisation method

The induced polarisation (IP) method is based on a current-stimulated electrical phenomenon observed as a delayed voltage response in earth materials. The IP effect is observed as a residual voltage decay after the current flow is interrupted (time domain IP) or as a frequency-dependent resistivity (frequency domain). In the time domain, the voltage decay is recorded during a time interval $\Delta t = t_2 - t_1$ (ms) after the current flow is interrupted. Conrad Schlumberger probably was first to report the induced polarisation phenomenon, which he called "provoked polarisation. While making conventional resistivity measurements, he noted that the potential difference, measured between the potential electrodes, often did not drop instantaneously to zero when the current was turned off. Instead, the potential difference dropped sharply at first, then gradually decayed to zero after a given interval of time. Certain layers in the ground can become electrically polarised, forming a battery when energised with an electric current. Upon turning off the polarising current, the ground gradually discharges and returns to equilibrium. The study of the decaying potential difference as a function of time is now known as induced polarisation (IP) in the time domain (Figure 3.1a). In this method the geophysicist looks for portions of the earth where current flow is maintained for a short time after the applied current is terminated. Another technique is to study the effect of alternating currents on the measured value of resistivity, which is called IP in the "frequency domain" (Figure 3.1b). In this method the geophysicist tries to locate portions of the earth where resistivity decreases as the frequency of applied current is increased. The induced electrical polarisation method is widely used in exploration for ore bodies, principally of disseminated sulfides. Use of IP in geotechnical and engineering applications has been limited, and has been used mainly for groundwater exploration.

Groundwater IP studies generally have been made with time-domain.
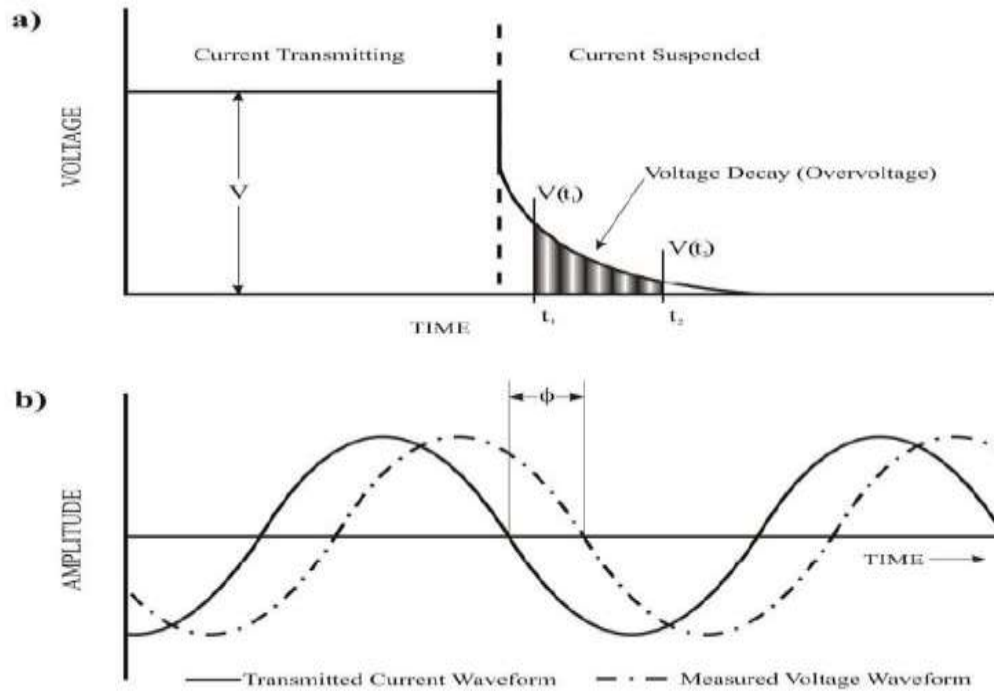
Figure 3.1. (a)Time domain and (b) frequency domain waveform illustrations

3.3.3 Current flow in a continuous medium

Considering an element of a homogeneous material in Figure 3.2 with length L and crossectional area A, there is a potential drop between the ends of the material when current I is passed through as a result of the resistance (R) by the medium. Ohm's law links the current (I), potential difference (V) and resistance (R) according to equation 3.1.
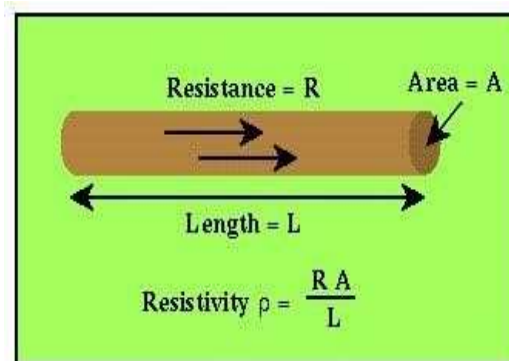
Figure 3.2: Schematic diagram of a current carring conductor.

$$V = R * I \qquad (3.1)$$

$$R = \frac{\rho L}{A} \qquad (3.2)$$

The resistance of the medium is given by equation 3.2 where ρ is the "true resistivity" which is the property of the isotropic conducting medium that opposes the current flow. For an anisotropic medium, resistivity varies and the output resistivity is not the true value of the medium but "apparent resistivity (ρ_a)".

A single electrode on a surface with a uniform subsurface of resistivity (ρ) (Figure 3.3) requires a current sink at a large distance from the electrode to complete the circuit. Current flows radially away from the electrode so that the current distribution is uniform over hemispherical shells centred on the source electrode (Kearey *et al.,* 2009). A shell at any point r in the medium from the electrode has a surface area (A) of $2\pi r^2$. The current density (J) and potential gradient ($\frac{\partial y}{\partial x}$) are given by equation 3.3.
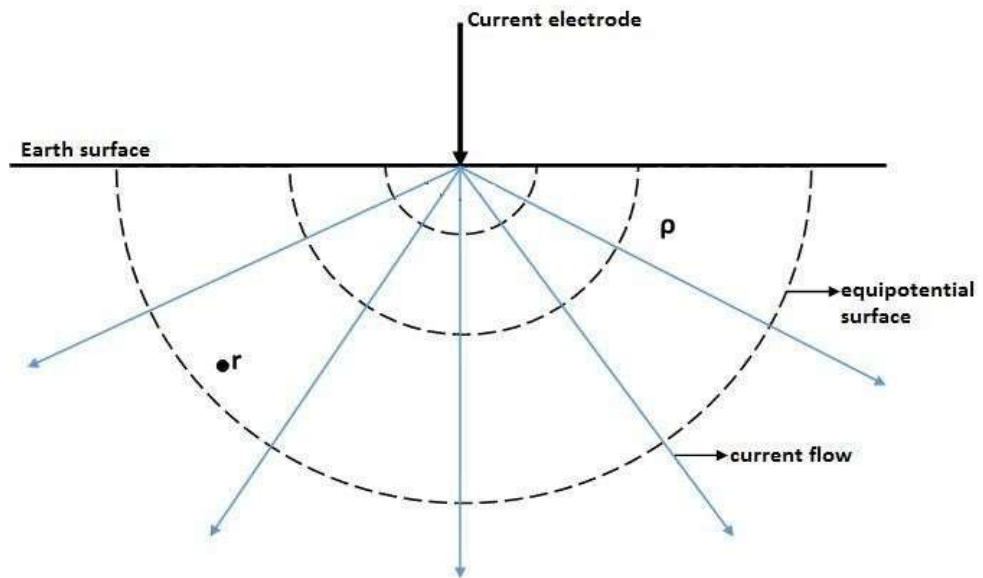
Figure 3.3: Current flow from an electrode through an isotropic subsurface.

$$J = \frac{I}{A} = \frac{I}{2\pi r^2} \qquad (3.3)$$

Also

$$J = \sigma E \qquad (3.4)$$

But

$$E = -\frac{\partial y}{\partial x} \qquad (3.5)$$

and

$$\sigma = \frac{1}{\rho} \qquad (3.6)$$

$$J = \frac{1}{\rho}\left(\frac{\partial y}{\partial x}\right) \qquad (3.7)$$

hence

$$\frac{\partial y}{\partial x} = \rho J = -\frac{\rho I}{2\pi r^2}$$

(3.8)

The potential (V) measured at any point r in the homogeneous subsurface is the integral of the potential gradient given by equation 3.9.

$$V_r = \frac{\rho I}{2\pi r}$$

(3.9)

Electrical resistivity surveys are carried out with the conventional four electrode or continuous vertical electrical sounding (CVES)/multi-electrode system. In either case, an artificially generated electric current is injected into the ground through two current electrodes and the resulting potential at point in the subsurface measured with two potential electrodes to compute the resistivity.

3.3.4. The four electrode system

The four electrode system uses two current and two potential electrodes for the survey. The current is sent into the ground through the electrodes A and B and the potential at any two points on the surface measured with electrodes M and N (Figure 3.4).
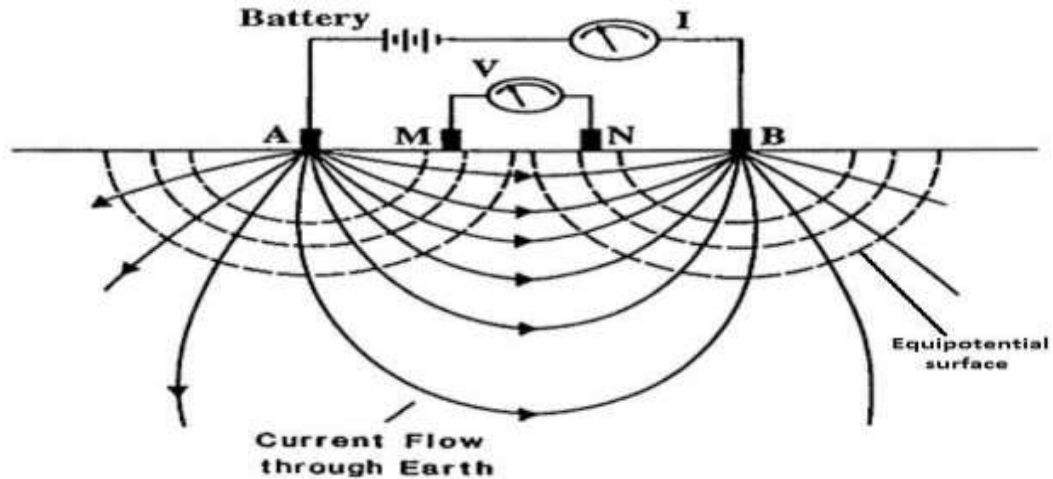
Figure 3.4: A diagram of the conventional four electrodes showing current flow pattern and the equipotential surface.

A and B are current electrodes with M and N as potential electrodes. Given the geometric factor k (equation 3.10) which is strictly determined by the arrangement of the electrodes, the apparent resistivity is given by equation 3.11.

$$K = \pi \frac{\left[\left(\frac{AB}{2}\right)^2\right] - \left[\left(\frac{MN}{2}\right)^2\right]}{2\left(\frac{MN}{2}\right)}$$
(3.10)

$$\rho_a = \frac{\Delta V}{I} k$$
(3.11)

3.3.5 Array types

There are different configurations of the electrodes used in electrical resistivity survey. The choice of an array in a particular work may depend on the anticipated depth of probe and other objectives of the survey, such as mapping of dykes. For this work wenner array was adopted.

3.3.6. The Multi-electrode system

The multi-electrode system also known as the electrical resistivity tomography (ERT) or continuous vertical electrical sounding (CVES) is a 2D method that combines profiling and sounding at the same time in measuring the subsurface distribution of earth resistance.

In this method, four equally spaced electrodes were layed on the profile line. The resistivity meter chooses a suitable electrode permutation at a time for measurements based on the selected configuration. This is repeated by the device until there is no permutation. The resulting apparent resistivity plots take the shape of a trapezium showing the covered part of the subsurface. Loke (2001) gives more information on the electrical resistivity method using multi-electrode. Figure 3.8 demonstrates the multi-electrode configuration using the Wenner array. The data points 1-17 in Figure 3.9 use a permutation such that the electrode separation is "a". The separation would then increase to twice the initial (a) for the next readings, thus"2a" for data points 18-31. This value keeps increasing till a value for the factor "n" where no four electrodes on the profile can be used for the separation "na". Knowing the geologic setting of the area, the apparent resistivities computed would predict the kind of formations present in the subsurface (Table 3.1).
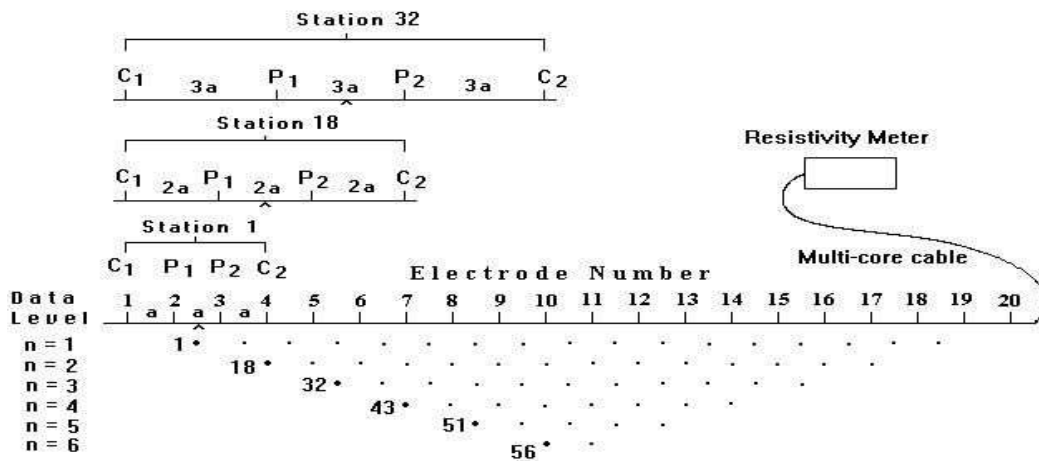
Figure 3.5: A 2D pseudosection from a multi-electrode resistivity survey using twenty electrodes (Loke 2001).

In profiling (Figure 3.6), the whole set of the electrode configuration is moved along the profile line at regular intervals without any change in the electrode spacing. Profilling resolves vertical structures such as dykes and shear zones (Kearey *et al.*, 2009).
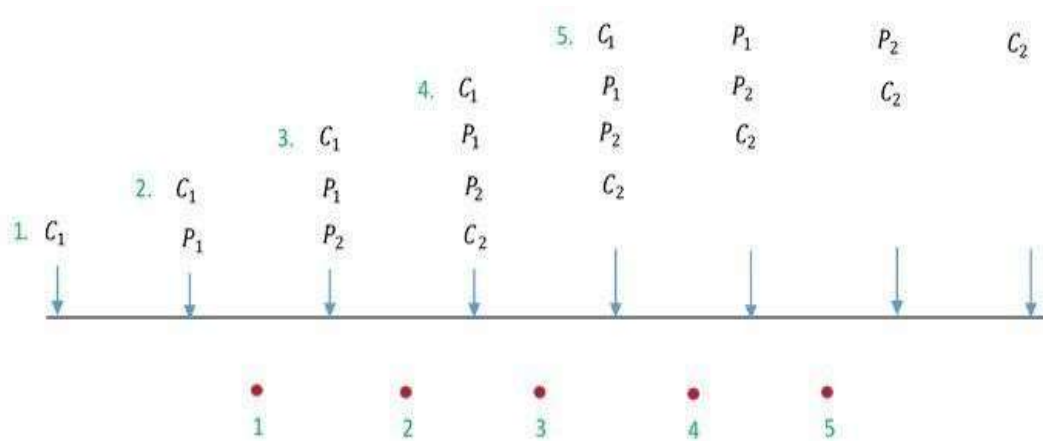
Figure 3.6: Profilling method showing the movement of electrodes using the Wenner array.

In VES, resistivity measurements are taken vertically by varying the electrode spacing about a fixed central point (Figure 3.8).   The 1D sounding resolves horizontal structures and good for mapping overburden thickness and delineating aquifers in bedrocks with complex geology (Kearey *et al*., 2009).
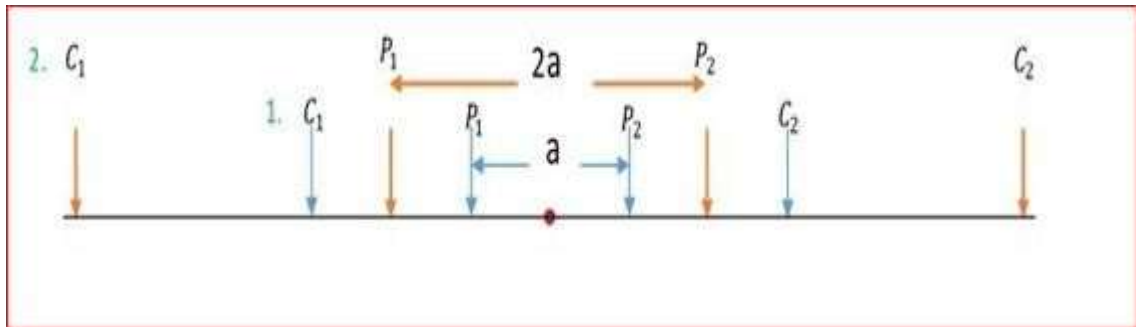
Figure 3.7: Sounding resistivity measurements using wenner array. The electrode spacings are increased about the midpoint.

3.3.7. Resistivity value of rock type

Table 3.1 shows the resistivity values of different rock types in a basement complex Nigeria. This was used for the interpretation of resistivity data throughout the research work.

Table 3.1 Resistivity Value of Rock Types (Salako *et al.,* 2009)

Rock Types	Resistivity (Ωm)
Fadama loam	30 – 90
Sandy clay and sandy silt	100 – 200
Sand and general laterite	150 – 1000
Weathered laterite	150 – 900
Fresh laterite	900 – 3500
Weathered basement	20 – 200
Fractured basement	500 – 1000
Fresh basement	>1000

3.4 Theory of Seismic Method

Seismic waves are in the form of packets of elastic strain energy that travel from a naturally or artificially generated source. It has two major components, the body and surface waves (Reynolds 2011). Body waves propagate through the whole internal structure of the earth. It comprises primary waves (P) and shear [secondary wave (S).

P-waves are longitudinal and cause the particle of the medium to vibrate in the same direction as the wave propagate while s-waves are transverse and cause the particles of the medium to vibrate perpendicular to direction of propagation of the wave. In the same medium, p-wave travels faster than s-wave. Surface waves are in the form of Rayleigh and Love waves. These waves travel along the surface of the Earth with a more complicated particle motion and are responsible for damages during the release of energy from earthquakes (Kearey *et al.*, 2009) and (Sheriff 2002). The velocities with which seismic pulses move are determined by the density (ρ), the bulk (K) and shear moduli (μ) of the medium through which they pass. The seismic velocities are given by the following relations:

$$v_p = \sqrt{k} + \frac{4}{3}\frac{\mu}{\rho}$$

(3.12)

and

$$v_s = \sqrt{\frac{\mu}{\rho}}$$

(3.13)

The estimated primary wave velocity from a refraction seismic survey is linked to porosity (φ) of a rock with the equation below.

$$\frac{1}{v_p} = \frac{\varphi}{V_f} + \frac{1-\varphi}{V_m}$$

(3.14)

V_f is pore fluid velocity typically 1500m/s and V_m is the velocity of the rock matrix (2800 m/s) (Wyllie *et al*., 1958 & Reynolds, 2011).

In near surface seismic exploration geophysics, elastic p-wave velocity is normally utilised but developments in recent years combine s-waves with p-waves for lithostratigraphic characterization (Telford & Sheriff, 1990).

3.4.1 Seismic refraction method

Seismic refraction tomography is based on the determination of time interval that elapses between an initiation of a seismic waves at a certain shot point and the arrival of refracted waves at one or more seismic detector. Seismic refraction tomography uses a wave's propagation in ground surface which is dependent on the velocity variation in different medium. The wave return to the surface as refracted waves which are sometimes called head waves.

Seismic waves propagate with different velocity when travelling in different geological layer and refracted when they crosses a boundary between different types of geological layer (Salisbury & Snyders 2007). The thickness and velocity of layers can be calculated by determining the arrival times for direct and refracted waves from seismic section.

A single shot seismic record has direct, refracted and reflected waves. In an environment with faulted zone in the bedrock, diffracted waves are also recorded. In this work only refracted seismic wave are made use of.

In a homogeneous earth layer, a wave travels in a straight path but changes direction as it enters a different acoustic layer (Figure 3.8). The ratio of the sine of the incident angle to the sine of the angle of refraction is equal to the ratio of the velocity of the first layer to that of the second layer given by equation 3.15. As the incident

angle increases, the refracted angle in the second layer also increases. Critical refraction is reached when the angle of refraction in the second layer equals 90^0 as the incident angle is further increased. At critical refraction, the refracted ray travels along the interface separating the two acoustic layers.
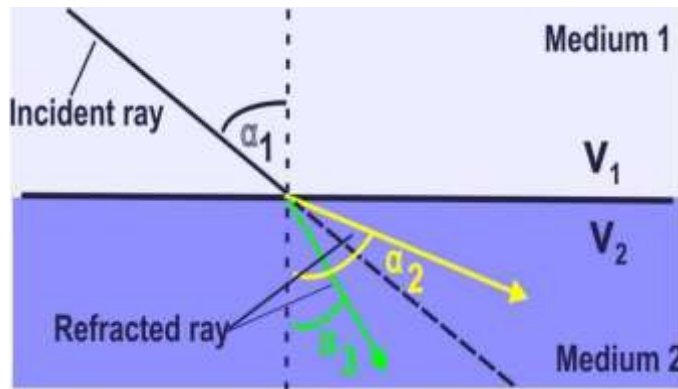
Figure 3.8: Schematic diagram of a p-wave travelling from a top layer with velocity V_1 into a layer with velocity V_2

$$\frac{\sin \alpha_1}{\sin \alpha_2} = \frac{v_1}{v_2}$$

(3.15)

In refraction seismology, part of the seismic impulses sent into the subsurface are critically refracted in response to changes in acoustic impedance of the earth layers. Acoustic impedance is the product of the density (ρ) of a given formation and its velocity. The critically refracted waves travelling along the discontinuous boundary break off to the surface as head waves (Figure 3.9) as points on the wave front act as secondary wave sources based on the Huygens'principle. Equation 3.16 and 3.17 give the relationship between the critical angle (i_c), refracted angle (90^0) and the layer velocities (V_1 and V_2)
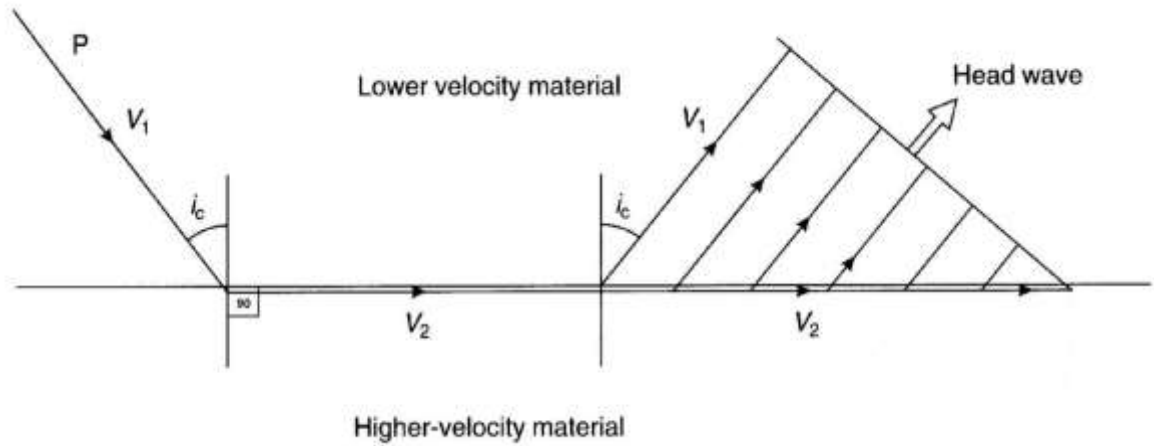
Figure 3.9: Schematic diagram showing critically refracted p-wave at a plane boundary generating upward moving header waves.

V_1 and V_2 are the velocities of the overburden and underlying layers respectively and i_c the critical angle (Telford & Sheriff 1990).

$$\frac{sin i_c}{sin 90^0} = \frac{V_1}{V_2}$$

(3.16)

$$sin i_c = \frac{V_1}{V_2}$$

(3.17)

3.4.2 Travel time curve, velocity and layer thickness

The time taken for seismic pulse to arrive at the receivers (geophones) are plotted against the distance of the receivers from the shot location in order to compute the velocities of layers present using the slopes of the T-X curves (Figure 3.10). The direct wave plot passes through the origin and has velocity V_1 given by the inverse of its slope (equation 3.18). The distance from the shot location to the point the refracted waves start arriving at the geophones is the critical distance (X_{crit}). From the crossover

point (X_{cross}), the refracted waves take over as first arrivals. Velocity of the refracted

waves (V_2) is given by equation 3.19.
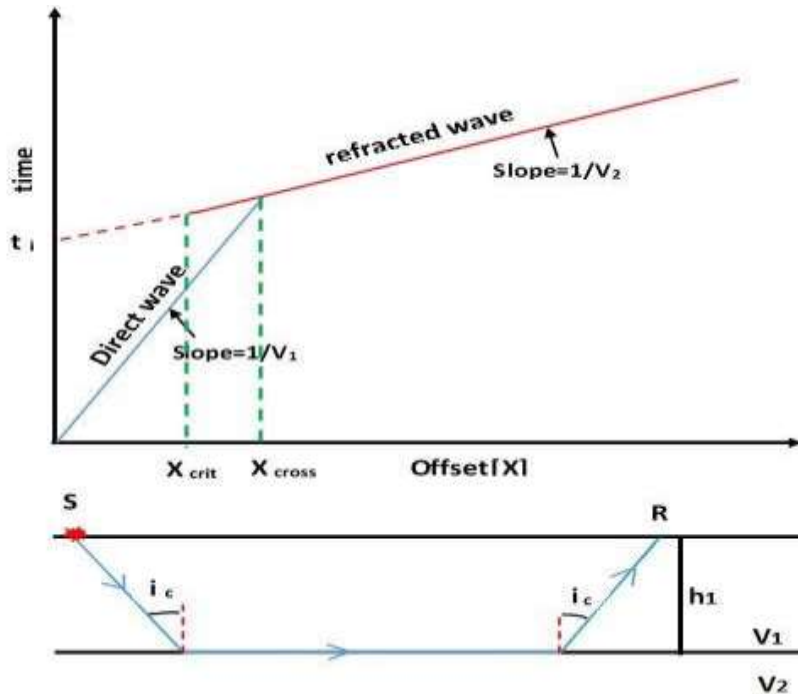
Figure 3.10: A travel time curve of seismic refraction first arrivals.

V_1 and V_2 are velocities of the first and second layers respectively. Note: V_2 is assumed to be greater than V_1.

The layer velocity is related to the slopes of the travel time plot according to the following equations:

$$\text{Slope\_direct} = \frac{1}{V_1} \tag{3.18}$$

$$\text{Slope\_refracted} = \frac{1}{V_2} \tag{3.19}$$

The velocities obtained from the slopes of the travel time curve are used to find the

layer thicknesses.   Refraction seismology uses velocity and layer thickness to describe

the subsurface geology. The arrival time t_x of a pulse at the receiver placed at a distance X from the shot point is given by equations 3.21 and 3.22.

$$t_x = \frac{X}{V_2} + \frac{2h_1\sqrt{V_2^2 - V_1^2}}{V_1 V_2}$$

(3.20)

$$t_x = \frac{X}{V_2} + t_i$$

(3.21)

t_i is intercept time and h_1 the depth to the refracting interface. If the shot and receiver locations are assumed to be at the same point, then X = 0 and $t_x = t_i$. The following equation therefore holds for t_i and h_1 (thus the depth to the first refracting interface).

$$t_i = \frac{2h_1\sqrt{V_2^2 - V_1^2}}{V_1 V_2}$$

(3.22)

$$h_i = \frac{t_i V_1 V_2}{2\sqrt{V_2^2 - V_1^2}}$$

(3.23)

3.4.3 Multiple layer

For a subsurface with multiple acoustic horizontal layers (Figure 3.11), the principle of reciprocity is valid. Both the forward and reverse travel time curves are of the same nature with a symmetrical crossing point of the refraction curves about the profile. The arithmetic mean of the apparent velocities obtained from the refraction curves is equal to the true velocity of the refractor.

Seismic Refraction
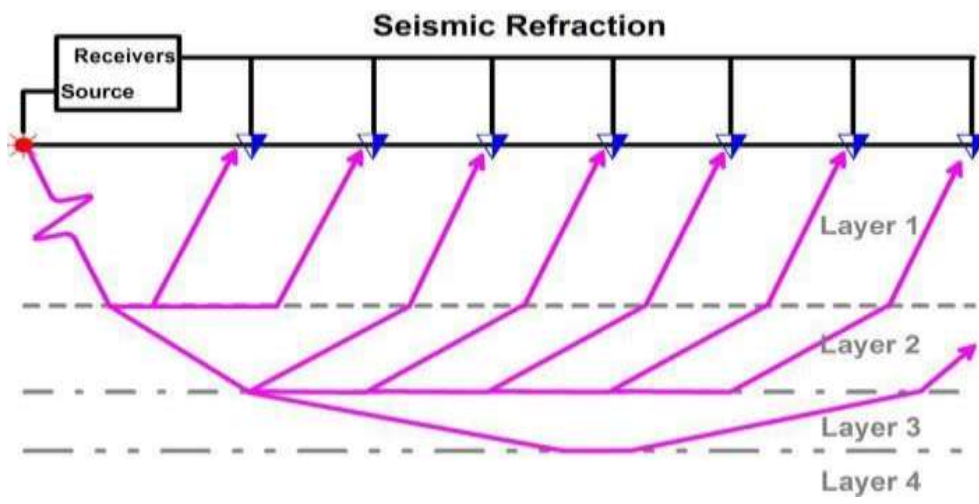
Figure 3.11: Refraction at multiple horizontal interfaces (Telford and Sheriff 1990).

3.4.4 Dipping layers

Travel time curve for a nonparallel or dipping refractor gives apparent velocity which can result in incorrect depth computation. The crossing point [CP] of the forward and reverse refraction curves is non symmetrical about the profile. It always shift towards the down-dip direction. Interchanging the shot and receiver positions would not produce the same travel-time curves (Figure 3.12).

The dip angle (γ) is related to the velocity of the first layer (V_1), refractor's velocity in up-dip

Direction (V_{2U}) and that in the down-dip direction (V_{2D}) by equation 3.24
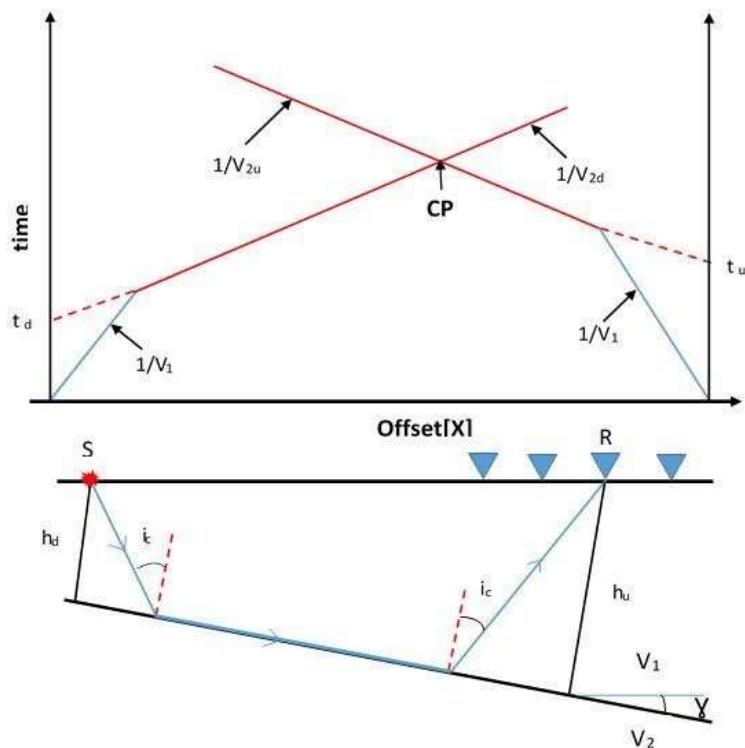
Figure 3.12: Schematic diagram of a dipping interface.

t_d is the down-dip intercept time, t_u is up-dp intercept time, V_{2d} and V_{2u} are the velocities of the refractor in the down and up-dip directions respectively and CP is the crossing point of the refracted travel time curves.

Velocity in the up-dip shot is always greater than that in the down-dip. The extent of dip of the refractor determines the magnitude of its apparent velocity.

$$V_{app} = V_{true} \text{ when } \gamma = 0_0 \quad\quad\quad (3.24)$$

$$V_{app} = \infty \text{ when } \gamma = 90^0 \quad\quad\quad (3.25)$$

The true velocity of the half-space is given by the product of the cosine of the dip angle and the harmonic mean but not the arithmetic mean of the measured up and down dip velocities (equation 3.25). The velocity of the seismic waves predicts the kind of material present in the propagating medium (Table 3.2) with the aid of geologic information of the area.

Table 3.2: Elastic wave velocity for some earth materials. Depend strongly on temperature (Kohnen,1974)

Material	V_p(m /s)
Air	330
Water	1450-1530
Sand(Loose)	200-2000
Sand(Loose, dry) 200-1000 Sand(Water saturated, 1500-2000 $^lF^{oose}$loodp$^)$ lain alluvium 1800-2200	
Sandstone	1400-4500
Limestone	1700-4200
Dolomite	2500-
Shale	20006500- 4500
Rock salt	4000-5500
Granites	4600-6200
Gabbro	6400-7000
Basalts	5500-6500
Gneiss	3500-7600

3.5 Theories of the Adopted Magnetic Interpretation Methods

3.5.1 Reduction to equator (RTE)

The Reduction to magnetic equator (RTE) is a filter that is usually applied to the TMI anomalies in order to centre structures and anomalous bodies over their respective causative positions.

The RTE filter depend on the inclination and declination of the body's magnetisation of the local earth's field and orientation of the body with respect to the magnetic north (Baranov, 1957). The RTE is governed by the equation below (Leu, 1981);

$$L\,\square\,\square\,\square\frac{\qquad\qquad\qquad\qquad\qquad}{\cos_2\square\square I_{ai}.\square.\cos\cos\square_2 I\square\square.D\cos\square\square\square D\square} \square\sin_2\square I_a\square\square$$

$$\square\square\square\cos\cos_2\square_2 D\square I\square\square.\square\cos\square\square_2\square D\ \square\square\square\square\ (3.26)\ \square\sin\square I\square$$

If $\square\left|I_a\right|\square I\ \square$, $I_a = I$ \hfill (3.27)

Where $L\,\square\,\square\,\square$ is the reduction to equator (RTE), I is the geomagnetic inclination, I_a is the inclination for amplitude correction and D is the geomagnetic declination.

3.5.2 First vertical derivative (FVD) map

The first vertical derivative (FVD) is applied to the reduced to pole anomaly data. The FVD allows the vertical imaging of the shallow causative structures. This is the FVD refines the effect of high frequency (short wavelength) magnetic features at the expense of the short frequency (long wavelength). It also enhances the textural variation in the data and hence helps to visualised subsurface structural features such as folds, faults, fracture and contact zones which could not be depicted clearly from the reduced to

equator map. The FVD computes the high frequency anomalies using the Laplace transformation expressions as thus;

$$\nabla^2 f = 0 \qquad\qquad (3.28) \text{ where } \nabla^2 f \text{ is}$$

the Laplace transform which can be expressed in full as;

$$\nabla^2 f = \frac{\partial^2 f}{\partial x^2} + \frac{\partial^2 f}{\partial y^2} + \frac{\partial^2 f}{\partial z^2} \qquad (3.29)$$

∂z, ∂y and ∂x are the differentials in z, y and x coordinate.

Then nth vertical derivative can be computed once the Fourier transformation is known by using the equation (3.30).

$$F\left[\frac{\partial^n f}{\partial z^n}\right] = K^n \, F[f] \qquad\qquad (3.30)$$

where F is the Fourier representation of the field, K is the wave number or frequency and f is the input to be filtered (Okpoli & Akingboye, 2016). As such, the n is taken as one (1) for the first vertical derivative filter.

3.5.3 Centre for exploration targeting (CET) structural lineaments

The CET plugin on the Oasis montaj software identifies and enhances linear geologic structures on from a potential field data (Core *et al.*, 2009). This technique was applied to the RTE grid using the following steps;

(a). The textural analysis which involves the calculation of the standard deviation in order to determine the magnetic discontinuities and complex textures zones. The standard deviation works based on the equation as thus; For a window containing N cells, whose mean value is μ, the standard deviation σ of the cell values x_i is given as;

$$\sigma = \sqrt{\frac{1}{N}\sum_{i=1}^{N}\left(x_i - \mu\right)^2} \qquad (3.31)$$

(b). The created standard deviation grid was subjected to the lineation and vectorisation transformation to producing the structural complexity map of the study

area.

3.6 Estimation of Depths to the Concealed Structures

3.6.1 3-D Euler deconvolution method

The 3-D Euler deconvolution method is also independent of the direction of source magnetization, which makes it deem fit for low-latitude region. The 3-D Euler deconvolution technique detect the subsurface structural features as well as estimate their respective depths. It makes use of the x, y, and z derivatives of the TFA anomaly data to determine the depth and boundaries of different geologic model of interest using a structural index (N). For example; N = 0 for geologic contact, N = 1 for thin dyke or sill, N = 2 for horizontal or vertical cylinder and N = 3 for magnetic sphere or dipole (Reid *et al.,* 2013). The structural index of one (1) for thin dykes or sills was used. The

3-D Euler deconvolution is based on the Euler's homogeneity equation (Thompson, 1982) given as:

$$(x - x_0)\frac{\partial F}{\partial x} + (y - y_0)\frac{\partial F}{\partial y} + (z - z_0)\frac{\partial F}{\partial z} = N(B - F)$$

(3.32)

Where, x_0, y_0 and z_0 are the position or coordinate of the magnetic source, (x, y, z) are the location of the field measurement, F is the total field value, B is the regional value of the total field and N is the degree of homogeneity is also referred to as structural index (Reid *et al.,* 2013). The 3-D Euler deconvolution map of the study area was produced using 6000 m width window size and a maximum depth tolerance of 50%.

3.7 Quality Control for Geochemical Analysis

Appropriate quality procedures and precautions were carried out to assure the reliability of the results. Reagents used to calibrate the instrumentation were of analytical grades. A spike-and recovery analysis was performed to assess the accuracy of the analytical techniques used. Post-analysed samples were spiked and homogenized with varying amounts of the standard solutions of the different metals. The spiked samples were then processed for the analysis by the dry ashing method. Quality control measures were taken to assess contamination and reliability of data. The coefficients of variation of replicate analysis were determined for precision o f analysis; the variations were found to be less than 10%.

3.8 Soil Chemical Analysis

Chemical analysis was done on the soil sample collected close to and away from the mining site. Preliminary assessment of the extent pollution with respect to exchangeable metals was carried out at the Federal Ministry of Water Resources, Regional Water Quality Laboratory,

Minna and American Public Health Association (19th Edition). Soil samples from five sampling points at about horizon C were obtained and analysed for their chemical concentrations in mg/L. The sample point were designated as S_1 to S_5 with each sampling point separated with a distance of 10 m and S_5 serves as the control point and distanced of 100 m away from S_4.

Table 3.3: Maximum permissible concentration of constituents in soil (Yusuf *et al.,* 2018a)

Constituents	WHO/EU/CSQG (mg/Kg)
Hydrogen iron (pH)	6 – 8
Arsenic	9.8
Iron	20
Cadmium	1.4
Chromium	6.4
Copper	270
Acidity	NS
Total Hardness	NS
Mercury	0.18
Lead	70
Zinc	200
Nitrate	35
Chloride	NS

NS* = Not specified, CSQG = Canadian Soil Quality Guideline

3.8.1 Sources of heavy metals in contaminated soils

The heavy metals essentially become contaminants in the soil environments because (i) their rates of generation via man- made cycles are more rapid relative to natural ones,

(ii) they become transferred from mines to random environmental locations where higher potentials of direct exposure occur, (iii) the concentrations of the metals in discarded products are relatively high compared to those in the receiving environment, and (iv) the chemical form in which a metal is found in the receiving environmental system may render it more bioavailable (Khan *et al.*, 2008).

3.8.2 Remediation of heavy metal in contaminated soils

The overall objective of any soil remediation approach is to create a final solution that is protective of human health and the environment. For heavy metal-contaminated soils, the physical and chemical form of the heavy metal contaminant in soil strongly influences the selection of the appropriate remediation treatment approach. Information about the physical characteristics of the site and the type and level of contamination at the site must be obtained to enable accurate assessment of site contamination and remedial alternatives. The contamination in the soil should be characterized to establish the type, amount, and distribution of heavy metals in the soil. Once the site has been characterised, the desired level of each metal in soil must be determined (Smith *et al*., 1995).

This is done by comparison of observed heavy metal concentrations with soil quality standards for a particular regulatory domain, or by performance of a site-specific risk assessment. Remediation goals for heavy metals may be set as total metal concentration or as leachable metal in soil, or as some combination of these (USEPA, 2007). As present a variety of approaches have been suggested for remediating contaminated soil (USEPA, 2007) has broadly classified remediation technologies for contaminated soil into (i) source control and (ii) containment remedies. Source control involve *in situ* and *ex situ* treatment technologies for sources of contaminated soil is treated in its original place,

unmoved, unexcavated. *Ex situ* means that the contaminated soil is moved, excavated, or removed from the site or subsurface. Implementation of *ex situ* remedies requires excavation or removal of the contaminated soil. Containment remedies involve the construction of vertical engineered barriers (VEB), caps, and liners used to prevent the migration of contaminants.

3.9 Hydrochemical Analysis

In order to carry out pollution assessment of the study area, hydrochemical analysis of water samples were collected from five wells/pits around the mining site. The sampling wells were designated W_1 to W_5 which stand for well $_1$ to well $_5$. The physiochemical parameters that are indicative of groundwater pollution such as copper, cadmium, zinc, chromium, lead, iron, mercury, nitrate and arsenic were analysed. All samples were analysed using standard methods recommended by the American Public Health Association (APHA 19th edition, 1995). Results were compared with Nigerian Standard for Drinking Water Quality (NSDWQ, 2015) and WHO. HM 5000 Metelyser and Colorimeter was used to ascertain the concentration of heavy metals in groundwater at the Federal Ministry of Water Resources, Regional Water Quality

Laboratory, Minna, Nigeria.

Table 3.4: Maximum permissible concentration of constituents in water (WHO, 2004) and (NSDWQ, 2015)

Constituents	WHO	NSDWQ
Arsenic	0.01 mg/L	0,01 mg/L
Nitrate	50 mg/L	50 mg/L
Hydrogen-iron concentration (pH)	7-8.5 μS/cm	6.5-8.5
Sulphate	200 ppm	100 mg/L
Total dissolved solids	1000 ppm	500 mg/L
Calcium	75 ppm	NS*
Magnesium	50 ppm	20 mg/L
Electrical conductivity	1000 μScm^{-1}	1000 μScm^{-1}
Iron	0.3 mg/L	0.3 mg/L
Mercury	0.006 mg/L	0.001 mh/L
Cadmium	0.003 mg/l	0.005 mg/l
Chromium	0.05 mg/l	0.05 mg/L
Copper	2.0 mg/l	1.5 mg/L
Acidity	NS*	NS*
Total Hardness	500 mg/l	150 mg/L
Alkalinity	200 mg/l	NS*
	0.001 mg/l	0.001 mg/L
Lead		
Zinc	3.0 mg/l	3.0 mg/L

NS* = Not specified, WHO = World Health Organisation, NSDWQ = Nigerian Standard for Drinking

Water Quality

CHAPTER FOUR

4.0   RESULTS AND DISCUSSION

4.1 Results of Aeromagnetic Data

Interpretation of Aeromagnetic Data (Bida Sheet 184 NE) was done in order to get a regional overview of the study area and to correlate the results (secondary data) and that of the primary data of the study area. Figure 4.1 represent the total magnetic intensity (TMI) map of Kataeregi mining site. The TMI map was formed by adding a

constant value of 33000 nT to the field anomaly data. The analysis of the TMI data were used to delineate the geologic structures that are concealed within the study area.

4.1.1 Interpretation of total magnetic intensity (TMI) anomaly map

In general, the northern, mid and southeastern parts (Figure 4.1) of Kataeregi mining site are characterised by high magnetic intensities denoted in red to pink colours with values between 331168.7 and 33176.9 nT respectively. The regions of moderate magnetic intensities (green to yellow colours) had values between 33005.4 and 33072.9 nT. The areas characterised by low magnetic intensities (blue to magenta colours) had values between 32728.2 and 32985.2 nT. However, the present study area (Kataeregi) marked by mine symbol falls within the moderate to high magnetic intensity zones. The TMI map was spatially correlated with the geologic map of the study area (Figure 2.3). It was observed that two major lithologic units namely; Migmatite gneiss and amphibolites schist were observed in the northern and southern part of the study area respectively. Migmatite gneiss and amphibolites schist usually have high and low magnetic intensities respectively. The study area falls within the low latitude region there is therefore the need to place the magnetic sources anomalies directly above the causative sources. This can be achieved by subjecting the total magnetic intensity anomaly data to reduction to equator (RTE), for easier
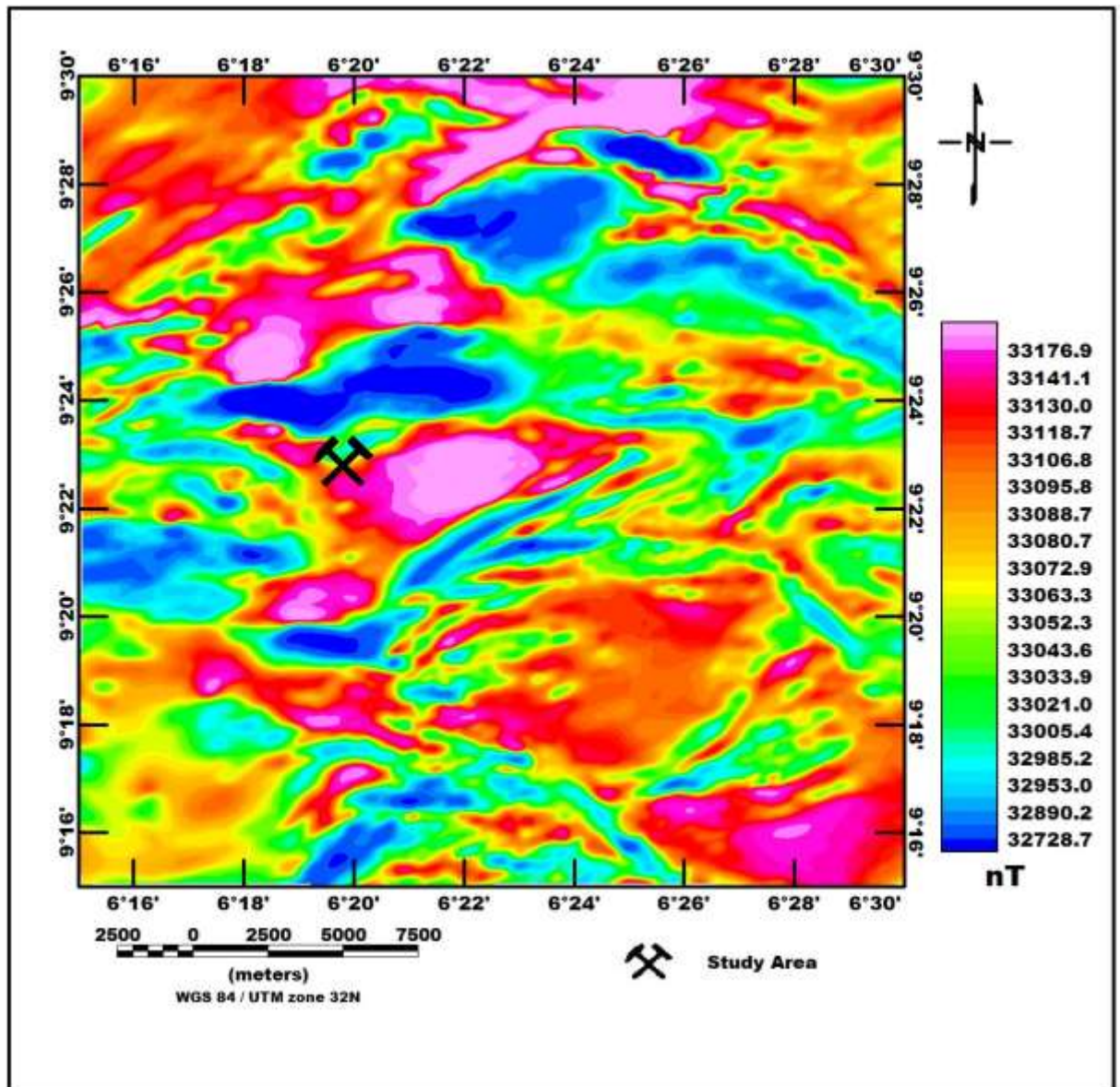
interpretation and understanding.

Figure 4.1: Airborne total magnetic intensity anomalies map of the study area

4.1.2 Interpretation of the Reduced to Equator (RTE) anomaly map

The TMI anomalies (Figure 4.1) were reduced to equator in a bid to subdue the effects of the low latitude region. It is important to note that, at low latitude with which the study area falls into. There is decrease in the magnetic field intensity which causes local magnetic bodies to have lower magnitude than those produced by an identical structure at high latitude (Beard *et al.,* 2000). As such, the reduced to equator anomaly map (Figure 4.2) represents a well-positioned magnetic anomalies directly above their respective sources. In contrast, there is a slight shift in the position of the magnetic

112

anomalies in TMI map (Figure 4.1) and the reduced to equator map (Figure 4.2). It is worth knowing that the area of interest Kataeregi denoted by black mining symbol, is bounded relatively low (yellow to green) to high magnetic (red to pink colours) intensity anomalies north to south. The relatively low to high magnetic intensity anomalies coincide with migmatite gneiss and amphibolites schist respectively.
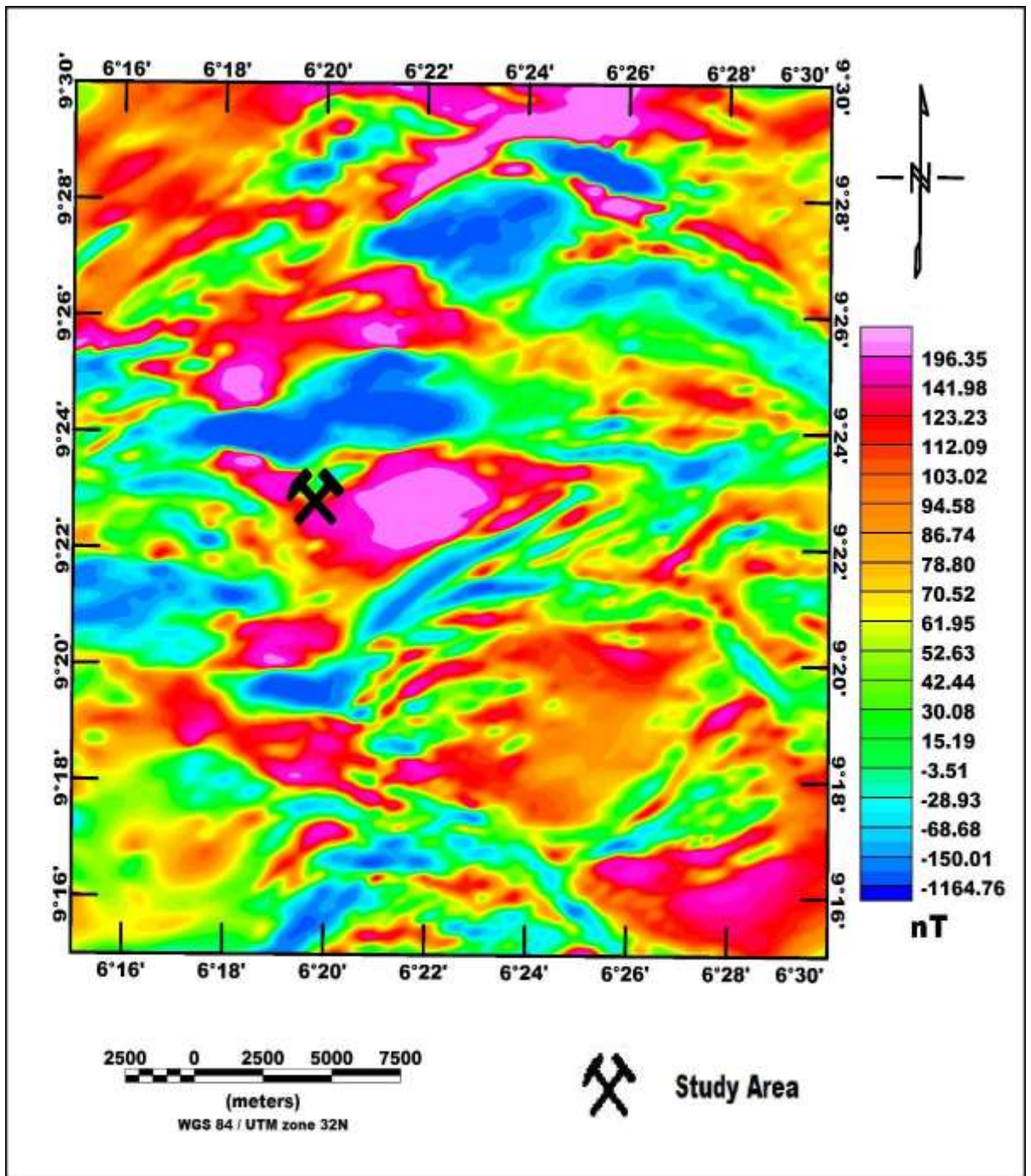
Figure 4.2: Reduced to equator (RTE) anomaly map derived from TMI data

4.1.3 Interpretation of the reduce to equator (RTE) structural lineaments map The RTE structural lineaments map (Figure 4.3) denotes the subsurface structural features such as; faults, folds, fractures and shear zones which are concealed in and around the study area. The subsurface structural features were automatically extracted and produce for better pictorial view in contrast to the TMI and RTE figures 4.1 and

114

4.2 maps respectively. The unveiled subsurface structural features (lineaments) are possibly responsible for hosting mineralised deposits. The study area (Kataeregi mining site) is dissected by series of trending lineaments (ENE-WSW, NNE-SSW and ESE-WNW). The highlighted lineament represents the short wavelength magnetic anomalies which cut across the migmatite gneiss and amphibolites schist of the study area.
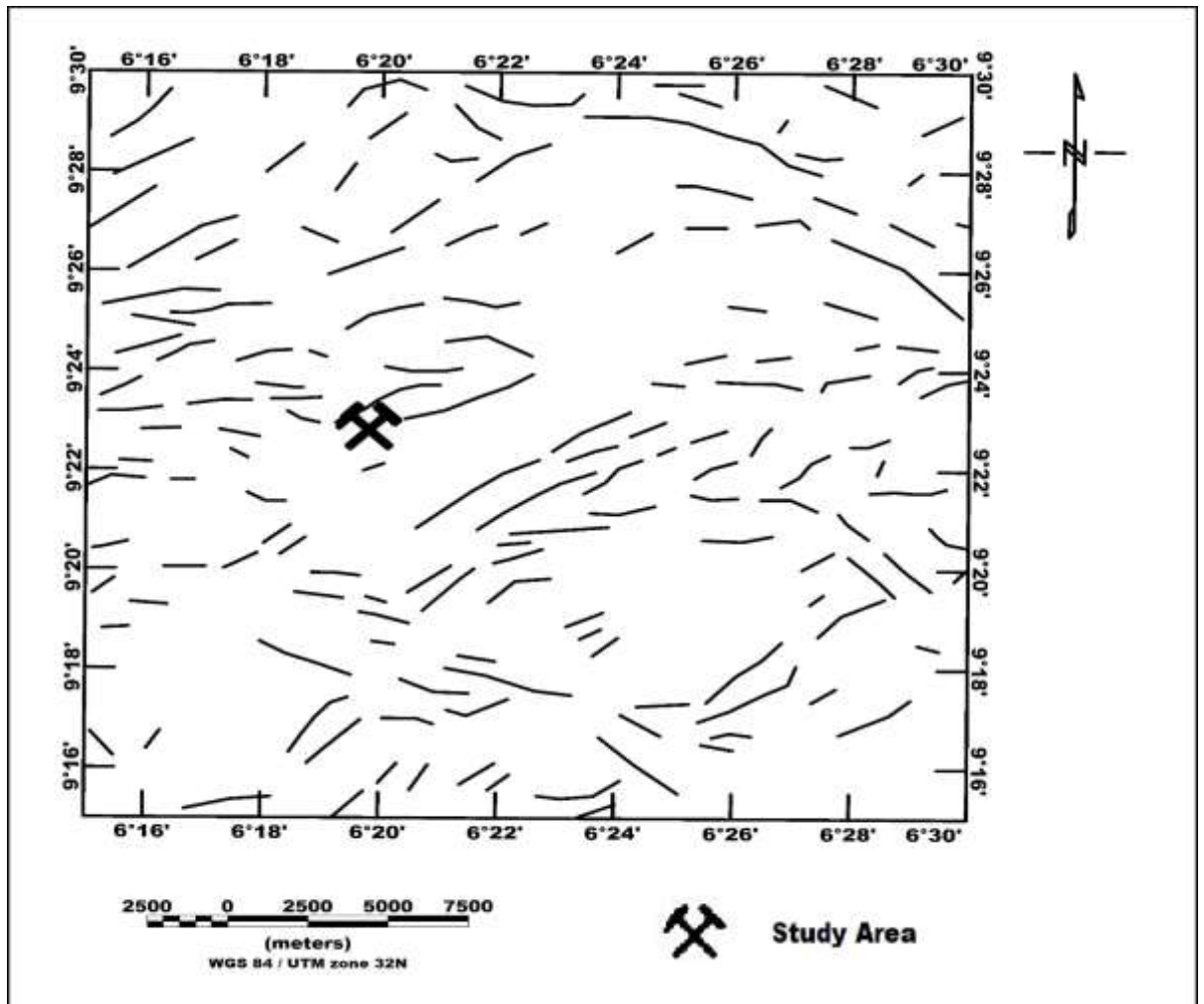

Figure 4.3: Subsurface structural lineaments map derived from the RTE data

In addition, the Rose diagram (Figure 4.4) of the reduced to equator, reveals the lineaments predominantly trending in the ENE-WSW directions. However, the observed ENE–WSW trends could be due faults of Eburnean 2000 Ma event of deformation (Obaje, 2009). The NNE-SSW trends on the other hand are attributed to the Pan-African

600 Ma orogenic event of deformation (McCurry, 1976). Meanwhile, the ENE-WSW, NNE-SSW and ESE-WNW obtained from this study correlated with most of the NNE-SSW trends that host mineralised deposits in accordance with (Ejepu *et al.,* 2018 and Salawu *et al*., 2019).
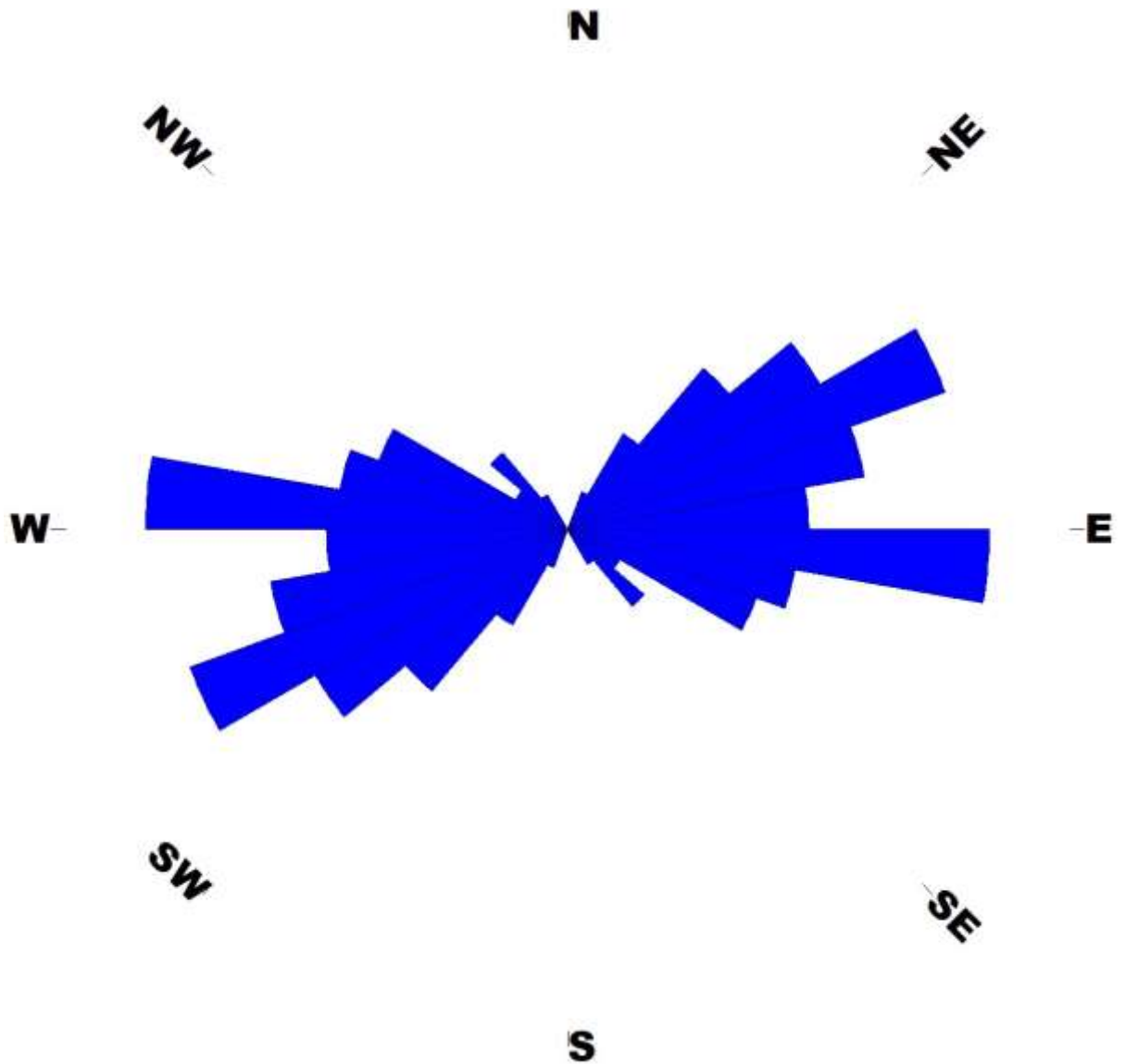

Figure 4.4: Rose diagram derived from reduced to pole lineaments of the study area

4.1.4 Interpretation of the reduced to equator first vertical derivative (FVD) maps

The visual inspection of the FVD map (Figure 4.5) reveals negative and positive FVD anomalies of different amplitudes. This map reveals both (positive and negative)

anomalies. Evidently, the study area falls within the low to high negative FVD anomalies in yellow to pink colours with values between -5.78 and 0.34 nT/m. The low to high negative FVD anomalies over the study area coincided with the relatively low RTE anomalies (Figure 4.2).
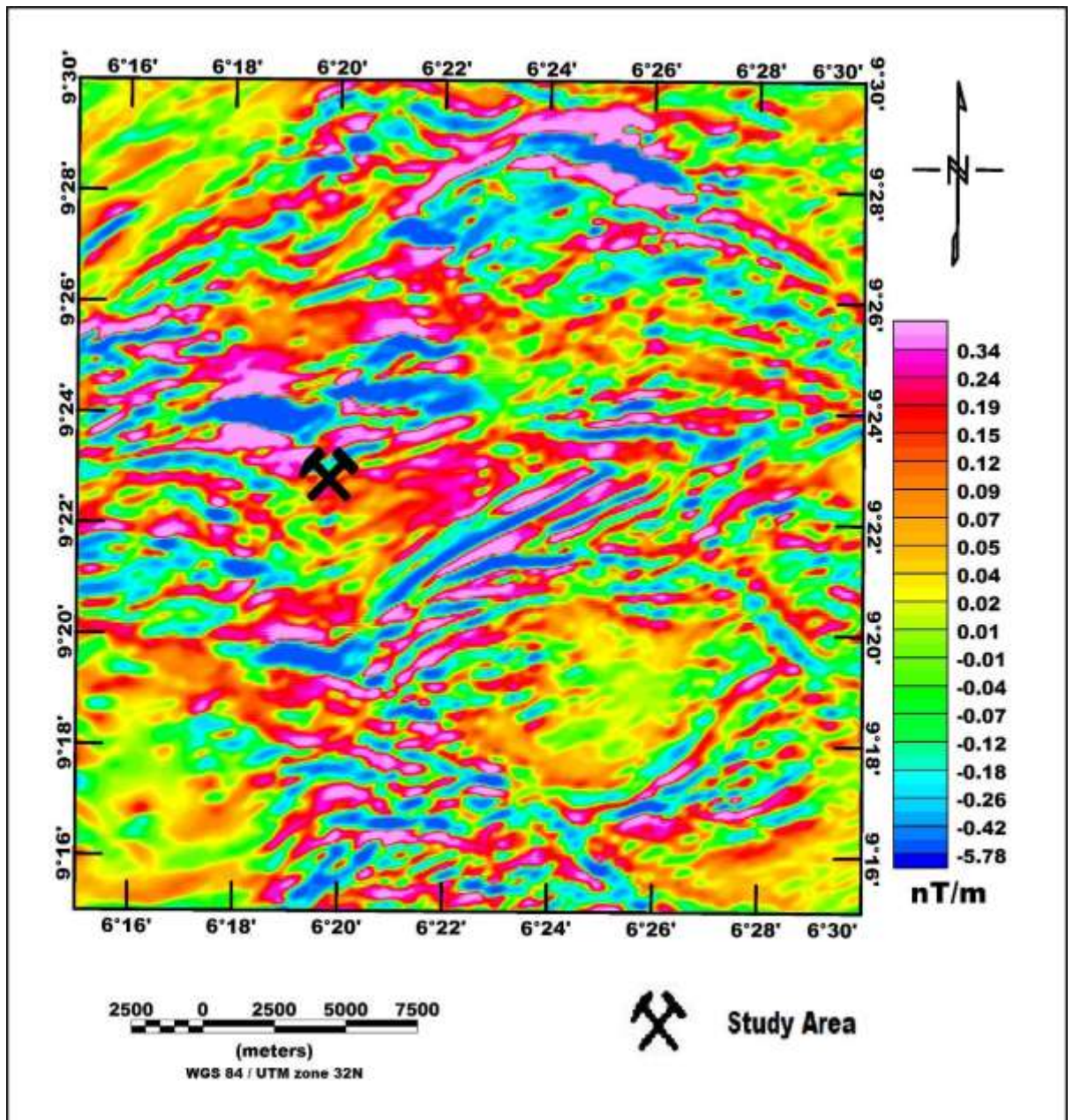
Figure 4.5: First vertical derivative map derived from the RTE data

The FVD map (Figure 4.3) enhanced the visibility of the short wavelength anomalies such as; faults, folds, shear zones among others, which were veiled up by the long wavelength anomalies in contrast to the RTE map (Figures 4.2). In a bid to examine the structural geologic features, the FVD anomalies were transformed into grayscale colour to have an enhanced view of the subsurface lineaments. The grayscale colour map (Figure 4.6) of the FVD unveils the distribution of the various oval and elongated

subsurface structural features. These structural features can be observed in bright white colour segments over the entire map. Interestingly, part of this bright white colour (lineament) cut across the study area. The RTE lineaments (Figure 4.6) were superimposed on the FVD grayscale map and a good correlation was observed. Thus, implying that the adopted methods complimented each other.
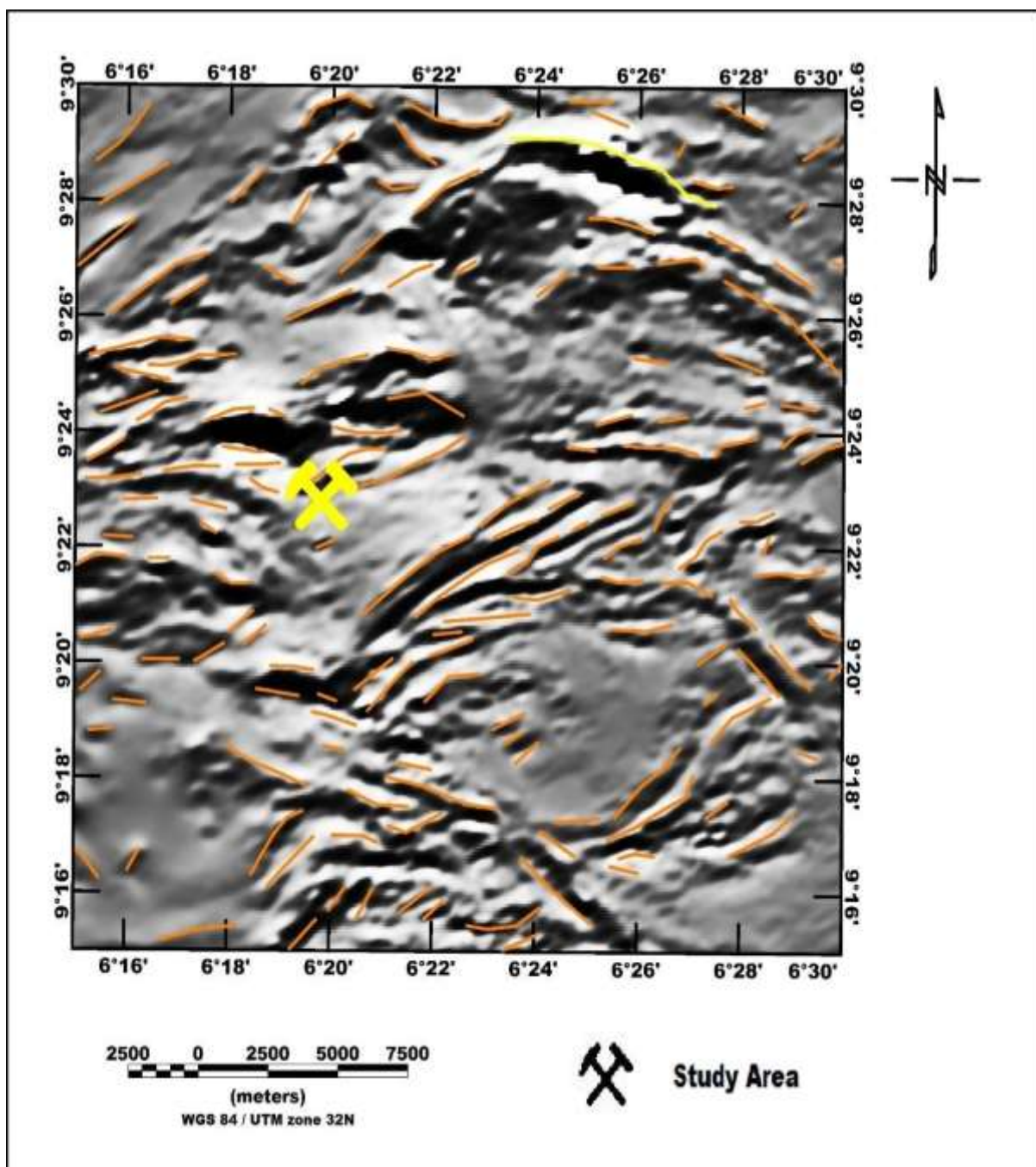

Figure 4.6: Grayscale first vertical derivative map derived from RTE anomalies

4.1.5: Interpretation of the reduced to equator Analytic signal (ASA) map The analytic signal (AS) amplitude map (Figure 4.7) displays the subsurface variations in the magnetic responses of the study area. The AS amplitude was estimated through the integrated calculations of both vertical and horizontal field components of the RTE anomalies. The AS amplitude map reveals wide range of values between 0.03 to 0.76 nT/m. Although, the regions of low RTE anomalies (Figure 4.2) signifies high AS amplitude (Figure 4.7) and vice versa. This sudden variation could be attributed to the suitability of analytic signal method at low latitude region. The AS method unlike first vertical derivative is independent of the direction of magnetisation. The present study area lies between high AS amplitude from the north and moderate AS amplitude from the south. The observed high and moderate AS amplitudes are due to short-wavelength anomalies that could be associated with mineralised deposits. These high and moderate AS amplitudes are quite similar to the short-wavelength as observed in Figures 4.5 and 4.6, resulting from the first vertical derivative maps.
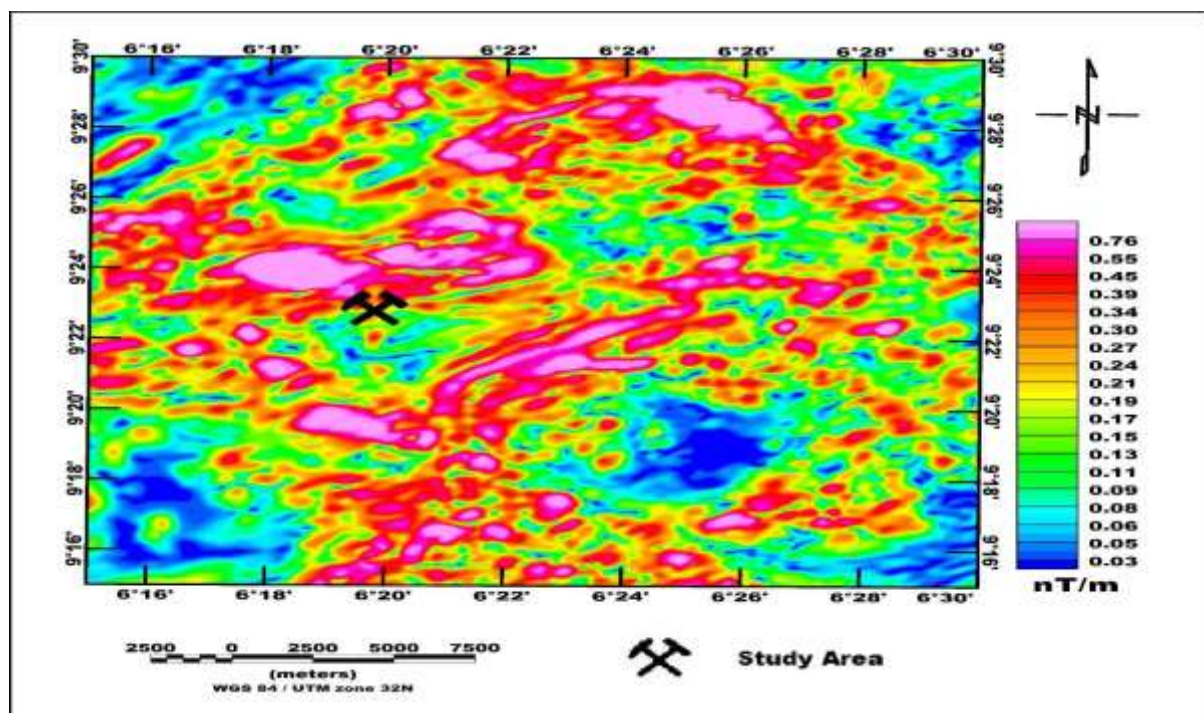

Figure 4.7: Analytic signal amplitude map produced from RTE anomaly

120

4.1.6 Interpretation of the reduced to equator Tilt derivative (TDR) map Tilt derivative (TDR) map (Figure 4.8) is an output of one of the shallow enhancement techniques is similar to first vertical derivative (FVD) and analytic signal (AS) amplitude. The TDR technique is less vulnerable to noise and thus, is suitable for mapping shallow basement structures and mineral exploration targets (Verduzco *et al.,* 2004). This technique depends on locating particular set of contours resulting from tilt angles (Salem *et al.,* 2008). The Tilt derivative is an effective technique used in locating vertical contacts from the reduced to magnetic equator (RTE) in low latitude region like the study area. The zero contours are employed to depict the spatial position of the edges of magnetic bodies. In general, the tilt derivative technique works under the presumption that source bodies are having vertical edges with no remnant magnetisation (Miller and Singh, 1994). The TDR map (Figure 4.8) show broad ranges of variations in anomalies with values from -0.06 to 1.42 rad/m, covering the study area and its environs. This map enhanced the edges of sources in contrast to the FVD and AS maps as shown in Figures 4.5 and 4.7.
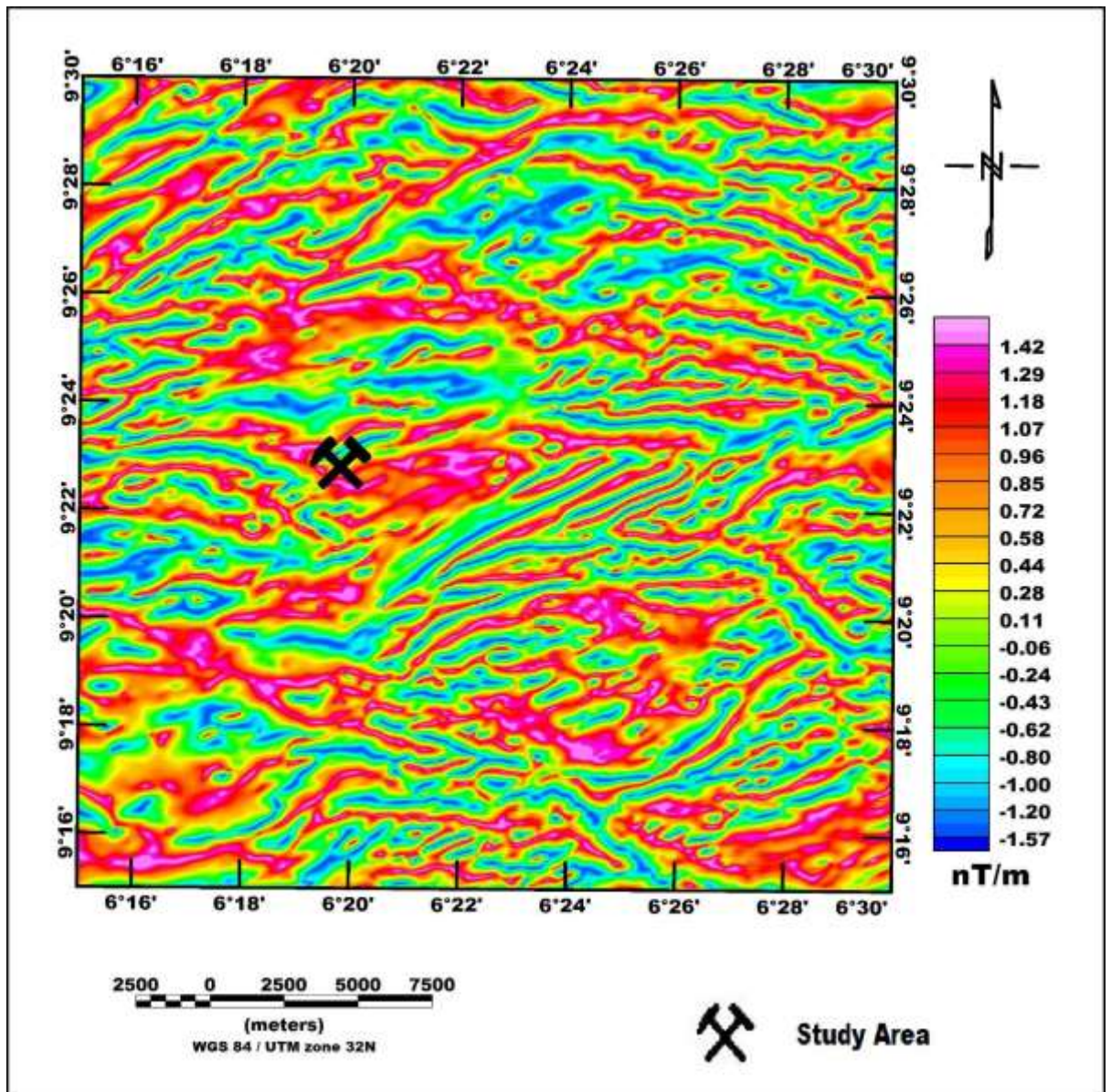
Figure 4.8: Tilt derivative (TDR) map produced from RTE anomaly

4.1.7 Interpretation of the 3-D Euler deconvolution depths map

The 3-D Euler deconvolution map (Figure 4.9) reveals the trend as well as estimate their

respective causative depths to the structural features. The depths obtained from these

structures varies between 38.0 and 428.5 m. The 3-D Euler deconvolution technique was

carried out on the total magnetic intensity anomaly data. This is because the 3-D Euler

deconvolution method is independent of the direction of magnetisation i.e., it does not

require the inclination and declination information prior to the depth estimation. The

depth was estimated using a window size of 2550 m width and a maximum depth

tolerance of 14%. In addition, structural index of one for sills and dykes geological model was used. Additionally, the subsurface structural lineaments

(Figure 4.3) map is similar to the 3-D Euler deconvolution depth trends (Figure 4.9). Though, the trends from the 3-D Euler deconvolution depths solutions yields a better result in contrast to the subsurface structural lineaments (Figure 4.3). This is because a linear structure with NNE-SSW cut across the study area (Kataeregi mining site) which was not well captured in the RTE lineament map (Figure 4.3).
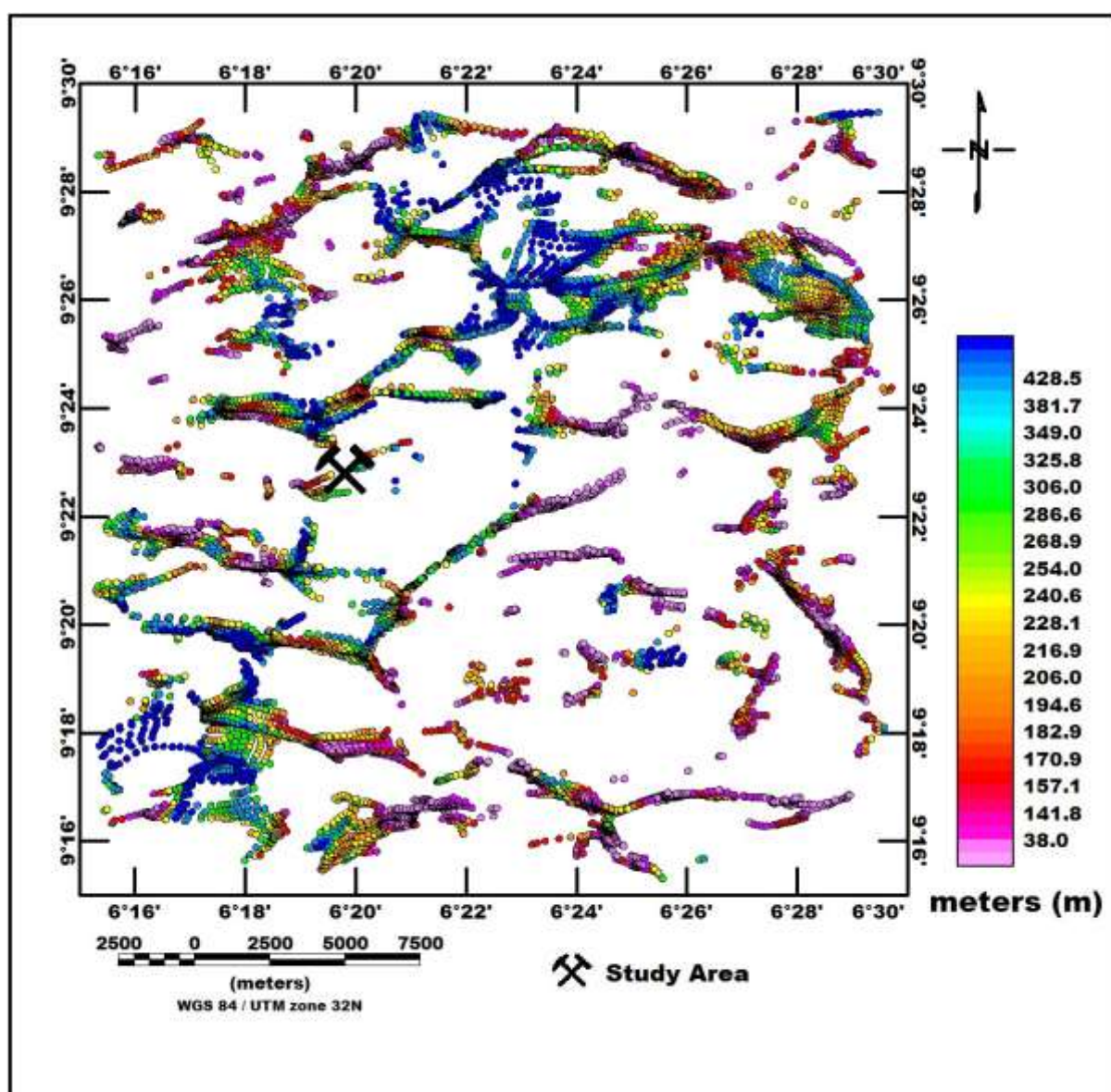

Figure 4.9: 3-D Euler deconvolution map computed from TMI data

4.2 Interpretation of structures associated with prospective heavy metals contamination from airborne data

The delineated RTE lineaments (Figure 4.3), FVD anomalies lineaments (Figure 4.5) and the 3D-Euler deconvolution lineaments (Figure 4.9) has aided in depicting the trends as well as the depths to the mineralised subsurface structures in and around the study area. These delineated lineaments represent structures like; faults, folds, fractures, shear zones among others, which acts as pathways for the migration and accumulation of the mineralised deposits (heavy metals). Thus, along these structures heavy metallic such as; arsenic, zinc, copper, nickel, lead, tin, zinc cobalt, gold among others are found. These heavy metals if properly harness can be of high economic importance to a country like Nigeria. In this regards, the artisanal miners that are operating over the present study area mainly focused on their primary target (gold). Thus, arrogantly, discharging other heavy metals as waste into air and waterways which perhaps contaminate in and around the study area. Heavy metals are metallic element that has relatively high density which are toxic in mild concentrations over time (Brempong *et al.,* 2016).. The possible coincidence between heavy metals and magnetic susceptibility has been affirmed in studies like (Hanesch and Scholger, 2002; Wang & Qin, 2005; Brempong *et al.,* 2016 and El Baghdadi *et al.,* 2012).

4.3 Resistivity Data Interpretation

The results of the 2D resistivity and chargeability inversion around the mining site as shown in figures 4.10 to 4.15 (5 profiles) as 2D inverted resistivity depth models with the help of RES2DINV software.

4.3.1 Interpretation of 2D models (Traverse 1)

The length of the entire profile (Laterally) is 500 m Figure 4.10a. The blue colour represent the horizontal distance starting from 30 m – 100 m extending to 110 – 190 m and continue laterally from 200 m to about 450 m. The resistivity value for the entire

profile ranges from 7.09 – 339 Ωm. The top soil along the traverse has resistivity values ranging from about 7.09 - 116 Ωm and thickness of about 2.58 m (vertically) with sandy - clay lithology (Table 3.1). The second layer extends from 2.58 - 43.0 m depth with resistivity values ranging between 117 – 198 Ωm representing a highly weathered/fractured layer composition, the layer has the possibility of aiding slimes or leach residue. The traverse is indicative of lateral and vertical migration of contamination at the top soil. Three distinctive layers were delineated as top soil, weathered/fractured layer and fresh basement.
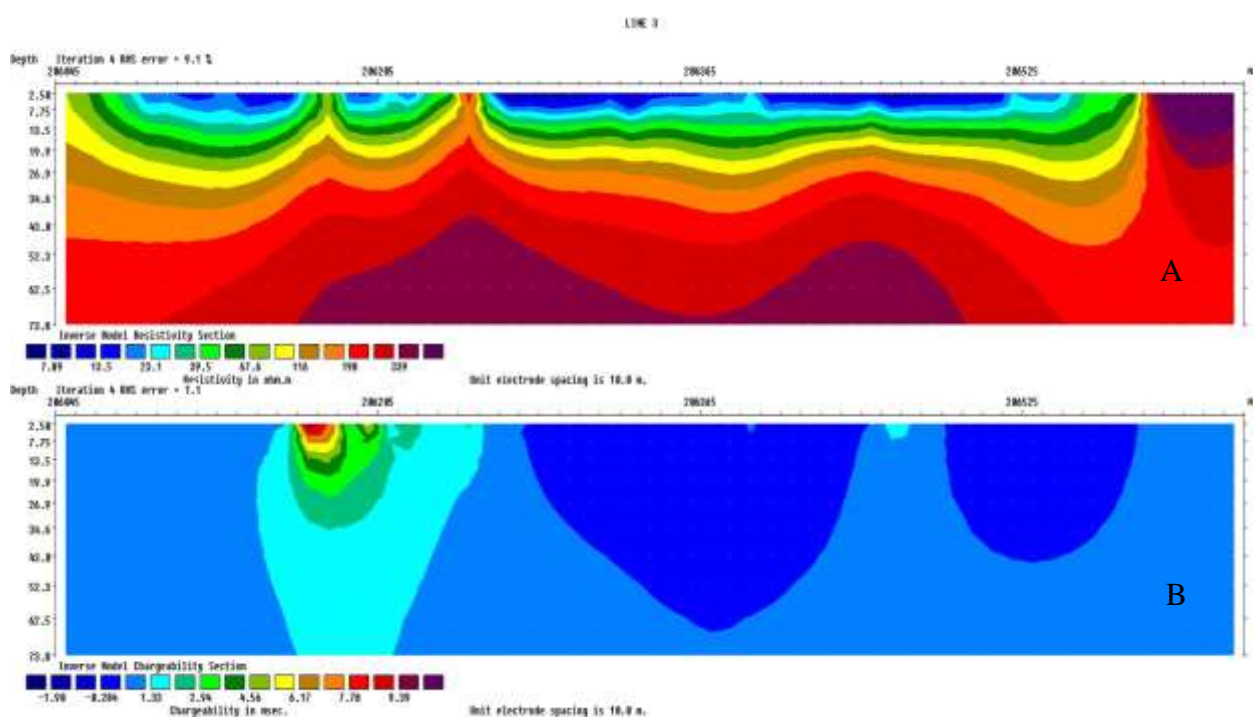
Figure 4.10: Inverse model resistivity section and inverse model chargeability section for traverse one

In order to obtain a better recognition of the different structural contacts and to define the alignment of mineralised vein in the study area, electrical tomography was employed. The first zone is at a distance of 160 m from the profile, (at a depth approximately13.5 m), its chargeability value exceed 6 m-sec, Figure 4.10b and its resistivity is around 200 ohm –m. The orientation of the electrical tomography profiles

is selected based on the direction of the vein portions noticed at the outcrop. The mineralisation zone is oriented NE – SW and E - W as seen in Figures 4.10, 4.11, 4.12, 4.13 and 4.14.

4.3.2 Interpretation of 2D models (Traverse 2)

The length of the entire profile (Laterally) is 500 m Figure 4.11a. The blue colour represent the horizontal distance starting from 100 m – 300 m and continue laterally extending to 350 – 450 m. The resistivity value for the entire profile ranges from 8.23 – 273 Ωm. The top soil along the traverse has resistivity values ranging from about 8.23 - 100 Ωm and thickness of about 2.58 m (vertically) with sandy - clay lithology (Table 3.1). The second layer extends from 2.58 - 62.5 m depth with resistivity values ranging between 111 and 273 Ωm representing a highly weathered/fractured layer composition. The inverse model sections of the subsurface and resistivity distribution derived from 2-D inversion in Figure 4.6a show continuous spread of leachate plume from horizontal distance of about 200 – 400 m in the north – south direction with

resistivity values below 10 Ωm, an indication of accumulation up to 11 m depth beneath the surface and may have reach the water table due to weathered basement below the basin shaped slimes or leach residue. The depth to water table is about 12 m as asserted by Idris-Nda *et al.* (2018) and Omanayin *et al*. (2016). Three distinctive layers were delineated as top soil, weathered/fractured layer and fresh basement. The mining residue (tailing) migration on the traverse originates the northern trends of the traverse to the surface.
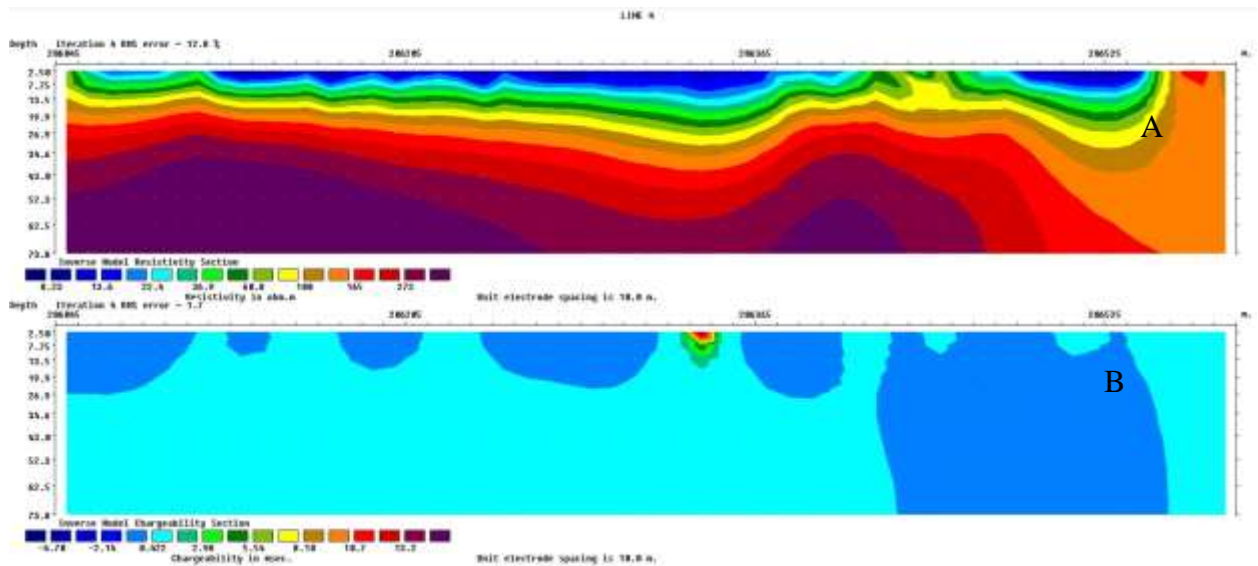
Figure 4.11: Inverse model resistivity section and inverse model chargeability section for traverse two

The inverse model chargeability of the profile figure 4.11b shows mineralised veins at about 300 m (laterally) in the traverse, trending NE – SW located at about 9 m (vertically) and its chargeability value exceeds 10 msec.

4.3.3 Interpretation of 2D models (Traverse 3)

The range of resistivity values along the profile varies from 2.5 to 377 Ωm (Figure 4.12). The resistivity distribution can be grouped into three different major zones corresponding to firstly the very low resistivity ($2 - 11$ Ωm) as the top soil which is believe to be large amount of mining waste or slimes originated from the mining trending along the entire profile (laterally) and the depth of about 2- 8 m. The second layer has a resistivity values ranging from $211 - 377$ Ωm and depth of about $9 - 27$ m which is indicative of weathered/fractured zone. Weathered/Fracture zone is well pronounced at 300 m and 470 m on the traverse. Three distinctive layers were delineated as top soil, weathered/fractured layer and fresh basement.
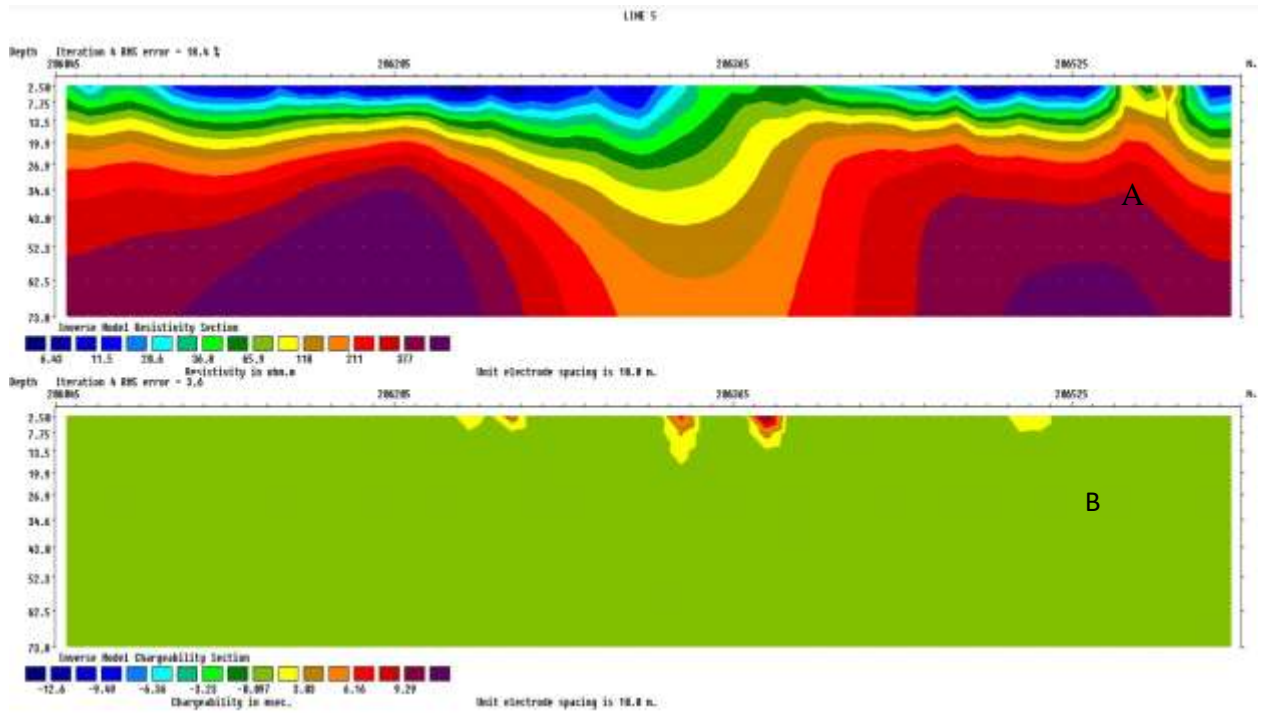
Figure 4.12: Inverse model resistivity section and inverse model chargeability section for traverse three

The results of the profile (Figure 4.12b) show structures in the prospected traverse (about 250 m on the profile). Its chargeability is around 9.3 msec. The anomaly is close the surface at NE, the veins is relatively small and these is attributed to the mining activity that is going on in the study area.

4.3.4 Interpretation of 2D models (Traverse 4)

The inverse models shows zone of low resistivity similar to the model in the Figure 4.13 but with slight differences. The profile consists of very low resistivity (6 – 12 Ωm) representing most likely the nines waste with depth less than 10 m (Figure 4.13a). The contamination is more pronounce in the central area of the traverse. The combination of faults and fractures (Figure 4.8a) are considered zones of permeability and have high transmissivity values than the surrounding massive bedrock, therefore, represent pathway for contamination migration, these is typically the definition of second layer of the profile with resistivity values ranging from 175 – 447 Ωm with estimated depth of about 10 – 27 m and the layer is above the water table. The depth to water table is about

128

12 m as asserted by Idris-Nda *et al.* (2018) and Omanayin *et al*. (2016). Three distinctive

layers were delineated as top soil, weathered/fractured layer and fresh basement.

Figure 4.13: Inverse model resistivity section and inverse model chargeability section for traverse four

The chargeability signatures in Figure 4.13b disseminated on the surface display large

IP were common on the center and towards the NE of the profile (200 m – about 400 m)

with depth range from 2 to 20 m, its chargeability is around 2- 7 msec (Figure

4.13b).

4.3.5 Interpretation of 2D models (Traverse 5)

The length of the entire profile (Laterally) is 500 m and the traverse is at the extreme

end of the profile in which the mining activity is fresh (Figure 4.9a). The resistivity value

for the entire profile ranges from 2 – 572 Ωm and the depth of entire profile is 2

– 74 m. The top soil along the traverse has resistivity values ranging from about 5 - 11

Ωm and thickness of about 2 – 7.5 m (vertically). The second layer extends from 10 - 35

m depth with resistivity values ranging between 155 and 572 Ωm representing a highly

weathered/fractured layer composition, the layer has the possibility of aiding

contamination. The traverse is indicative of lateral and vertical migration of

contamination at the top soil. Three distinctive layers were delineated as top soil, weathered/fractured layer and fresh basement.
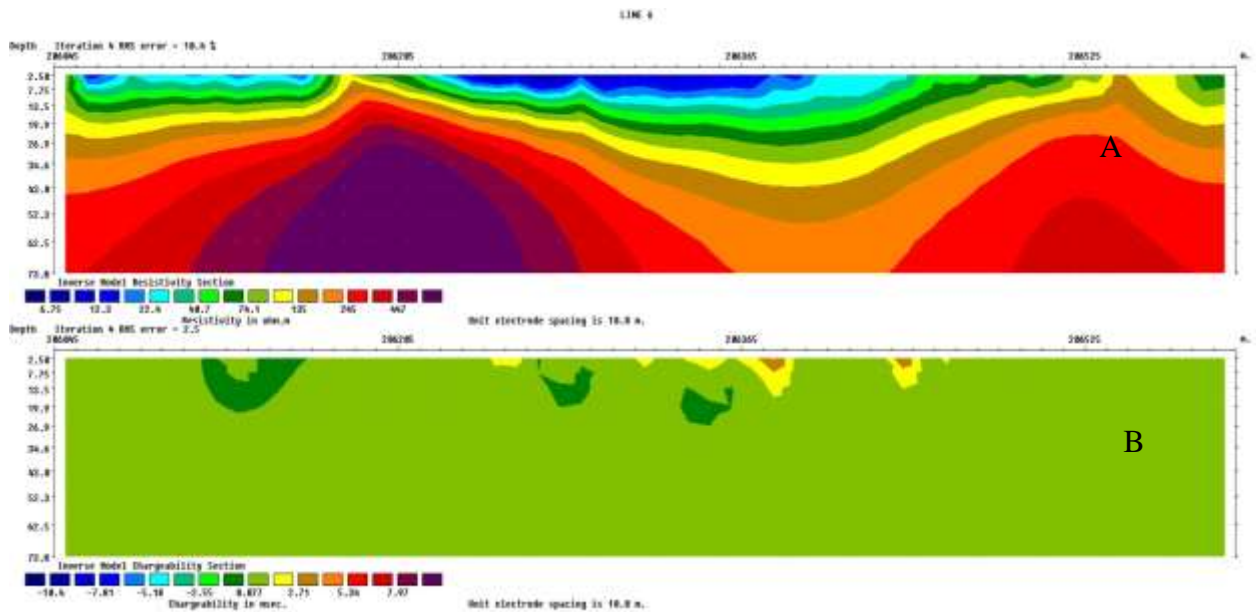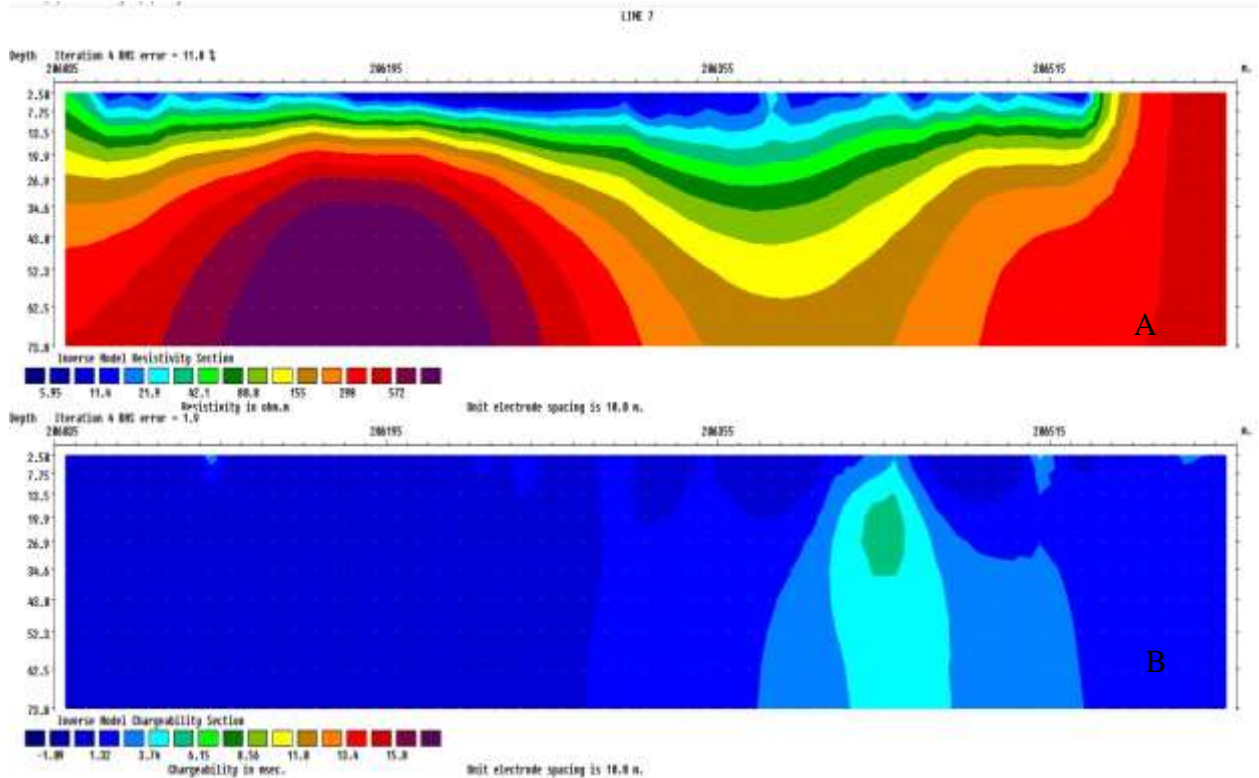

Figure 4.14: Inverse model resistivity section and inverse model chargeability section for traverse five

The chargeability value for figure 4.14b exceed 16 msec and its resistivity is around 500 ohm –m with depth of the vein clearly above 73 m. The orientation of the electrical tomography profiles is selected based on the direction of the vein portions noticed at the SW (Figure 4.14).

4.4. Interpretation of Travel Time Curve and Velocity Models through Profile after Tomography

Travel time curve and velocity models through profiles after tomography showing the time of arrival of initiation and refracted wave, distribution of velocities within the profile. Three distinctive layers (top layer, weathered/ fractured layer and consolidated layer). The travel time curves and tomograms which were transformed into velocity models after tomography are given in appendix. Four seismic profiles were taken but

only one profile was interpreted due to the noise encountered in the field. The use of 2D tomography in the interpretation of the seismic data provided accurate depth sections and precise velocities for different layers.

4.4.1 Interpretation of travel time curve

The travel time curve Figure 4.15 is a graph showing the time taking for seismic wave to travel from the epicentre of an earth disturbance to seismograph stations varying distance away. The travel time taking were between 0 to 60 ms while the distance of the seismic wave represented with 6 unit. The distance covered was between 0 to 60 m each.
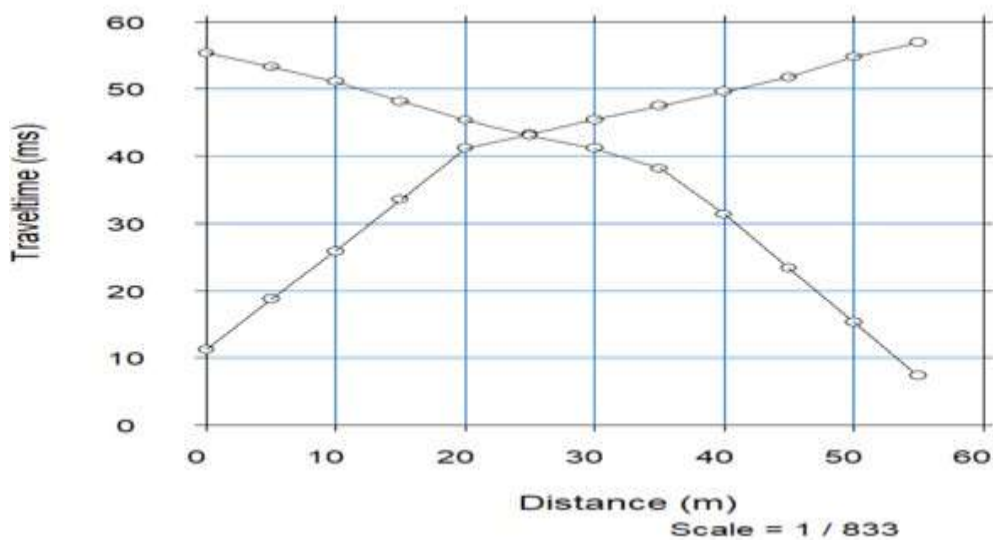
Figure 4.15 Travel time curve

4.4.2 Velocity model of profile after tomography

The velocity model of the subsurface is represented in 2D tomography as shown in Figure 4.16 The top layer which is characterised as the top soil has a velocity of 600 m/s and thickness of about 1.0 to 12 m. The velocity in this zone may be suggestive of unconsolidated materials. The top soil is underlain by a highly weathered/fractured basement with a velocity of 2000 m/s. The weathered basement intruded with fresh basement at a depth 26.0 m and lateral distance of about 30 – 60 m. The consolidated

layer has a velocity of 2850 m/s. Three distinctive layers were delineated as top soil, weathered/fractured layer and fresh basement.
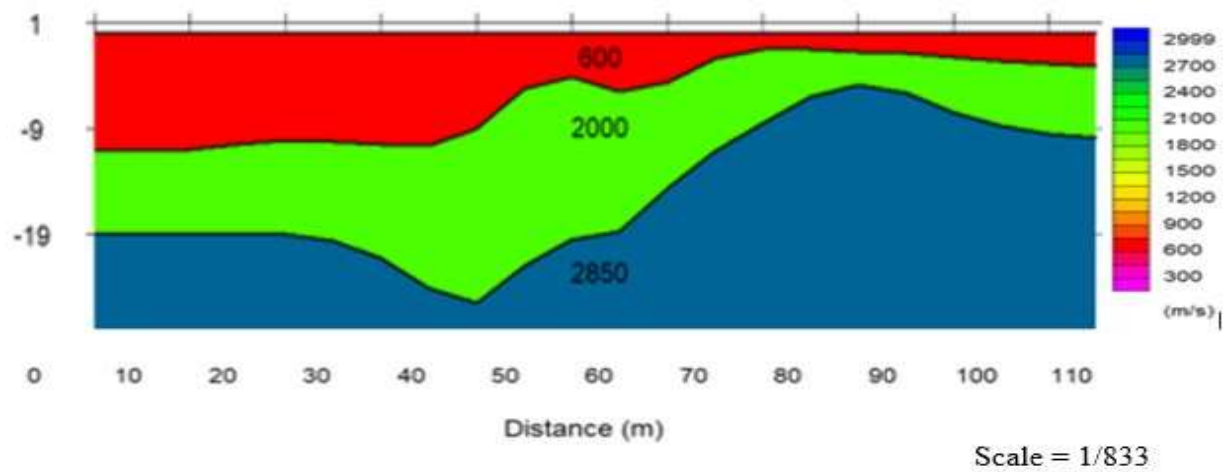
Figure 4.16 Velocity model of profile after tomography

4.5 Groundwater quality

Groundwater qualities were assessed via the physiochemical analysis of some parameters like pH, Zn, Pb, Fe, Cu, Cr, Cd, Ni, Hg, and Ar to ensure that standard set by World Health Organisation (WHO) and Nigerian Standard for Drinking Water Quality (NSDWQ) is adhered to. Assessment of the extent pollution with respect to exchangeable metals was carried out at the Federal Ministry of Water Resources, Regional Water Quality Laboratory, Minna and American Public Health Association (19th Edition).

4.5.1 Physical parameters of water

Table 4.1 shows the values of physiochemical parameters determined. Temperature ranges from 30.9 to 31.9 ^{0}C which is lower than the World Health Organisation (WHO) limit. Lower temperature may indicate the presence of pollutants (Omanayin *et al.*, 2016). The pH values ranges from 6.70 to 7.04 and within the allowable consumption

limit. Total Dissolve Solids varies from 210 to 338 mg/L falls below the standard and thereby recommended for domestic purposes. Electrical Conductivity varies from 323 to 520 μScm^{-1}, this is also within the prescribed values by World

Health Organisation (WHO) and Nigerian Standard for Drinking Water Quality (NSDWQ).

4.5.2 Physiochemical parameters of water, uses and percentage compliance

Maximum and minimum concentration of determined parameters and percentage compliance for the sampled parameters were shown in Table 4.2: Control site, well 1 – 4 were analysed and the distance of 100 m away from one well to the other was considered. The concentration level of Cadmium ranges from 0.000 mg/L and 0.003 mg/L while the control site is 0.000 mg/L, Copper ranges between 0.000 mg/L and 0.515 mg/L likewise the control site is 0.055 mg/L, Zinc ranges from 0.000 mg/L and 0.111 mg/L control site is 0.095 mg/L, all three analysed samples fell far below the permissible limit, and the percentage compliance level is 100%. Iron concentration varies between 0.03 mg/L and 13.6 mg/L with control site of 0.15 mg/L as shown in Table 4.1 with W_1, W_2, all above tolerable limit and the percentage compliance is 50%, arsenic ranges from 0.002 mg/L to 0.026 mg/L with well $_1$ and $_4$ been the affected, the control site value was 0.00 mg/L and the percentage compliance is 50%, nitrate concentration level far above the WHO and NSDWQ standard with the values ranging from 323.7 mg/L and 16.50 mg/L with control well stands at 29.0 mg/L, well $_1$, $_3$ and $_4$ all above tolerable limit and the percentage compliance is 25%. Mercury has concentration ranging level between 0.000 mg/L and 0.022 mg/L with well $_2$ been the possible contaminant, the control site remain at 0.000 mg/L and the percentage compliance is 75% while chromium has values ranging from 0.000 mg/L to 0.080 mg/L with well $_1$ having the value above the standard and the percentage compliance is 75%

with control site value of 0.00 mg/L and lead concentration value ranging between 0.000

mg/L and 0.001 mg/L with control well of 0.000 mg/L and the percentage compliance

is 100%.

Table 4.1: Summary of Physiochemical parameters of Water Samples

Parameters	Method	Control well	W_1	W_2	W_3	W_4	WHO	NSDWQ	Health Impact (NSDWQ, 2015, Ezugwu, 2015)
Temperature (^{0}C)	APHA 2550 B	30.9	31.5	31.5	31.1	31.9	35-40	-	-
Arsenic (mg/L)	APHA 3130 A	0.000	0.026	0.007	0.009	0.019	0.01	0.01	Cancer, Damages Kidney & Liver
Nitrate (mg/L)	APHA 4500 NO$_3$	29.0	109.2	16.50	288.0	323.7	50	50	Cyanosis and asphyxia
(pH)	APHA 4500H*B	3.70	6.73	6.76	6.70	7.04	7-8.5	6.5-8.5	Bitter taste
TDS (mg/L)	APHA 2510 B	210	338	312	232	312	1000	500	Shorten the life of hot water heaters
Electrical conductivity c	APHA 2510 B	323	520	466	357	480	1000	1000	None
Iron (mg/L)	APHA 3500 -Fe D	0.15	3.00	0.62	0.04	0.03	0.3	0.3	Bitter taste, brownish colour to clothing
Mercury (mg/L)	APHA 3130 A	0.000	0.000	0.022	0.005	0.004	0.006	0.001	Kidney and nervous system
Cadmium (mg/L)	APHA 3130 A	0.000	0.000	0.000	0.000	0.000	0.003	0.005	Toxic to liver & kidney, High blood pressure etc.
Chromium (mg/L)	APHA 3500 –Cr D	0.00	0.08	0.03	0.05	0.05	0.05	0.05	Cancer, respiratory damage
Copper (mg/L)	APHA 3500 Cu-D	0.055	0.515	0.000	0.000	0.000	2.0	1.5	Stomach & intestinal distress, liver & kidney damage
Lead (mg/L)	APHA 3130 A	0.000 mg/L	0.003	0.000	0.001	0.000	0.001	0.001	Cancer, toxic to central & nervous system, red blood cell
Zinc (mg/L)	APHA 3500 Zn-D	0.095	0.111	0.000	0.000	0.000	3.0	3.0	Aid in healing of wounds

Table 4.2: comparison of Physiochemical parameters of Water Samples with percentage compliance to WHO & NSDWQ

Parameters	Minimum	Maximum	Percentage compliance (%)	Water quality	Possible ranges for uses	WHO	NSDWQ
Temperature (^{0}C)	30.9	31.9	100	Excellent	Drinking, irrigation & industrial	35-40	-
Arsenic (mg/L)	0.002	0.026	50	Fair	Irrigation & industrial	0.01	0.01
Nitrate (mg/L)	16.50	323.7	25	Poor	Irrigation	50	50
(pH)	6.70	7.0 4	100	Excellent	Drinking, irrigation & industrial	7-8.5	6.5-8.5
TDS (mg/L)	210	338	100	Excellent	Drinking, irrigation & industrial	1000	500
Electrical conductivity µScm^{-1}	323	520	100	Excellent	Drinking, irrigation & industrial	1000	1000
Iron (mg/L)	13.6	0.03	50	Fair	Irrigation & industrial	0.3	0.3
Mercury (mg/L)	0.0000	0.0061	75	Good	Domestic, irrigation & industrial	0.006	0.001
Cadmium (mg/L)	0.000	0.003	100	Excellent	Drinking, irrigation & industrial	0.003	0.005
Chromium (mg/L)	0.00	0.08	75	Good	Domestic, irrigation & industrial	0.05	0.05
Copper (mg/L)	0.000	0.515	100	Excellent	Drinking, irrigation & industrial	2.0	1.5
Lead (mg/L)	0.00	0.017	100	Excellent	Drinking, irrigation & industrial	0.001	0.001
Zinc (mg/L)	0.000	0.111	100	Excellent	Drinking, irrigation & industrial	3.0	3.0

4.6 Physiochemical Properties of Soil

Table 4.3 shows the results of analysed soil samples within the vicinity of Kataeregi

mining site compared with the control site and the standard set up by the Canadian Soil

Quality Guidelines/World Health Organisation (CSQG/WHO) for the protection of the agricultural and human health values for each metal. Descriptive statistics using computed mean and standard deviation were employed to interpret the measured soil parameters (pH, Zn, Pb, Fe, Cu, Cr, Cd, Ni, Hg, and Ar) concentration. The results indicates that the measured soil pH for both the control site and the mining site are within the CSQG standard signifying a moderately alkaline soil type with normal distribution. Some parameters with high concentration as observed in Table 4.3 (S_1 for pH, S_1, S_2, and S_4 for Ar, , S_1, S_2, for Ni, S_1, S_3, and S_4 for Hg, S_1, S_2, S_3 and S_4 for Cd, S_1, S_2, S_3 and S_4 for Cr) were above the limit thereby causing harm to soil, crop and human health. For the parameters that have insignificant level of concentration, the contaminants may have been seeped down the soil to ground water (Yusuf *et al.*, 2018a).

Soil pH values of various locations ranged from 6.08 to 8.12 which is indicative of moderately alkaline, Ar values ranged from 4.23 mg/kg to 12.05 mg/kg which is above the standard, Ni values ranged from 4.00 mg/kg to 70.0 mg/kg is also above the standard set for agricultural and human health, Fe ranged from 0.72 mg/kg to 16.03 mg/kg is below the standard set by CSQG, Hg values ranged from 0.11 to 1.01 which is above the standard, Cd values ranged from 4.76 mg/kg to 9.32 mg/kg is also indicative of high concentration of chemical parameters and Cr ranged from 9.89 mg/kg to 27.00 mg/kg is above standard.

Cu values ranged from 99.78 mg/kg to 111.9 mg/kg while Pb values ranged from 1.0 mg/kg to 6.07 mg/kg and Zn values ranged from 9.91 mg/kg to 13.0 mg/kg all those parameters are within the standard.

Table 4.3: Chemical properties of soil Samples

Parameters (mg/Kg)	Control site	S1	S2	S3	S4	Min.	Max.	Mean	S.D.	CSQG/WHO (mg/Kg)

Temperature (°C)	25.2	25.0	25.0	25.0	25.0	25.0	25.2	25.0	0.1	-
Ph	2.27	8.12	7.57	6.08	6.62	6.08	8.12	7.13	0.79	6 – 8
Arsenic	4.23	9.89	12.05	9.92	11.00	4.23	12.05	9.42	3.03	9.8
Nitrate	7.01	49.41	70.0	8.60	4.00	4.00	49.41	33.8	27.8	35
Iron	3.6	3.00	0.72	16.03	5.05	0.72	16.03	7.68	6.75	20
Mercury	0.10	0.20	0.12	0.19	1.01	0.11	1.01	0.33	0.49	0.18
Cadmium	0.76	9.32	6.00	8.70	6.50	4.76	8.70	7.06	1.91	1.4
Chromium	1.89	20.10	18.43	27.00	12.00	9.89	27.00	17.5	6.82	6.4
Copper	86.00	100.1	111.1	99.78	111.9	86.00	111.9	102	10.6	270
Lead	1.04	4.44	1.00	1.50	6.07	1.00	6.07	2.40	0.81	70
Zinc	9.91	13.0	11.55	11.01	10.00	9.91	13.0	11.1	1.27	200

CHAPTER FIVE

5.0   CONCLUSION AND RECOMMENDATIONS

5.1 Conclusion

In an attempt to assess the level of contamination over Kataeregi mining site integrated geophysical investigation and geochemical analyses of water and soil were carried out. Good correlation exist between interpreted airborne magnetic data and electrical resistivity inversion in groundwater and soil quality assessment. Generally inverse models of all the electrical resistivity tomography lines show low resistivity values of less than 10 Ωm for all the top soil which is indicative of slimes as a result of the mining activities, the depth to mine waste was estimated to be around 0 - 2 m and resistivity

values were observed as representing the most contaminated zones in all inverse models. The distinction of weathered and fractured formation, faults, folds, fractures and shear zones helped in conceptualising the groundwater contamination. The chargeability of all the profile suggest the continuity of the vein or the high chargeability of the models with the depth not exceeding 30 m.

Seismic refraction methods delineated three distinctive layers (top soil has velocity of 600 m/s, weathered/fractured layer has velocity of 2000 m/s with a depth of 26 m and fresh basement has a velocity of 2850 m/s) with different thickness and lithology. The velocity increases with depth. The correlation between the seismic refraction and electrical resistivity exists, with all the method having three layers of top soil, weathered/fractured layer and fresh basement, even though the same number of layers is delineated, a thickness variation exists due to different properties measured by the two methods but the resistivity as indicated mine waste (dump) at the top soil.

The result of geochemical parameters on the analysed groundwater are within the specified limit set by World Health Organisation, Nigerian Standard Drinking Water Quality. However the activity of artisanal mining in the area has impacted on the environment with about 20% of the area directly or indirectly contaminated (Tables 4.1, 4.2 and 4.3). The possible contamination may be as a result of element migration and extent of migration depth. Consequently the activities has led to environmental degradation, erosion and loss of vegetation. The research has shown significant relationship between magnetic susceptibility and heavy metals. Magnetic method has proved suitable for measuring and indicating heavy metal pollution.

5.2 Recommendations

i.   It is recommended that groundwater be monitored periodically and treated before use to ensure that it is fit for intended purpose. There may be possible contamination of shallow and deep groundwater system in the nearest future if proper and possible mitigation measures are not taken into consideration at the mining site.

ii.   The area delineated with high chargeability should be harnessed for mineralisation using a modern instrument that will reduce indiscriminate dumping of mine waste/slimes and thereby degrading the environment.

iii.   Regulations and remediation methods should be in place to checkmate the effect of mining during and after the mining activity. Source control and containment remedies can be put in place.

iv.   Remediation of heavy metal contaminated soils is necessary to reduce the risks associated with mining, make the land resources suitable for agricultural production, enhance food security and scale down land tenure problems arising from changes in the land use pattern.

v.   Other researchers should focus in identifying the individual minerals in the study area so as to reduce over reliance on gold deposit.

5.3 Contribution to Knowledge

The thesis established that the tomography model delineated three distinctive layers of top soil with velocity of 600 m/s, weathered/fractured layer has a velocity of 2000 m/s and fresh basement with a velocity of 2850 m/s. The 3-DEuler revealed lineaments trending in NE-SW directions. The FVD map showed the oval and linear shapes anomalies with values between -5.78 to 0.34 nT/m, the ASA amplitude map revealed wide range of values between 0.03 to 0.76 nT/m, the TDR map established variations in

anomalies with values ranging from -0.06 to 1.42 rad/m. The research has presented a guide to water portability of the study area. The low resistivity values of <10 Ωm was observed at the top soil and may be suggestive of mine waste. The research has shown that the activities of artisanal miners has led to environmental degradation, dust pollution, soil erosion and loss of vegetation in the study area. All these findings imply that the activity of artisanal miners in the study area has impacted negatively on the environment.

REFERENCES

Adebayo A. S., Ariyibi E. A., Awoyemi M. O. & Onyedim G. C. (2015). Delineation of Contamination Plumes at Olubonku Dumpsite Using Geophysical and Geochemical Approach at Ede Town, Southwestern Nigeria. *Geosciences,* 5(1):39-45.

Adebiyi S. Adebayo, Emmanuel A. Ariyibi, Oluwaseyi A. Dasho, Charles I. Adenika & Emmanuel O. Olagunju (2021) Structural Interpretation Of Magnetic and Satellite Remotely Sensed Data of Osun State, Southwestern, Nigeria, *NRIAG Journal of Astronomy and Geophysics*, 10:1, 347-360.

Adegoke Anthony & Ajayi O. W. (1988): Groundwater Prospects in Basement Complex Rock of South Western Nigeria. *Journal of African Earth Sciences,* Vol. 7, No. 1. pp. 227-235.

Adelusi. A. O. Akinlalu A. A. & Adebayo S. S. (2013). Geophysical and Hydrochemistry Methods for Mapping Groundwater Contamination around Aule area, Akure, Southwestern Nigeria, *International Journal of Water Resources and Environmental Engineering, 5(7):* 442-451.

Adesoye, S.A., (1986). Master plan of Federal University of Technology, Minna, permanent site. Unpublished Report, 46-48.

Ajakaiye D. E., Hall D. H., Ashiekaa JA. & Udensi E. E. (1991). Magnetic anomaliesin the Nigerian Continental mass based on aeromagnetic surveys. *Tectonophysics* 192(1):211-230

Ajibade, A.C., Anyanwu, N.P.C., Okoro, A.U. & Nwajide, C.S. (2008). The Geology of Minna Area: Explanation of 1:250,000 Sheet 42 (Minna). Nigeria *Geological Survey agency Bull*. No 43, p. 112.

Ajibade, A. C. (1976). Provisional Classification and Correlation of the Schist Belt in Northwestern Nigeria. *Elizabethan Publishing Company*, Ibadan, 85-90.

Akinloye (1983): Hydro-geological Investigation or Groundwater Development at Obada Oko, Abeokuta Technical Brink Zones and Company Ltd. Ibadan. *Geology*. Vol 26, No.1. pp. 10

Alabi, A. A., Ogungbe A. S, Adebo B. & Lamina O. (2010) Induced polarization interpretation for subsurface characterisation: A case study of Obadore, Lagos State, *Scholars Research Library, Archives of Physics Research,* 1(3):34-43

Alexandros Liakopoulos, Bruno Lemiere, Konstantinos Micheal, Catherine Crouzet & Valerie Laperche (2010). Environmental Impacts of Unmanaged Solid Waste at a Former Metal Mining and Ore Processing Site, *Waste Management and Research*, 28(11), 996-1009.

Alex Gore D. and G. A. Olyphant (2010) Mapping the Variability of Groundwater Quality in an Abandoned Tailings Deposit Using Electromagnetic Geophysical Techniques, *Proceedings America Society of Mining and Reclamation*, 403414.

Alvin K. Benson, Kelly L. Payne & Melissa A. Stubben (1997) Mapping groundwater contamination using dc resistivity and VLF geophysical methods—A case study. *Geophysics,* 62(1): 80–86.

Ameloko A. A. & Ojigbo O. O. (2015): 2D Geophysical Evaluation of Subsoil Contamination, *Petroleum and Coal* 57(2): 135 – 142

Amstrong M. & Rodegheiro A (2006). Airborne Geophysical Techniques in Aziz. Coal Operators' Conference, *University of Wollongong and the Australasian Institute of Mining and Metallurgy* 113-131

Andres Gonzales Amaya, Torleif Dahlin , Gerhard Barmen & Jan-Erik Rosberg (2016): Electrical Resistivity Tomography and Induced Polarization for Mapping the Subsurface of Alluvial Fans: A Case Study in Punata (Bolivia). *Geosciences 6(51)1-13.*

Annapoorna H. & Janardhana M.R. (2015). Assessment of Groundwater Quality for Drinking Purpose in Rural Areas Surrounding a Defunct Copper Mine. *Aquatic Procedia*, (4). 685–692.

Bayode & Adeniyi, (2014). Integrated geophysical and hydrochemical investigation of pollution Associated with the Ilara-Mokin Dumpsite, Southwestern Nigeria. *American International Journal of Contemporary Research,* 4(2): 150-160.

Balasubramanian A. (2017) Chemical Properties of Soils, Centre for Advanced Studies in Earth Science, University of Mysore, Mysore Page 1-11

Beard, L. P. & Goitom, B. (2000). Some Problems in Interpreting Low Latitude Magnetic Surveys.6th EAGE/EEGS Meeting.

Baranov, V. (1957). A new method for interpretation of aeromagnetic maps: pseudogravimetric anomalies. *Geophysics* 22, 359-383.

Beatrice Abila & Jussi Kantola (2013). Municipal Solid Waste Management Problems in Nigeria: Evolving Knowledge Management Solution. *International Journal of Environmental and Ecological Engineering,* 7(6): 303-308.

Benson Nsikak U. Paul A. Enyong, & Omowunmi H. Fred-Ahmadu (2016). Trace Metal Contamination Characteristics and Health Risks Assessment of *Commelina africana* L. and Psammitic Sandflats in the Niger Delta, Nigeria*, Applied and Environmental Soil Science,* http://dx.doi.org/10.1155/2016/8178901

Blight G. & Fourie A. (2005) Catastrophe revisited disastrous flow failure of mine municipal solid waste. *Geotechnical Geology & Engineering,* 23: 219-248.

Brempong F., Mariam Q & Preko K. (2016). The use of magnetic susceptibility measurements to determine pollution of agricultural soils in road proximity. *African Journal of Environmental Science and Technology*. 10 (9), pp. 263271.

Bityukova L, Scohlger R & Birke M. Magnetic susceptibility as indicator of environmental pollution of soils in Tallin. *Physical Chemistry Earth* 1999. 24:829-835.

Cabala, J., Zogala, B. & Dubiel, R. (2008). Geochemical and Geophysical Study of Historical Zn – Pb Ore Processing Waste Dump Areas, Southern Poland, *Polish Journal of Environmental Studies*, 17(5): 693-700.

Custodio, E, (2013). Trends in groundwater pollution: Loss of groundwater quality & related services - Groundwater Governance. *Global Environmental Facility* (GEF).

Commission of the European Communities, Communication from the Commission on safe operation in mining activities: a follow-up to recent mining accidents, COMM (2000) 264 final, dated 23.10.2000.

Core, D., Buckingham, A & Belfield, S. (2009). Detailed structural analysis of magnetic data done quickly and objectively, SGEG Newsletter.

David L. Campbell & David V. Fitterman (2014). Geoelectrical Methods for Investigating Mine Dumps, Proceeding of the Symposium on the Application of Geophysics to Engineering and Environmental Problems, march 23 – 26, 19 Reno Nevada, 261 – 270.

Dimitri Ilich Kerbauy Veloso, Cesar Augusto Moreira & Ariane Raissa Pinheira Cortes (2015) Integration of Geoelectrical Methods in the Diagnostic of a Diesel Contaminated site in Santa Ernestina (Sp. Brazil), *Revista Brasilera de Geofisica* 33(4): 667-676.

Douglas I. & Lawson N. (2000) An earth science approach to assessing the disturbance of the Earth's surface by mining, School of Geography, the University of Manchester.

Ejepu J. S., Unuevho C. I., Ako T. A. & Abdullahi S. (2018). Integrated geosciences prospecting for gold mineralization in Kwakuti, North-Central Nigeria. *Journal of Geology and Mining Research*, 10(7):81-94.

El Baghdadi M., Barakat, A., Sajieddine, M. & Nadem, S. (2012). Heavy metal pollution and soil magnetic susceptibility in urban soil of Beni Mellal City (Morocco). *Environmental Earth Sciences,* 66(1):141-155.

Eugeniusz Koda , Andrzej Tkaczyk , Mariusz Lech & Piotr Osin´ski (2017)Application of Electrical Resistivity Data Sets for the Evaluation of the Pollution Concentration Level within Landfill Subsoil, *Applied. Science*, 7, 262.

Ezugwu C. N. (2015). Groundwater Contamination and Potential Health Effects, *International Journal in IT and Engineering.* 3(1): 83-93.

Ganiyu S. A., B. S. Badmus, M. A. Oladunjoye, A. P. Aizebeokhai, V. C. Ozebo, O. A. Idowu & O. T. Olurin (2016). Assessment of Groundwater Contamination around active dumpsite in Ibadan Southwestern Nigeria using integrated Electrical Resistivity and hydrochemical Methods. *Environmental Earth* Science, 75:621-643.

Ganiyu S. A., Badmus B. S., Oladunjoye M. A., Aizebeokhai A. P., Ozebo V. C., Idowu O. A. & Olurin O. T. (2015). Delineation of Contamination Plumes Migration using Electrical Resistivity Imaging on Lapite Dumpsite in Ibadan Southwestern Nigeria. *Environmental Earth* Science, 5(2):70-80.

George, I. L. (1992). Geology and Environment of Western Europe, Oxford University Press, Oxford, England. Waste disposal site: A case study from Isparta, Turkey. *Environmental Geology,* 40(6): 725-731.

Harish E. & David M. (2015) Assessment of Potentially Toxic Cyanide from the Gold & Copper Mine Ore Tailings of Karnataka, India. *International Journal of Science and Technology*, 3: 171-178.

Hanesch M & Schloger R (2002). Mapping of heavy metal loadings in soils by means of magnetic susceptibility measurements. *Environmental. Geology*. 42:857-870

Ibrahim Dakir, Ahmed Benamara, Habiba Aassoumi, Abdessalam Ouallali, & Youssef Ait Bahammou (2019): Application of Induced Polarization and Resistivity to the Determination of the Location of Metalliferous Veins in the Taroucht and Tabesbaste Areas (Eastern Anti-Atlas, Morocco). *Hindawi International Journal of Geophysics* 1-12

Idris-Nda A., Waziri N.M., Bida A.D. & Abdullahi S. (2018) Socio-Economic Impacts of Artisanal and Small-Scale Mining in Parts of Niger State, North Central Nigeria. *International Journal of Mining Science (IJMS),* 4(3): 21 – 30

Idris-Nda A., Abubakar S. I., Waziri S. H., Dadi M. I. & Jimada A. M. (2015) Groundwater development in a mixed geological terrain: a case study of Niger State, central Nigeria. WIT Transactions on Ecology and the Environment, 196. 77-88

Jolanta Pierwoła (2013) Investigation of Soil Contamination Using Resistivity and Induced Polarization Methods, *Poland. Journal Environmental Studies,* 22(6):1781-1788.

Kalaivanan K., Gurugnanam , B., Hamid Reza Pourghasemi, Suresh, M. & Kumaravel S., (2017). Spatial assessment of groundwater quality using water quality index and hydrochemical indices in the Kodavanar sub-basin, Tamil Nadu, India. *Sustain Water Resources Management.* 15 pp. 5-7

Kearey, P., Brooks, M. & Hill, I. (2009). An introduction to geophysical exploration. John Wiley & Sons.

Kelvin M. Hiscock (2005): Hydrogeology Principles and Practice. *Blackwell Publishing Company*

Kohnen, H. (1974).   The temperature dependence of seismic waves in ice. *Journal of Glaciol,* 13(67):144–147.

Khan S., Cao Q., Zheng Y. M., Huang Y. Z., & Zhu Y. G. (2008) "Health risks of heavy metals in contaminated soils and food crops irrigated with wastewater in Beijing, China," *Environ- mental Pollution*,152 (3), 686–692

Leu, L. K. (1981). Use of reduction - to- equator process for data interpretation: presented at the 51st *Annual, international. Management of Sattelite Experimenntal Geophysics, Geophysics,* Vol 47, p 445.

Loke, M. (2001). Tutorial: 2-d and 3-d electrical imaging surveys. Copyright (19962012).

Manungufala T. E., M. Sabiti-Kalule & I. Aucamp (2005). Investigation into the slimes dams, mine dumps and lanfills (residue dposits) as environmental constraints to low-cost housing projects in Gauteng, South Africa. *World Congress on Housing*, XXXIII IAHS, 27(3).

Mara, D. and Evans, B. (2011). Sanitation and water supply in low-income countries. Ventus Publishing, 142 pp.

Massally, R-E.M., Sheriff, A.B., Kaitibi, D., Abu, A., Barrie, M. & Taylor,   E. T. (2017).Comprehensive Assessment of Groundwater Quality around a Major Mining Company in Southern Sierra Leone. *Journal of Water Resource and Protection*. (9), 601-613.

Mathias Ronczka, Kristofer Hellman, Thomas Gunther, Roger Wisen, & Torlief Dahlin (2017). Elecric Resistivity and Seismic Refraction Tomography: a Challenging Joint Underwater Surveya at Aspo Hard Rock Laboratory. *Solid Earth*, 8(671-682).

Médecins Sans Frontières (MSF) (2010). Roport The response to the mass lead poisoning in Zamfara State with funding of US$ 1.9 million.

Mccury, P. (1976). the geology of part of pre-Cambrian to lower paleozoic rocks of Northern Nigeria. A review in geology of Nigeria (Editor Kogbe, C.A) *Elizabeth & publishing co. Lagos Nigeria,* 7, 15-39.

McGlasshan N. D. (2004). Contrasts of Cancer rates among black gold miners from Transkei and Lesotho, *South African Journal of Science*, 100:491-497.

Milsom, J. (2007). Field geophysics, volume 25. John Wiley and Sons.

Miller, H.G. & Singh, V. (1994). Potential Field Tilt-A New Concept for Location of Potential Field Sources. *Journal of Applied Geophysics,* 32, 213-217.

Morrisson BL, Lawrence ARL, Chilton PJC, Adams B, Calow RC & Klinck BA (2003). Groundwater and its susceptibility to degradation: A global assessment of the problem and options for management. Early Warning and Assessment Report Series, RS. 03–3. Nairobi, Kenya: *United Nations Environment Programme*, p. 126.

Moghaddam S., S. Dezhpasand, A. Kamkar Rouhani, S. Parnow and M. Ebrahimi (2015): Detection & determination of groundwater contamination plume using time lapse electrical resistivity tomography (ERT) method, *Journal of Mining and Environment,* 523: 1- 10

Mücella Canbay (2010) Investigation of the relation between heavy metal contamination of soil and its magnetic susceptibility. *International Journal of Physical Sciences* 5(5), 393-400.

Nataliya Viktorovna Yurkevich, Natalya Aleksandrovna Abrosimova, Svetlana Borisovna Bortnikova, Yuriy Grigoryevich Karin & Olga Petrovna Saeva (2017) Geophysical investigations for evaluation of environmental pollution in a mine tailings area, Novosibirsk, Russia, *Toxicological and Environmental Chemistry*, 99(9–10): 1328–1345.

Obaje, N. G. (2009). Geology and Mineral Resources of Nigeria, Lecture Notes in the Earth Science Springer: Heidelberg.

Odeyemi, I.B. (1999). Late-Proterozoic metaconglomerates in the schist belt of Nigeria: Origin and tectonostratigraphic significance. *Journal of Technoscience*. Volume 3, pp.56-60

Okpoli C, & Akingboye A. (2016). Reconstruction and appraisal of Akunu–Akoko area iron ore deposits using geological and magnetic approaches. *RMZ – Materials and Geoenvironment Journal*, 63, 19-38.

Office for the Coordination of Humanitarian Affairs (OCHA) (2011): Lead poisoning from mining activities, Zamfara State - Update 1

Olasehinde, P. I. (1999): An Integrated Geologic and Geophysical Exploration Techniques for Groundwater in the Basement Complex of West Central Part

Part of Nigeria. *Journal of Nigeria Association.of Hydrogeologist* (Water Resources), 10(1). 46-49.

Olarewaju, V. O., Olorunfemi, M. O. & Alade, O. (1996): Chemical Characteristics of Groundwater from Some Parts of the Basement Complex of Central Nigeria. *Journal of Mining Geology*. 33(2). 135-139.

Olorunfemi M. O. and Olayinka A. I. (1992): Alteration of Geoelectric in Okene area and Implication for Borehole Sitting. *Journal of Mining and Geology*, pp. 403-411.

Olomo, K. O., Olayanju, G. M., Adiat K. A. N. & Akinlalu, A. A. (2018) Applied Integrated Approach Involving Aeromagnetic And Landsat For Delineating Structures And Its Implication On Mineralisation. *International Journal of Scientific & Technology Research*. (7)2, 208 - 217

Olubunmi Fagbote Emmanuel & Olanipekun Edward Olorunsola (2010) Evaluation of the Status of Heavy Metal Pollution of Sediment of Agbabu Bitumen Deposit Area, Nigeria
European Journal of Scientific Research 41(3) 373-382
http://www.eurojournals.com/ejsr.htm

Omanayin, Y. A., Ogunbajo, M. I., Waziri, N. M., Ako, T. A., Shuaibu, A. M & Alaku, I. O. (2016) Geochemical Investigation and Physical Impact Assessment of Artisanal Gold Mining, Kataeregi, North-Central Nigeria, *International Journal of Science for Global Sustainability,* 2(2). 21-35

Omanayin, Y. A., Ogunbajo, M. I., Amadi, A. N., Abdulfatai, I. A. & Mamodu, A. (2016) Water quality investigation within the neighbourhood of Kataeregi artisanal gold mining sites, North-Central Nigeria. Journal *of information, Education, Science and Technology* (JIEST), 3(2):123-130.

Orisakwe,Orish Ebere., John Kanayochukwu Nduka, Cecilia Nwadiuto Amadi, Daniel Onyekachi Dike & Onyinyechi Bede (2012) heavy metals health risk assessment for population via consumption of food crops and fruits in owerri, south eastern, Nigeria, *Chemistry Central Journal* (http://journal.chemistrycentral.com/content/6/1/77)

Osazuwa I. B. & Abdullahi N. K. (2008). Geophysics Techniques for the Study of Groundwater Pollution: A Review. *Nigerian Journal of Physics*, 20(1):163174.

Oyeyemi, K. D., Aizebeokhai, A. P., Adegunodo, T. A., Olofinnade, O. M., Sanuade, O. A. & Olaojo, A. A. (2017): Subsoil Characterisation using Geolectrical Investigation, *International Journal of Civil Engineering and Technology*, 8(10)

Rahman M. A. (1979). Review of the Basement Geology of Southwestern Nigeria. In: Geology of Nigeria. C. A. Kogbe (ed). *Elizabethan Publishing Co*.: Lagos, Nigeria. 41-58.

Rahaman, M.A. (1988). Recent Advances in study of the Basement Complex of Nigeria Precambrian geology of Nigeria. In: OLUYIDE, P.O. ET AL., (eds) Precambrian Geology of Nigeria., *Geological Survey of Nigeria Publication Kaduna*, 11-43.

Ramalho E., J. Carvalho, S. Barbosa, F.A. & Monteiro Santos (2009) used geophysical methods to characterize an abandoned uranium mining site, Portugal. *Journal of Applied Geophysics,* 67: 14–33

Raymond A. Wuana and Felix E. Okieimen (2011) Heavy metals health risk assessment for population via consumption of food crops and fruits in Owerri, South Eastern, Nigeria, *International Scholarly Research Network,* Article ID 402647

Reid, A. B., Ebbing., J & Webb., S. J (2013). Avoidable Euler errors-the use and abuse of
    Euler deconvolution applied to potential fields. *Geophysics Prospecting*.

Reynolds, J. M. (2011). An introduction to applied and environmental geophysics. *John Wiley & Sons.*

Ritcey G. M. (1989) Tailings Management Problems and solutions in the mining industry. *Elsevier* ISBN 0-444-87374-0.

Rolland Andrade & Karunakar Goud B. (2011).Geophysical prospecting as a tool for site characterisation for mining dump waste, *e-Journal Earth Science India.* Popular Issue. www.earthscienceindia.info.

Saad R., Muztaza M. A., Zakaria M. T. & Saidin M. M. (2017). Application of 2D Resistivity Imaging and Seismic Refraction Tomography to Identify Sungai Batu Sedimentary Depositional Origin. *Journal of Geology and Geophysics,* 6(1).

Salawu, N. B., Olatunji, S., Adebiyi, S. L., Olasunkanmi, K. N. & Dada, S. S. (2019). Edge detection and magnetic basement depth of Danko area, north western Nigeria, from low-latitude aeromagnetic anomaly data. *Springer Nature Switzerland Applied Sciences,* 1, 1056.

Salako K. A, Adetona A. A, Rafiu A. A, Ofor N. P, Alhassan, D. U, & Udensi E. E. (2009). VES method to investigate the ground water at the south-western part (Site A) of Nigerian mobile Police Barracks (Mopol 12), David Mark Road, Maitumbi, Minna, *Journal of Science, Education and Technology,* 2 (1), 350 – 362

Salem, A., Williams, S., Fairhead, D., Smith, R., & Ravat, D. (2008). Interpretation of Magnetic Data Using Tilt-angle Derivatives. *Geophysics,* 73, L1-L10

Sayed S. R. Moustafa, Elkhedr H. Ibrahim, Eslam Elawadi, Mohamed Metwaly & Naser Al Agami (2012).Seismic Refraction and Resistivity Imaging for Assessment of Groundwater Seepage Under a Dam Site, Southwestern Nigeria, *International Journal of Physical Sciences,* 7(48): 6230-6239

Salisbury M. & Snyders D., (2007). Application of Seismic Methods to Mineral Exploration, in Goodfellow, W.D., ed., Mineral Deposits of Canada: A Synthesis of Major Deposit-Types, District Mettalogeny, the Evalution of Geological Provinces, and Exploration Method: *Geological Association of Canada,* Mineral Deposits Division, Special Publication. 5, 971-982.

Salehi M. H., Jorkesh S. H. & Mohajer R. (2013) Relationship between Magnetic Susceptibility and Heavy Metals Concentration in Polluted Soils of Lenjanat Region, Isfahan *http://www.e3s-conferences.org or http://dx.doi.org/10.1051/e3sconf/20130104003 p 1 - 3*

Seidu J. & Ewusi A. (2018). Assessment of Groundwater Quality using Hydrogeochemical Indices and Statistical Analysis in the Tarkwa Mining area Ghana, *Journal of Environmental Hydrology, 26(1) 1-14*

Sheriff, R. E. (2002). Encyclopedic dictionary of applied geophysics.

Shtivelman V. (2003). Application of Shallow shallow seismic methods to engineering, environmental and groundwater investigations, *Bollettino Di Geofisica Teorica Ed Applicata*, 44(3-4): 209-222.

Smejkalora M., Mikanora O. & Borurka L. (2003) Effect of Heavy Metal Concentrations on Biological Activity of Soil Micro-Organism. *Plant Soil and Environment*, 49: 321 326.

Smith L., Means J. L. & Chen A. (1995) Remedial Options for Metals-Contaminated Sites, *Lewis Publishers*, Boca Raton, Fla, USA.

Tamma Rao G., V. V. S. Gurunadha Rao, G. Padalu, Ratnakar Dhakate & V. Subrahmanya Sarma (2014): Application of electrical resistivity tomography methods for delineation of groundwater contamination and potential zones, *Arab Journal of Geosciences,* 7: 1373 – 1384

Tawey M. D., Alhassan D. U., Adetona A. A., Salako K. A., Rafiu A. A. & Udensi E. E. (2020) Application of Aeromagnetic Data to Assess the Structures and Solid Mineral Potentials in Part of North Central Nigeria. *Journal of Geography, Environment and Earth Science International,* 24(5): 11-29

Telford, W. M. & Sheriff, R. E. (1990). Applied geophysics, volume 1. *Cambridge university press.*

Trustwell J. F. & Cope R. N (1963). The geology of part of Nigeria & Zaria province Northern Nigeria, *Bulletin of Geology Survey of Nigeria,* 29.

Thompson, D. T. (1982). EULDPH-A new technique for making computer-assisted depth Estimates from magnetic data. *Geophysics,* 47:31–37.

Umar Hamzah, Mark Jeeva & Nur Atikah Mohd Ali (2014). Electrical Resistivity Technique and Chemical Analysis in the study of Leachate Migration at Sungai Sedu Landfill. *Asian Journal of Applied Sciences,* 7:818-535.

Umar Hamza, Mohd Azmi Ismail & Abdulrahim Samsudin (2008). Geophysical techniques in the study of hydrocarbon-contaminated soil. *Bulletin of the Geological Society of Malaysia, 54:133 – 138*

Ugwu S. A. & Nwosu J. I. (2009). Effect of Waste Dumps on Groundwater in Choba Using Geophysical Method. *Journal of Science Environmental Management*, 3(1): 85-89

United Nations Environmental Programme (UNEP) (2011): Lead poisoning kills 100 children in the North

United Nations Children's Fund (UNICEF) report (2010): Lead Poisoning Investigation in Northern Nigeria

United Nations Environmental Programme (UNEP (1996) *Guide to Tailings Dams and Impoundment –* Bulletin 106)

USEPA, (2007) Treatment technologies for site cleanup: annual status report (12th Edition)," Tech. Rep. EPA-542-R-07-012, *Solid Waste and Emergency Response* (5203P), Washington, DC, USA, 2007

Vega F. A., Covelo E. F. & Andrade M. (2006) Comparative sorption and desorption of heavy metals in mine soil: influence of mine soil characteristic. *Journal of Colloid Interface Science*, 298: 582-592.

Verduzco, B., Fairhead, J.D., Green, C.M. & MacKenzie, C. (2004). New insights into Magnetic Derivatives for structural mapping. *The Leading Edge*. 23, 116-119

Wang, Z, S & Qin, Y. (2005). Correlation between magnetic susceptibility and heavy metals in urban topsoil: a case study from the city of Xuzhou, China. *Environmental Geology*. 49:10-18.

World Health Organization (WHO) (1996): Cholera and Other Epidemic Diarrhoel Diseases Control, *Fact Sheets on Environmental Sanitation*, World Health Organization (WHO), Geneva.

World Health Organization (WHO) (2004). Guideline for drinking water quality. Lenntech water treatment and air purification Holding *Rotterdamseweg.*

Wyllie, M., Gregory, A., & Gardner, G. (1958). An experimental investigation of factors affecting elastic wave velocities in porous media. *Geophysics*, 23(3):459–493.

Yi-Chun Lo; Dooyema, Carrie A.; Neri, Antonio; Durant, James; Jefferies, Taran; Medina-Marino, Andrew; Ravello, Lori de; Thoroughman, Douglas & Davis, Lora (2012). "Childhood Lead Poisoning Associated with Gold Ore Processing: a Village-Level Investigation—Zamfara State, Nigeria*. Environmental Health Perspectives. 120 (10): 1450–1455.*

Yusuf T. U., Udensi E. E., Rafiu A. A., Eze P. C & Salako K. A. (2018a). Assessing the Spatial Patterns in Soil Properties which Strongly Influences High Crop Yields,

through Electrical Resistivity Methods, in Mokwa, Niger State, Nigeria. *Lapai Journal of Applied and Natural Sciences*, 3(1): 9-19

Yusuf T. U., Udensi E. E., Rafiu A. A., Eze P. C. & Mohammed A. (2018b). Investigating Groundwater Quality and Soil Viability Using Geophysical and Geochemical Approach at a Dumpsite in Mokwa, Niger State, Nigeria. Nigeria. *Lapai Journal of Applied and Natural Sciences*, 3(1): 20-34

Zielke-Oliver & PD Vermeulen (2017) Utilizing Geophysics as a Delineation Tool for Groundwater Flow Paths and Contaminants along a Graben, Mine Water and Circular Economy 320 – 328.

Appendix A
Resistance, Apparent resistivity and Chargeability of the study area

A	RESISTANCE (Ω)	2*pi	APPARENTRESISTIVITY (Ωm)	CHARGEABILITY (msec)
10	0.324	6.284	20.36016	0.83
10	0.417	6.284	26.20428	0.88
10	0.283	6.284	17.78372	0.76
10	0.455	6.284	28.5922	0.94
10	0.34	6.284	21.3656	-0.21
10	0.468	6.284	29.40912	3.5
10	0.408	6.284	25.63872	-1.69
10	0.338	6.284	21.23992	-0.34
10	0.5	6.284	31.42	0.51
10	4.00	6.284	251.36	0.95
10	0.411	6.284	25.82724	0.42
10	0.41	6.284	25.7644	1.45
10	0.259	6.284	16.27556	0.2
10	0.29	6.284	18.2236	0.19
10	0.256	6.284	16.08704	-0.17
10	0.22	6.284	13.8248	0.71
10	0.185	6.284	11.6254	1.75
10	0.171	6.284	10.74564	-0.44
10	0.186	6.284	11.68824	2.98

10	0.146	6.284	9.17464	-0.11
10	0.178	6.284	11.18552	2.73
10	0.167	6.284	10.49428	0.69
10	0.207	6.284	13.00788	0.59
10	0.244	6.284	15.33296	-1.65
10	0.202	6.284	12.69368	1.83
10	0.256	6.284	16.08704	3.16
10	0.164	6.284	10.30576	0.91
10	0.246	6.284	15.45864	-0.045
10	0.205	6.284	12.8822	0.31
10	0.248	6.284	15.58432	0.33
10	0.281	6.284	17.65804	0.32
10	0.192	6.284	12.06528	0.063
10	0.345	6.284	21.6798	0.15
10	0.225	6.284	14.139	0.33
10	0.314	6.284	19.73176	0.5
10	0.328	6.284	20.61152	0.76
10	0.3	6.284	18.852	0.66
10	0.352	6.284	22.11968	1.02
10	0.43	6.284	27.0212	0.98
10	0.271	6.284	17.02964	0.39
10	0.44	6.284	27.6496	0.76
10	0.335	6.284	21.0514	0.49
10	0.486	6.284	30.54024	-0.64
10	0.352	6.284	22.11968	0.86
10	0.479	6.284	30.10036	0.87
10	0.39	6.284	24.5076	2.95
10	0.417	6.284	26.20428	0.38
10	0.293	6.284	18.41212	-0.086
30	0.478	6.284	90.11256	1.95
30	0.424	6.284	79.93248	2.61
30	0.366	6.284	68.99832	3.02
30	0.251	6.284	47.31852	0.86
30	0.181	6.284	34.12212	1.6
30	0.197	6.284	37.13844	2.37
30	0.128	6.284	24.13056	4.36
30	0.172	6.284	32.42544	0.56
30	0.156	6.284	29.40912	1.61
30	0.186	6.284	35.06472	0.6
30	0.244	6.284	45.99888	-0.24
30	0.337	6.284	63.53124	0.44
30	0.368	6.284	69.37536	1.7
30	0.368	6.284	69.37536	1.31

30	0.334	6.284	62.96568	1.24
30	0.336	6.284	63.34272	1.25
50	0.383	6.284	120.3386	1.03
50	0.335	6.284	105.257	-0.16
50	0.209	6.284	65.6678	2.68
50	0.192	6.284	60.3264	0.98
50	0.158	6.284	49.6436	1.16
50	0.2	6.284	62.84	17.6
50	0.342	6.284	107.4564	0.99
50	0.418	6.284	131.3356	0.96

Appendix B

Seismic Refraction Tomograms and travel time curves for all the profiles

Source= 60.0m

Ln4_4aR.dat

0 10 20 30 40 50 60 70 80 90 100 110 120 130 140 150 160 170 180 190 200 210 220 230 240 250 260 270 280 290 300 310 320 330 340 350 360 370 380 390 400 410 420 430 440 450 460 470 480 490 500 510 520 530 540 550 560

Distance (m) Scale = 1 / 2632

Distance (m)

Scale = 1 / 2632

LINE 4_ALL.VS

Distance (m)

Scale = 1 / 2632

LINE 4_ALL.VS

LINE 4_ALL.VS

LINE 4_ALL.VS

Status : No editing

LINE 5_ALL.VS

Scale = 1 / 2778

LINE 5_ALL.VS

Scale = 1 / 2703

#

154
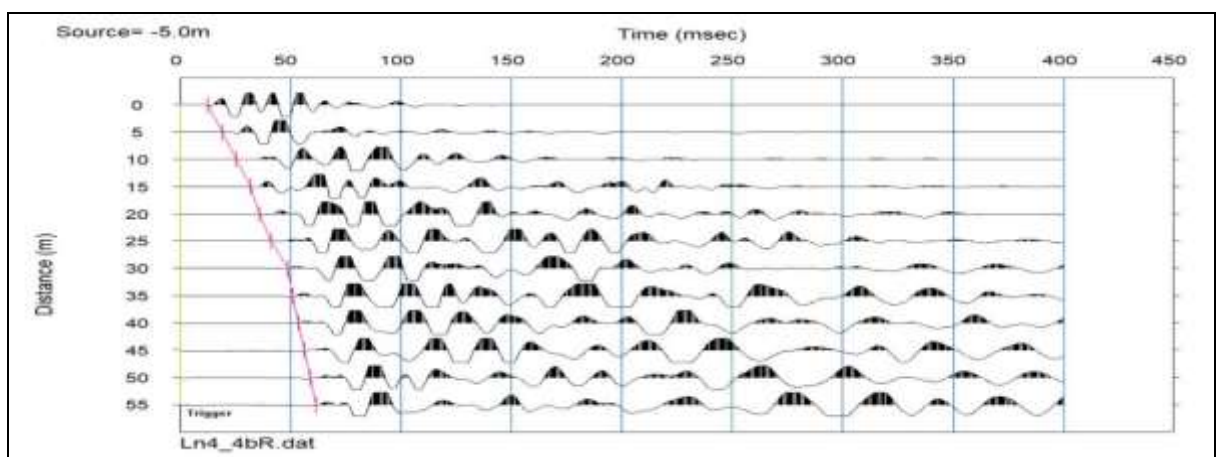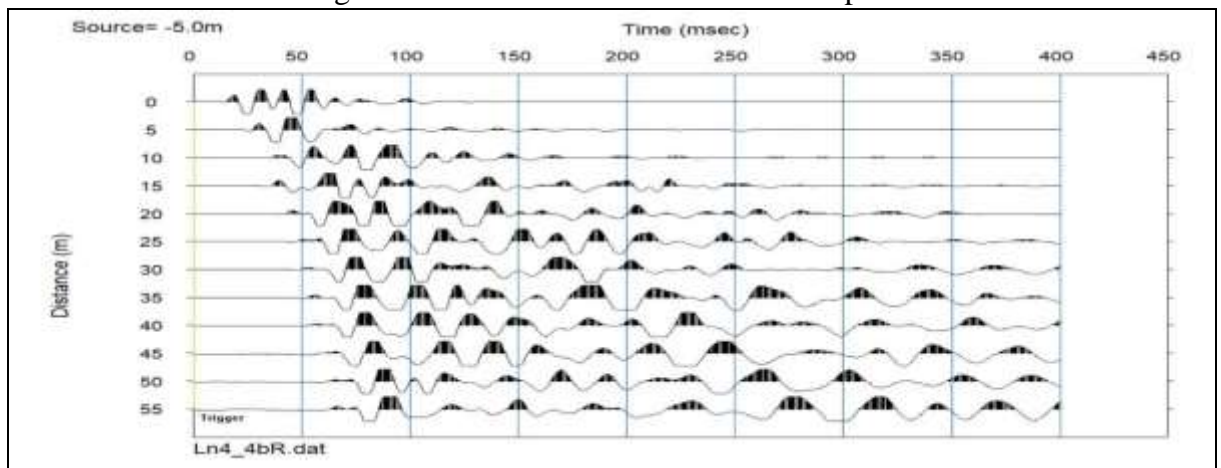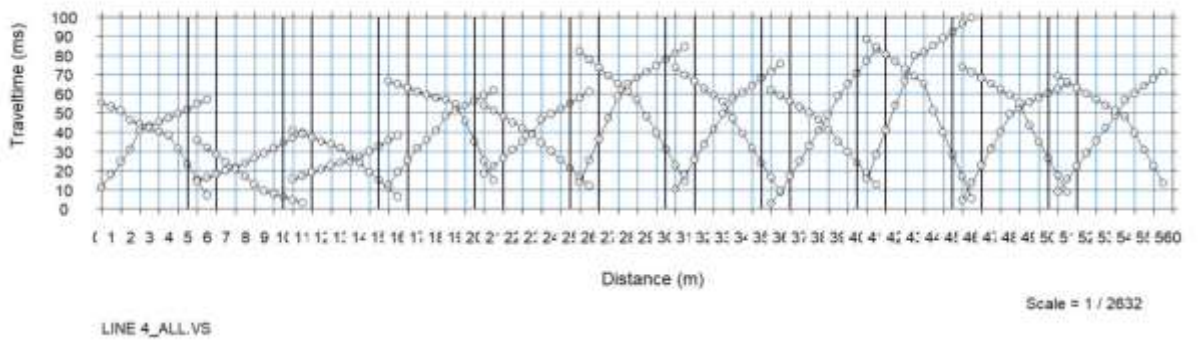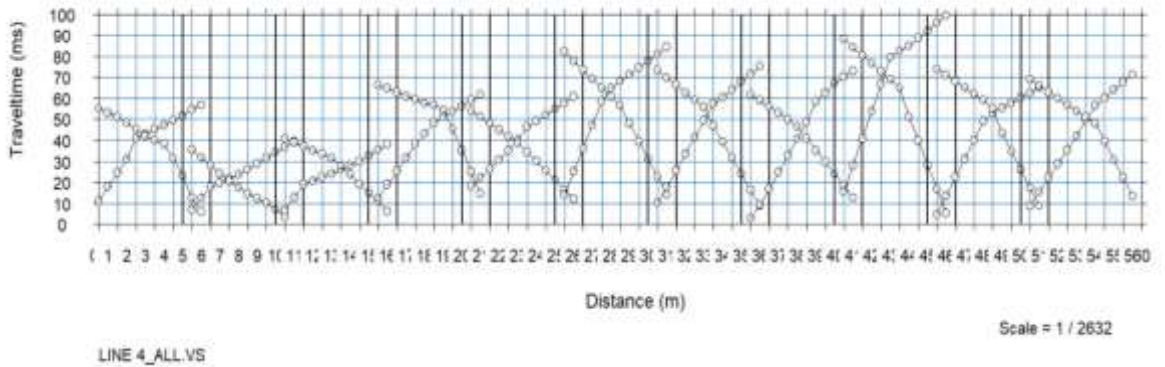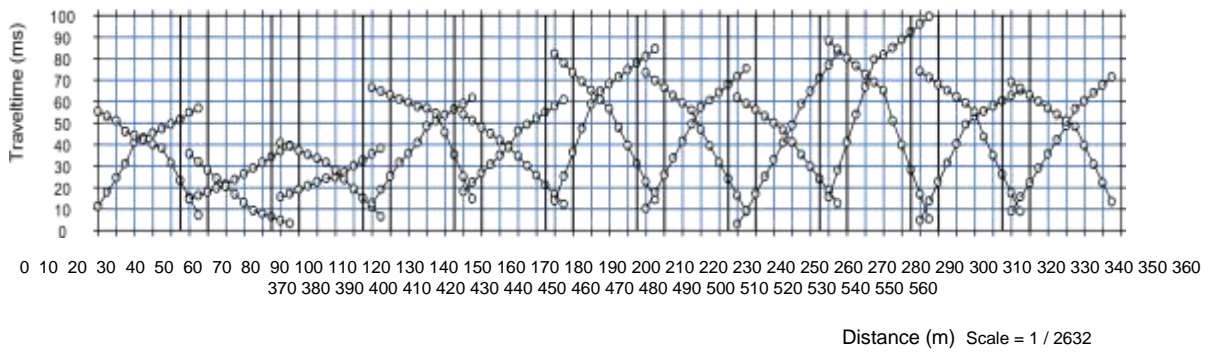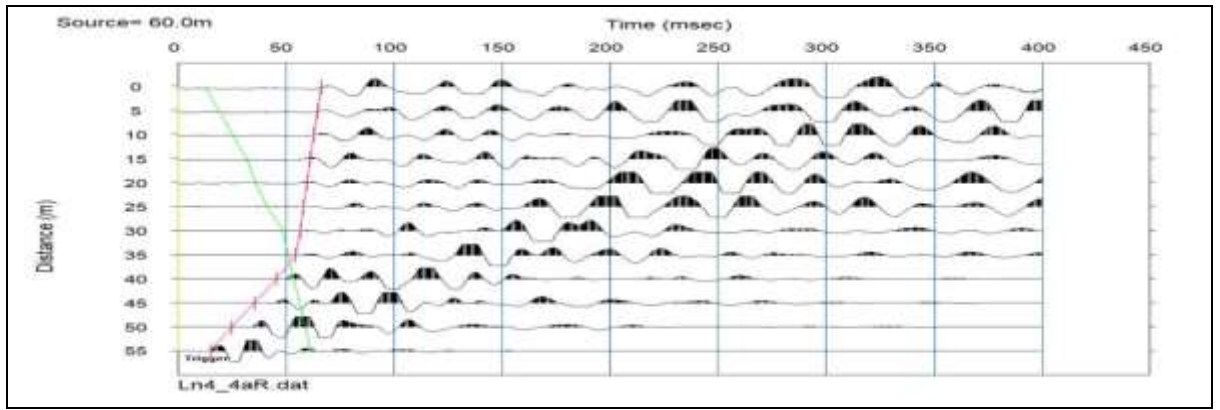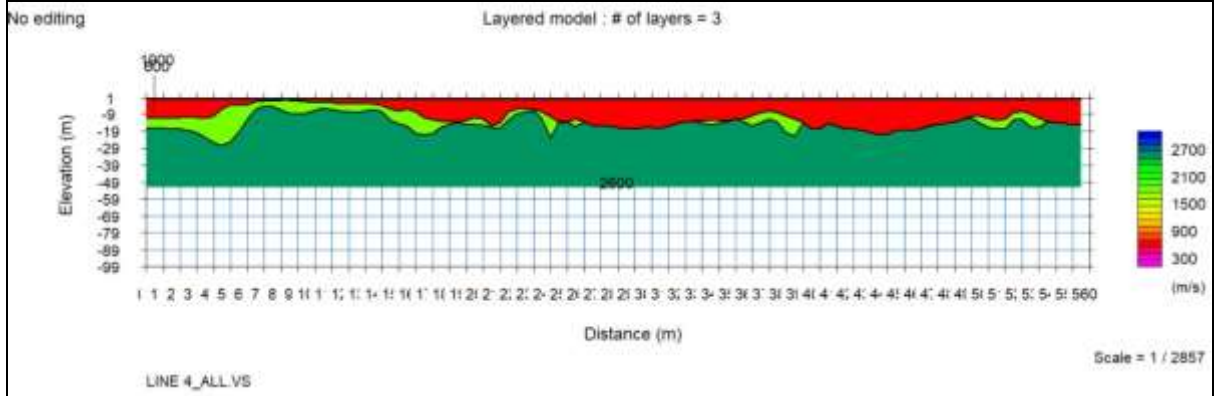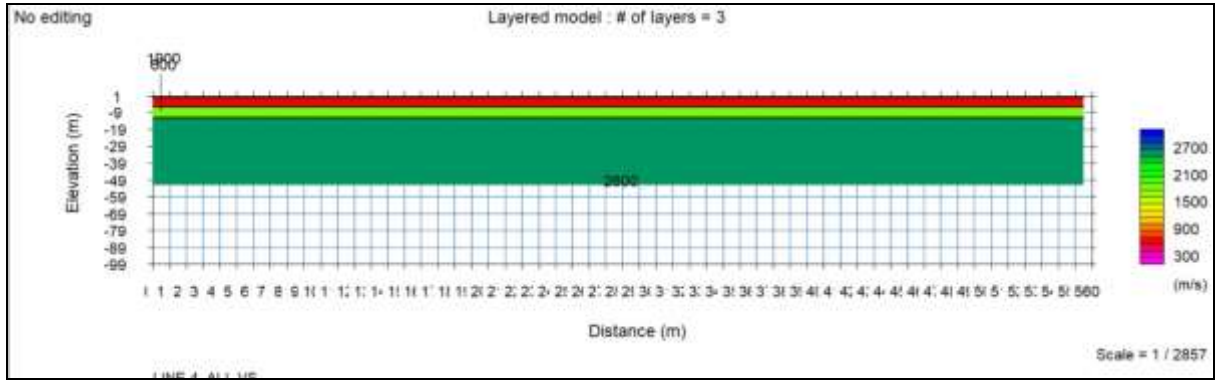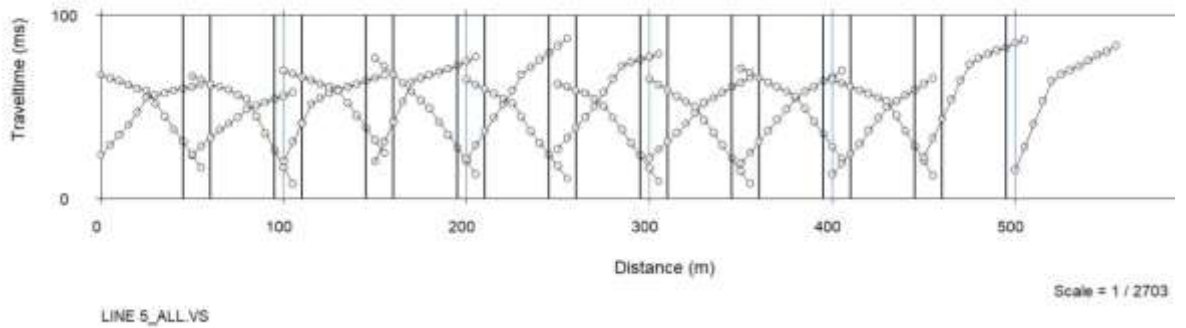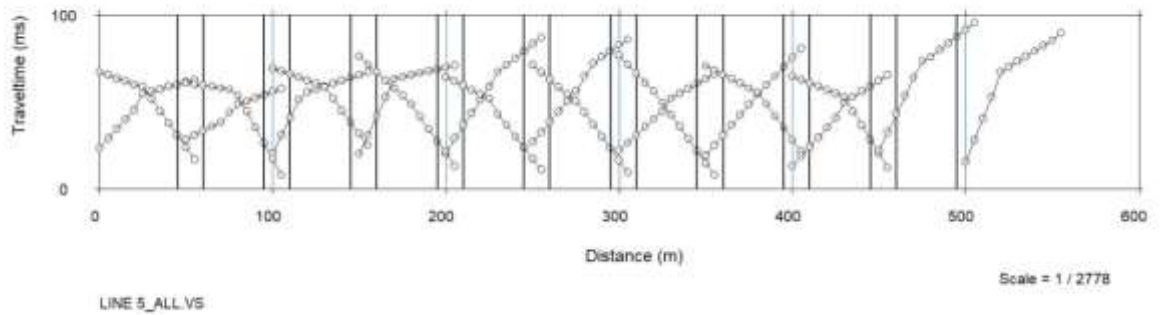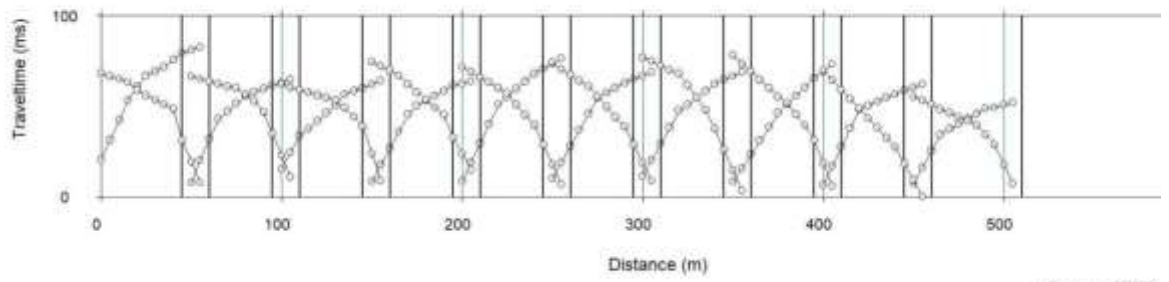
No editing

Layered model : # of layers = 3

LINE 5_ALL R.VS

Scale = 1 / 3226

155

LINE 6_ALL.VS
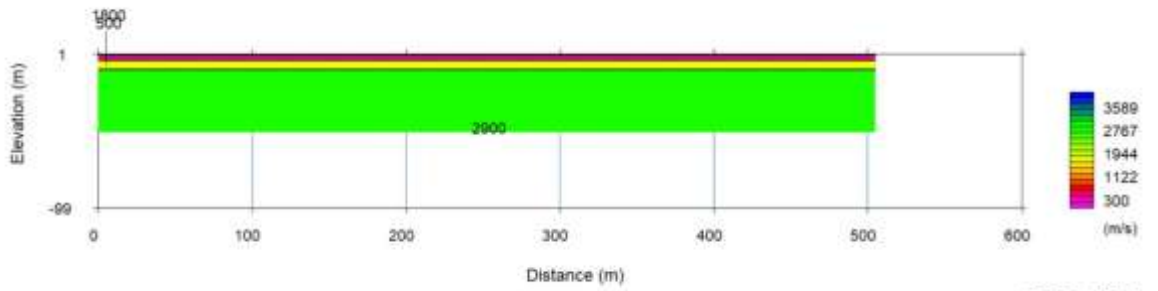
Scale = 1 / 2857

LINE 6_ALL.VS

Scale = 1 / 3125

No editing

Layered model : # of layers = 3

LINE 6_ALL.VS

Scale = 1 / 3125

No editing

Layered model : # of layers = 3

LINE 6_ALL.VS
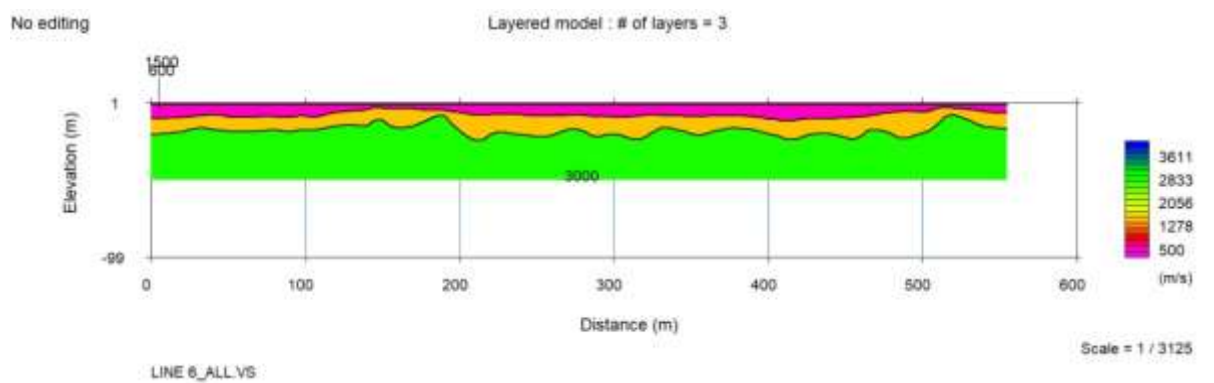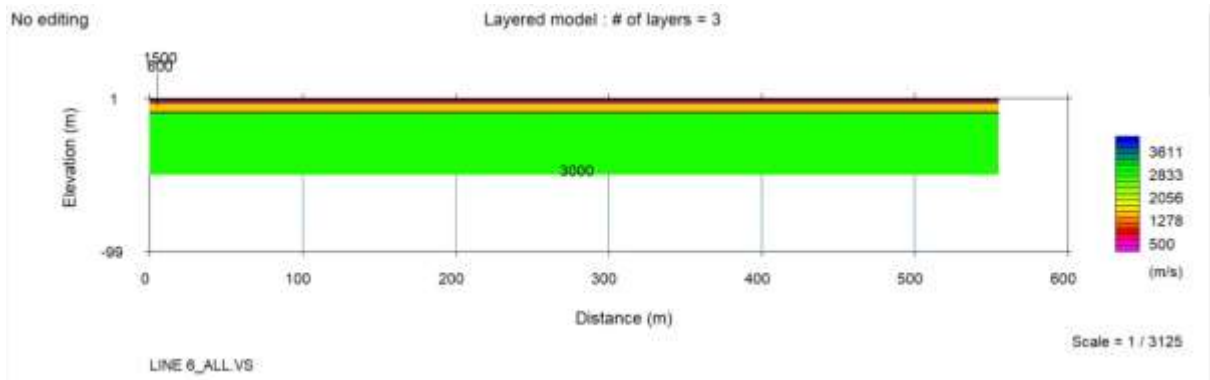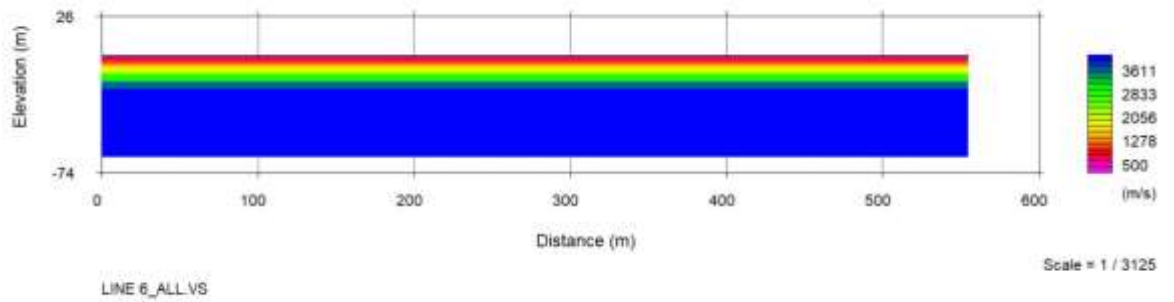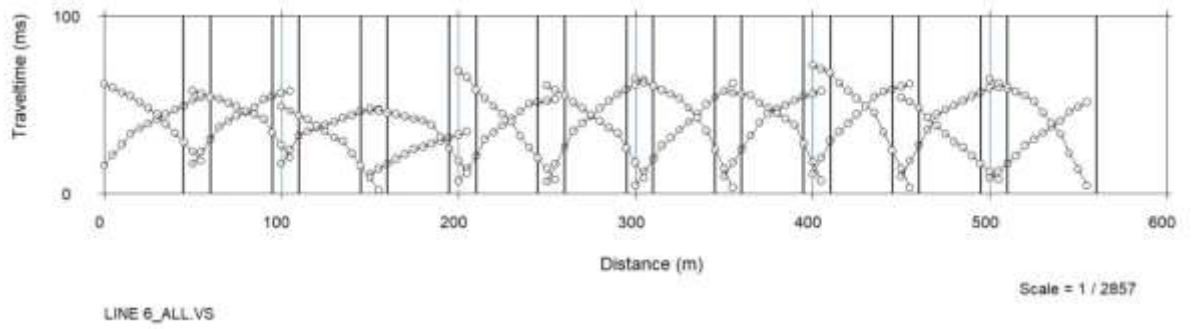
Scale = 1 / 3125

LINE 7_ALL.VS

Scale = 1 / 2703

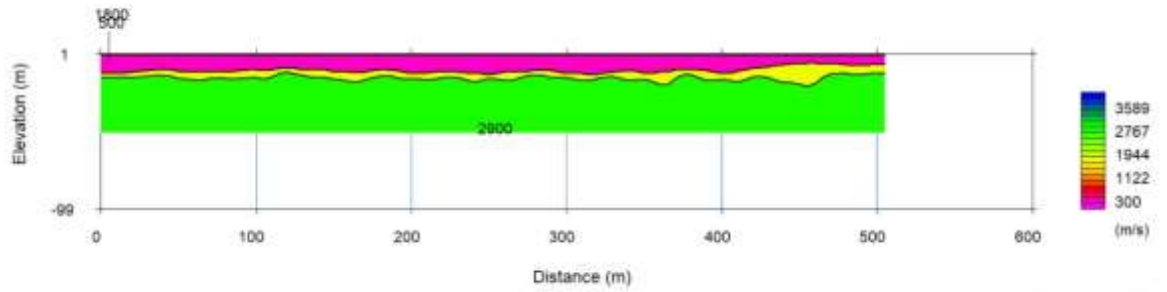No editing

Layered model : # of layers = 3

LINE 7_ALL.VS

Scale = 1 / 3125

No editing

Layered model : # of layers = 3

LINE 7_ALL.VS

Scale = 1 / 3125